Initial Relative-Orbit Determination Using Second-Order Dynamics and Line-of-Sight Measurements

by

Shubham Kumar Garg

A thesis submitted to the Graduate Faculty of
Auburn University
in partial fulfillment of the
requirements for the Degree of
Master of Science

Auburn, Alabama
May 10, 2015

Keywords: nonlinear dynamics, orbit
determination, angle-only navigation

Approved by

Andrew Sinclair, Chair, Associate Professor of Aerospace Engineering
David Cicci, Professor of Aerospace Engineering
John Cochran, Professor Emeritus of Aerospace Engineering

Abstract

This thesis addresses the problem of determining the initial relative-orbit state between a chief and a deputy satellite using line-of-sight unit vectors. An analytical solution is investigated for estimating the deputy satellite's initial states relative to the chief satellite, assuming circular chief orbit. The line-of-sight measurements and the relative motion of the deputy satellite, captured with a closed-form second-order solution of relative motion, leads to the nonlinear measurements equation. The measurement equations are transformed using the new proposed formulation which solves directly for the unknown ranges. The new formulation is applied to two solution procedures to solve the relative-orbit determination problem. Within the first solution method, the new formulation is computationally faster and requires fewer measurements, than the previous formulation. The second solution method requires the minimal number of measurements, but the new formulation provides reduced algebraic complexity in comparison to the previously published formulation.

Acknowledgment

I would like to thank my parents and elder sister for making my dream of higher education become possible. You all have been a motivation and a reason for me to focus on my work each and every day. I would also like to thank my cousin Mr. Ruchit Garg and his wife Mrs. Veebha Garg to have been my close family in this country. Without them being here, this experience would have been much less fun.

This work could not have been completed without the help and support of many individuals. I would like to sincerely appreciate Dr. Andrew J. Sinclair for his constant advice, patience and kindness throughout my study at Auburn University. He went above and beyond to help me succeed. His suggestions from time to time have been imperative to this work. Working with him has been a tremendous learning experience for me. I am very thankful for the insights and valuable time of my committee members Dr. David Cicci and Dr. John Cochran. I would like to thank Dr. Anwar Ahmed, Dr. Brian S. Thurow, and Dr. Normam Speakman, they all provided valuable support and suggestions whenever I needed. I would also like to thank the Department of Aerospace Engineering at Auburn University for giving me an opportunity to work as a teaching assistant. Being a TA has taught me a lot and given me an opportunity to understand how it feels to be on other side.

I can't imagine life without friends and would like to thank Aditya Agarwal, Amey Rane, Micah Bowden, Mikhail Zade, and Prachi Sangle for their tremendous support both during good and tough times. They all are like a second family to me. As an international student, sometime we all miss love of parents and home cooked food, I would like to thank

Mrs. Niranjana Nayak, Mr. Rajesh Nayak and Gayatri didi for being here and fulfilling that role. Their family has always showered us with love, respect, and the delicious home cooked food. I will be ever grateful for their assistance, and am sorry that Mr. Nayak has not lived to see me graduate. I would also like to appreciate the work that me and my committee member has done for Indian Student Association. It has been a wonderful and learning experience working with them for these two years. I must thank Dr. Sushil Bhavnani, faculty advisor, Hasitha Athotha, President, and all the members of Indian Student Association for relieving me of my duties during the preparation of this thesis.

There are many other people that I met during this period like Ajit bhai, Nakul bhai, Shantanu bhai, Kunal bhai, Jasma di, Vishai bhai, Bhumi di, Robin and they all helped me in gaining something good. I am sorry that I cannot write everyone's name and their importance, which would be whole another thesis, but I am thankful for everything that happened during this time. Thank you all.

Table of Contents

List of Tables

List of Illustrations

CHAPTER 1

INTRODUCTION

A major area in the field of orbital mechanics is the dynamics of multiple space objects with respect to each other, specifically when the relative distance between two objects is small in comparison to the distance from the central gravitational body. Knowing the dynamics of relative motion is very important for proximity operations because orbit maneuvers are performed not to correct the inertial orbit about the central body, but rather to adjust and control the relative orbit between two vehicles. The satellite from which all other satellites are referred is called 'chief' and the rest of the satellites are called 'deputy'. Relative-orbit determination has been fundamental for several decades with the beginning of human spaceflight in 1961. For example, rendezvous and docking in the context of mission staging, maintenance and supply, interferometric sensing, and cooperative flight depend on accurate knowledge of the relative-motion state. The theory and application of relative motion continues to receive high attention focused on precision, autonomous, multi-vehicle formation flight and close proximity operations.

In performing relative-orbit determination for satellites in close proximity, two types of observation sensors are typically used. These are cameras and range sensors onboard the satellites. The problem discussed here is a case of using only cameras. This means the only observation that can be obtained is line-of-sight (LOS) unit direction vectors. Woffinden and Geller[1] concluded that relative-orbit determination is an unobservable problem when the following three conditions are satisfied:

- angle-only measurements are taken,
- a linear Cartesian model of relative motion is used to estimate the dynamics, such as the Clohessy-Wiltshire (CW) model[2],
- there are no thrusting maneuvers during the span of measurements.

Ref. 1 showed that a family of relative orbits whose state histories are proportional to one another (i.e. differ by only a constant scalar multiple) will possess a common LOS history. Figure 1 shows what is meant by a family of relative orbits. This method can provide knowledge of shape and orientation of the relative trajectory, but not the size of the trajectory.

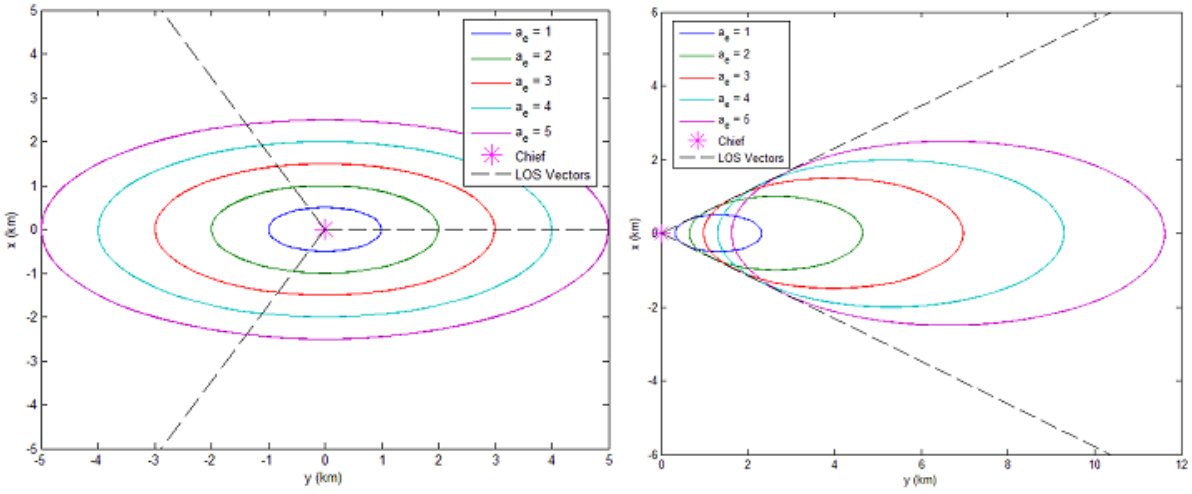

Figure 1. Families of Relative Orbits with Common LOS histories (trajectories generated using the Hills-Clohessy-Wiltshire equations[2, 3])

Reference 3 presented a linear matrix equation procedure for determining the non-unique state-vector solution. An unscaled vector in the direction of the initial conditions was determined, but it was not possible to determine the proper scaling of the vector because of the linear dynamics.

Current research is investigating the use of second-order nonlinear relative equations of motion to capture the motion between the chief and the deputy satellite. These equations offers two distinct advantages: first, these are able to capture the relative motion of two satellites better than the linear CW solution due to its inclusion of nonlinear terms; second, the nonlinear terms facilitate determination of the unique scaling of the state vector, rendering the Initial Relative-Orbit Determination (IROD) problem observable. References 4, 5 and 6 have applied a nonlinear relative dynamic model with angular measurements to remove the unobservability associated with linear dynamics. The second-order dynamics model and angle-only measurements produce a system of quadratic equations for the unknown initial conditions.

Two different solution procedures have been considered. The first method, minimum-measurement solution, provides direct solution of the quadratic equations by Macaulay polynomial resultant with minimal number of measurements. It requires a minimum number of measurements and is computationally very complex. The Macaulay resultant theory is a less familiar subject in engineering disciplines, when compared to linear algebra. In this theory, the system of multivariate polynomial equations is projected to a single univariate polynomial equation: the resultant polynomial equation: Using a matrix polynomial structure, this equation can be solved by computing a generalized Eigen decomposition.[11-16] Because the resultant polynomial is zero if and only if the polynomial system has a common root, this procedure is often interpreted as a means to finding the intersection of algebraic curves. The second method, redundant-measurement solution, treats the linear and quadratic components as independent variables and transforms the original second-order dynamics solution to a linear homogenous matrix equation with the

use of redundant measurements. The steps are to, first, solve the measurements for an eigenvector with linear and quadratic components; second, discard the quadratic components and reform them again using the scaled linear components; and third, substitute the reformed vector back into the measurement equations to solve for the scaling.

The main aim of this research is to determine the initial relative position vector and the velocity vector of the deputy satellite with respect to the chief satellite using angle-only measurements, i.e. to estimate the $x_0, y_0, z_0, \dot{x}_0, \dot{y}_0, \dot{z}_0$ components of the relative position vector and the relative velocity vector using azimuth and elevation angle observations provided by an on-board camera on the chief satellite. In this thesis, development of a new method for estimating the deputy satellite initial relative state with respect to the chief satellite is discussed. Compared to previous methods, the linear measurement equations of the proposed method are reformulated in a different set of unknowns. The reformulation of the measurement equations means that in the minimum-measurement solution, lower computational complexity is required, and in the redundant-measurement solution, fewer measurements are needed to perform the IROD. Also, another method for calculating the scalar ambiguity which utilizes all the constraint equations is studied along with its failure to give an accurate result. To illustrate the results, they are evaluated along several relative motions in the presence of varying noise types, noise levels, and sample periods.

CHAPTER 2

SECOND-ORDER DYNAMICS MODEL

This chapter reviews the development of the full nonlinear relative equation of motion using Cartesian coordinates. A spacecraft formation with two satellites is considered as shown in Figure 2.

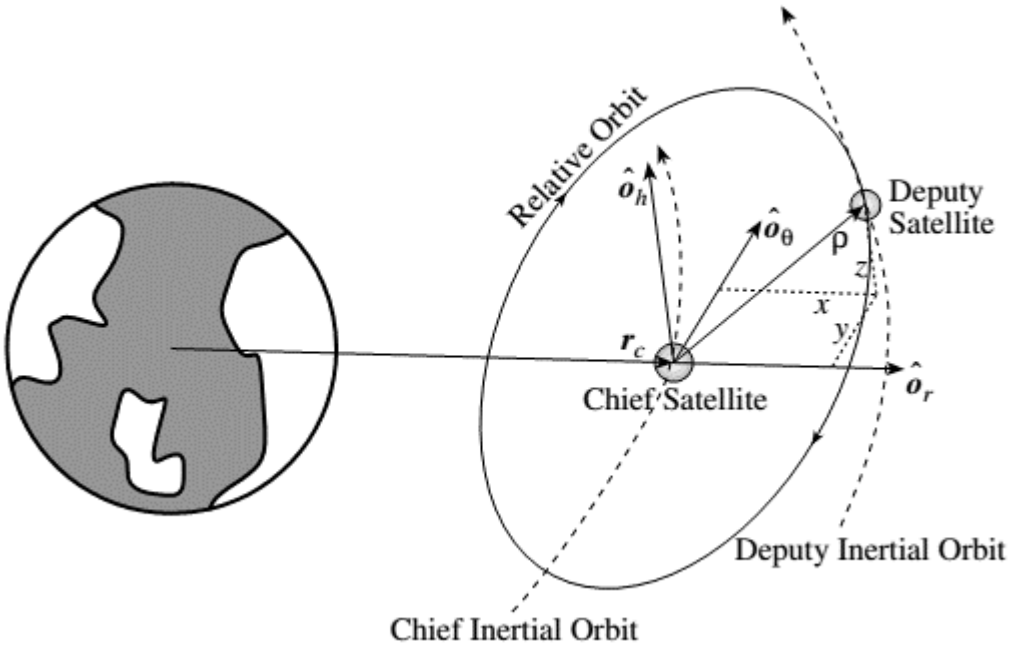

Figure 2. Relative Motion between Chief and Deputy Satellite[12]

The chief satellite is used as a reference to describe the motion of the deputy satellite. The inertial chief position is expressed through the vector $\boldsymbol{r}_c$ (t), while the deputy satellite position is given by $\boldsymbol{r}_d$ (t). The local-vertical local-horizontal (LVLH) frame is used as the reference system. One of the advantages of using this reference frame is that the physical

dimensions of the relative orbit can be clearly visualized. The (x, y) coordinates defines the relative-orbit motion in the chief satellite's orbital plane and the z coordinate indicates the relative motion out of plane. Its origin is at the chief satellite position and its orientation is given by the vector triad $\{\hat{\boldsymbol{o}}_r, \hat{\boldsymbol{o}}_\theta, \hat{\boldsymbol{o}}_h\}$ shown in Figure 2.

The vector $\hat{\boldsymbol{o}}_r$ points in the direction of chief satellite radius, the vector $\hat{\boldsymbol{o}}_h$ is in the direction of angular momentum of the chief satellite and the vector $\hat{\boldsymbol{o}}_\theta$ completes the right-handed coordinate system. Mathematically, the three unit direction vector can be shown as

$$\begin{aligned} \hat{\boldsymbol{o}}_r &= \frac{\boldsymbol{r}_c}{r_c} \\ \hat{\boldsymbol{o}}_h &= \frac{\boldsymbol{h}}{h} \quad (\boldsymbol{h} = \boldsymbol{r}_c \times \dot{\boldsymbol{r}}_c) \\ \hat{\boldsymbol{o}}_\theta &= \hat{\boldsymbol{o}}_h \times \hat{\boldsymbol{o}}_r \end{aligned} \tag{1}$$

Cartesian-coordinate Description

The relative orbit can be described in both Cartesian coordinates as well as orbital elements. Here, the relative orbit is described in terms of Cartesian coordinates. The relative position of the deputy satellite with respect to the chief satellite is the vector **ρ** expressed in LVLH frame as

$$\boldsymbol{\rho} = [x, y, z]^{\mathrm{T}} \tag{2}$$

From Figure 2, we can write the deputy satellite position vector as

$$\boldsymbol{r}_d = \boldsymbol{r}_c + \boldsymbol{\rho} = (r_c + x)\,\hat{\boldsymbol{o}}_r + y\,\hat{\boldsymbol{o}}_\theta + z\,\hat{\boldsymbol{o}}_h \tag{3}$$

Where r_c is the orbital radius of the chief satellite at any point of time. The angular velocity vector of the rotating LVLH frame is given by

$$\boldsymbol{\omega} = \dot{f}\,\hat{\boldsymbol{o}}_h \tag{4}$$

Where f is the chief's true anomaly. Double differentiation of the position vector of the deputy satellite with respect to the inertial frame will give the acceleration vector of deputy satellite as

$$\ddot{\boldsymbol{r}}_{\boldsymbol{d}} = (\ddot{r}_c + \ddot{x} - 2\dot{y}\dot{f} - \ddot{f}y - \dot{f}^2(r_c + x))\hat{\boldsymbol{o}}_r + (\ddot{y} + 2\dot{f}(\dot{r}_c + \dot{x}) + \ddot{f}(r_c + x) - \dot{f}^2)\hat{\boldsymbol{o}}_\theta + \ddot{z}\hat{\boldsymbol{o}}_h \tag{5}$$

Keeping in mind that the chief satellite angular momentum h is constant for Keplerian motion and is given by $h = r_c^2\dot{f}$, the first derivative of it yields

$$\dot{h} = 0 = 2r_c\dot{r}_c\dot{f} + r_c^2\ddot{f} \tag{6}$$

Equation (6) can be used to solve for the true anomaly acceleration:

$$\ddot{f} = -2\frac{\dot{r}_c}{r_c}\dot{f} \tag{7}$$

Further, we can write the chief satellite position as $\boldsymbol{r}_c = r_c\,\hat{\boldsymbol{o}}_r$. Taking the double derivative of the chief satellite position vector with respect to the inertial frame and equating it with orbit equation of motion can be expressed as:

$$\ddot{\boldsymbol{r}}_c = (\ddot{r}_c - r_c\dot{f}^2)\hat{\boldsymbol{o}}_{\boldsymbol{r}} = -\frac{\mu}{r_c^3}\boldsymbol{r}_c = -\frac{\mu}{r_c^2}\hat{\boldsymbol{o}}_{\boldsymbol{r}} \tag{8}$$

Equating vector component in Eq. (8), the chief satellite orbit acceleration can be expressed as:

$$\ddot{r}_c = r_c\ddot{f} - \frac{\mu}{r_c^2} = r_c\dot{f}^2(1 - \frac{r_c}{p}) \tag{9}$$

Substituting Eq. (7) and Eq. (8) into Eq. (5), the deputy satellite acceleration vector will reduce to:

$$\ddot{\boldsymbol{r}}_d = (\ddot{x} - 2\dot{f}(\dot{y} - y\frac{\dot{r}_c}{r_c}) - x\dot{f}^2 - \frac{\mu}{r_c^2})\hat{\boldsymbol{o}}_{\boldsymbol{r}} + (\ddot{y} + 2\dot{f}(\dot{x} - x\frac{\dot{r}_c}{r_c}) - y\dot{f}^2)\hat{\boldsymbol{o}}_\theta + \ddot{z}\hat{\boldsymbol{o}}_h \tag{10}$$

Next, the deputy satellite acceleration vector can also be expressed in terms of its orbital acceleration as:

$$\ddot{\boldsymbol{r}}_d = -\frac{\mu}{r_d^3}\boldsymbol{r}_d = -\frac{\mu}{r_d^3}\begin{bmatrix} r_c + x \\ y \\ z \end{bmatrix} \tag{11}$$

Here $r_d = \sqrt{(r_c + x)^2 + y^2 + z^2}$ Equating Eq. (10) and Eq. (11), the exact nonlinear relative equations of motion are given by

$$\begin{aligned} \ddot{x} - 2\dot{f}(\dot{y} - y\frac{\dot{r}_c}{r_c}) - x\dot{f}^2 - \frac{\mu}{r_c^2} &= -\frac{\mu}{r_d^3}(r_c + x) \\ \ddot{y} + 2\dot{f}(\dot{x} - x\frac{\dot{r}_c}{r_c}) - y\dot{f}^2 &= -\frac{\mu}{r_d^3}y \\ \ddot{z} &= -\frac{\mu}{r_d^3}z \end{aligned} \tag{12}$$

These three equations constitute sixth order full nonlinear relative equations of motion of the deputy satellite with respect to the chief satellite as seen in the LVLH reference frame. The only assumption that has been made is of an unperturbed Keplerian motion. These are valid for arbitrarily large relative orbits and for any value of chief eccentricity.

The relative equations of motion can be linearized about the origin of the chief-fixed LVLH frame, on the assumption that the relative-orbit separation is small in comparison to the chief satellite orbit radius (r_c) and the chief satellite is in circular orbit. The linearized equations of motion are called the Clohessy–Wiltshire equations (CW) or the Hill–Clohessy–Wiltshire equations (HCW). Since for a circular orbit, the chief radius is constant and the mean motion (n_0) is equal to the true anomaly rate $\dot{f}$, the relative equations of motion can be reduced into simpler forms as:

$$\ddot{x} - 2n_0\dot{y} - 3n_0^2 x = 0$$
$$\ddot{y} + 2n_0\dot{x} = 0 \qquad (13)$$
$$\ddot{z} + n_0^2 z = 0$$

The simple form of the differential relative equations of motion allows them to be solved analytically. It can be noticed that the linearization has decoupled the out-of-plane motion from the in-plane motion and is similar to simple spring-mass system which has a known solution.

As mentioned earlier, initial research in this area has used these linearized relative equations of motion for determining the initial relative orbit of the deputy satellite with respect to the chief satellite. But, with angle-only observations the problem is unobservable, and only shape and orientation of the relative orbit can be estimated. Hence, the exact nonlinear equations are used to obtain the second-order dynamic relative equation of motion. The second-order dynamics solution of relative motion make this problem observable, as will be seen.

The relative motion between the chief satellite and the deputy satellite can be modeled with the use of an analytically obtained approximate solution of a second-order approximation of the nonlinear equations[5].

$$x(t) = (4 - 3\cos(n_0 t_i))x_0 + \frac{1}{n_0}(\sin(n_0 t_i))\dot{x}_0 + \frac{2}{n_0}(1 - \cos(n_0 t_i))\dot{y}_0$$

$$+ \frac{3}{2R_0}(7 - 10\cos(n_0 t_i) + 3\cos(2n_0 t_i) + 12n_0 t_i \sin(n_0 t_i) - 12n_0^2 t_i^2)x_0^2$$

$$+ \frac{3}{2R_0}(1 - \cos(n_0 t_i))y_0^2 + \frac{1}{4R_0}(3 - 2\cos(n_0 t_i) - \cos(2n_0 t_i))z_0^2$$

$$+ \frac{1}{2n_0^2 R_0}(-3 + 4\cos(n_0 t_i) - \cos(2n_0 t_i))\dot{x}_0^2$$

$$+ \frac{1}{2n_0^2 R_0}(6 - 10\cos(n_0 t_i) + 4\cos(2n_0 t_i) + 12nt_i \sin(n_0 t_i) - 9n_0^2 t_i^2)\dot{y}_0^2$$

$$+ \frac{1}{4n_0^2 R_0}(3 - 4\cos(n_0 t_i) - \cos(2n_0 t_i))\dot{z}_0^2 + \frac{6}{R_0}(-\sin(n_0 t_i) + n_0 t_i)\, x_0 y_0$$

$$+ \frac{3}{n_0 R_0}(4\sin(n_0 t_i) - \sin(2n_0 t_i) - 4n_0 t_i + 2n_0 t_i \cos(n_0 t_i))x_0 \dot{x}_0$$

$$+ \frac{3}{n_0 R_0}(4 - 6\cos(n_0 t_i) + 2\cos(2n_0 t_i) + 7n_0 t_i \sin(n_0 t_i) - 6n_0^2 t_i^2)x_0 \dot{y}_0$$

$$+ \frac{3}{n_0 R_0}(-\sin(n_0 t_i) + (n_0 t_i))y_0 \dot{y}_0 + \frac{1}{2n_0 R_0}(2\sin(n_0 t_i) - \sin(2n_0 t_i))z_0 \dot{z}_0$$

$$+ \frac{1}{n_0^2 R_0}(7\sin(n_0 t_i) - 2\sin(2n_0 t_i) - 6n_0 t_i + 3n_0 t_i \cos(n_0 t_i))\dot{x}_0 \dot{y}_0 \qquad (14)$$

$$y(t) = 6(\sin(n_0 t_i) - n_0 t_i)x_0 + \{1\}y_0$$

$$+\frac{2}{n_0}(-1 + \cos(n_0 t_i))\dot{x}_0 + \frac{1}{n_0}(4\sin(n_0 t_i) - 3n_0 t_i)\dot{y}_0$$

$$+\frac{3}{4R_0}(40\sin(n_0 t_i) + 3\sin(2n_0 t_i) - 22n_0 t_i - 24n_0 t_i\cos(n_0 t_i))x_0^2$$

$$+\frac{3}{R_0}(\sin(n_0 t_i) - n_0 t_i)y_0^2 + \frac{1}{R_0}(4\sin(n_0 t_i) + \sin(2n_0 t_i) - 6n_0 t_i)z_0^2$$

$$+\frac{1}{4n_0^2 R_0}(8\sin(n_0 t_i) - \sin(2n_0 t_i) - 6n_0 t_i)\dot{x}_0^2$$

$$+\frac{1}{n_0^2 R_0}(10\sin(n_0 t_i) + \sin(2n_0 t_i) - 6n_0 t_i - 6n_0 t_i\cos(n_0 t_i))\dot{y}_0^2$$

$$+\frac{1}{4n_0^2 R_0}(8\sin(n_0 t_i) - \sin(2n_0 t_i) - 6n_0 t_i)\,\dot{z}_0^2 + \frac{3}{R_0}(1 - \cos(n_0 t_i))x_0 y_0$$

$$+\frac{3}{2n_0 R_0}(-5 + 4\cos(n_0 t_i) + \cos(2n_0 t_i) + 4n_0 t_i\sin(n_0 t_i))x_0\dot{x}_0$$

$$+\frac{3}{n_0 R_0}(12\sin(n_0 t_i) + \sin(2n_0 t_i) - 7n_0 t_i - 7n_0 t_i\cos(n_0 t_i))x_0\dot{y}_0$$

$$+\frac{1}{3n_0 R_0}(-\sin(n_0 t_i) + n_0 t_i)y_0\dot{x}_0$$

$$+\frac{1}{2n_0 R_0}(-3 + 4\cos(n_0 t_i) - \cos(2n_0 t_i))z_0\dot{z}_0$$

$$+\frac{1}{n_0^2 R_0}(-3 + 2\cos(n_0 t_i) + \cos(2n_0 t_i) + 3n_0 t_i\sin(n_0 t_i))\dot{x}_0\dot{y}_0$$

$$z(t) = \cos(n_0 t)z_0 + \{\frac{1}{n_0}\sin(n_0 t)\}\dot{z}_0 + \{\frac{3}{2R_0}(-3 + 2\cos(n_0 t) + \cos(2n_0 t)$$

$$+4n_0 t\sin(n_0 t))\}x_0 z_0 + \{\frac{3}{2n_0 R_0}(2\sin(n_0 t) + \sin(2n_0 t) - 4n_0 t\cos(n_0 t))\}x_0 \dot{z}_0$$

$$+\{\frac{1}{2n_0 R_0}(2\sin(n_0 t) - \sin(2n_0 t))\}z_0 \dot{x}_0 + \{\frac{1}{n_0 R_0}(-3 + 2\cos(n_0 t) + \cos(2n_0 t)$$

$$+3n_0 t\sin(n_0 t))\}z_0 \dot{y}_0 + \{\frac{1}{2n_0^2 R_0}(3 - 4\cos(n_0 t) + \cos(2n_0 t))\}\dot{x}_0 \dot{z}_0 + \{\frac{1}{n_0^2 R_0}(\sin(n_0 t)$$

$$+\sin(2n_0 t) - 3n_0 t\cos(n_0 t))\}\dot{y}_0 \dot{z}_0$$

The results are obtained from the 0^{th} order kernel in the Volterra expansion of the initial value problem[8]. In these equations, the subscript '0' denotes the value of a quantity at the initial time (t_0). The time term in the right hand side of the equations represents the relative time elapsed since the initial time, and the time term in the left hand side denotes the absolute time measured from the zero reference. In equations, it can be shown as:

$$x(t) = x_0$$

$$t_i = t - t_0$$

The other variables in the equations are the radius of the chief satellite (R_0) and the mean motion of chief satellite (n_0).

These solutions represent the time-dependent deputy position as a linear, quadratic, and bilinear combination of the initial relative position and velocity components ($x_0, y_0, z_0, \dot{x}_0, \dot{y}_0, \dot{z}_0$). All combinations of terms are present at least once in the expressions except for terms $y_0 z_0$ and $y_0 \dot{z}_0$. There are few points in the second-order solution which can be noticed and compared with the first-order solution. The linear terms of the first-order solution is present in the second-order solution. Along with that there are few extra terms in the second-order solution which makes it more accurate than the first-order solution. The

first-order solution has only one secular term, in the y equation, but the second-order solution has introduced new secular terms in x, y, and z. Secular terms in x include $n_o t$, $n_o t\cos(n_o t)$, $n_o t\sin(n_o t)$, $(n_o t)^2$, while secular terms in y include only $n_o t$, $n_o t\cos(n_o t)$, $n_o t\sin(n_o t)$, and secular terms in z are limited to just $n_o t\cos(n_o t)$, $n_o t\sin(n_o t)$. The secular term in the first-order solution provides the drift in only transverse (y) axis, but the secular terms in the second-order solution reflects the local three-dimensional drift of the deputy satellite away from the chief satellite in radial (x) and normal (z) axes also. Although the second-order solution is able to capture the true relative motion between the deputy and chief satellite, it will eventually fail since the secular terms will grow with time, and cause it to diverge from the true solution. Also, it is true that for a given separation distance between the chief and deputy satellite, the second-order solution may provide higher accuracy than first-order solution, but the error growth rate associated with second-order solution may exceed the level of first-order solution as the separation distance gets larger. Further, the cross-track and in-track motion is coupled in the full nonlinear equation and the second-order solution but it is lost in the first-order solution.

The problem is unobservable when the first-order solution is used with angle-only observations, and observable when the second-order solution is used with angle-only observations. Figure 3 and 4 show how the change in dynamic model helped in achieving the observability. Figure 3 shows the relative motion of a deputy satellite with respect to the chief satellite, captured with the first-order solution. The trajectory generated with true initial conditions is labelled as “First-Order Motion”. For this trajectory, the three line-of-sight direction of the deputy satellite at three different time in future are shown with black color. The trajectory generated with initial conditions that are twice of the true initial

conditions, is labelled as “First-Order Motion with 2 time initial condition”. For this trajectory, the line-of-sight direction of the deputy satellite at three different time in future are shown with green color. It can be seen, the line-of-sight unit-direction-vectors of the two different trajectory are overlapping each other. With these line-of-sight unit-direction-vector as measurements, the initial conditions cannot be estimated with first-order dynamic model since a family of trajectory will provide same unit-direction vector. Figure 4 shows the relative motion of a deputy satellite with respect to the chief satellite, captured with second-order solution. The trajectory generated with true initial conditions is labelled as “Second-Order Motion”. For this trajectory, the three line-of-sight direction of the deputy satellite at three different time in future are shown with black color. The trajectory generated with initial conditions that are twice of the true initial conditions, is labelled as “Second-Order Motion with 2 time initial condition”. For this trajectory, the line-of-sight direction of the deputy satellite at three different time in future are shown with green color. It can be seen, different set of measurements of unit-direction-vectors will estimate the trajectory corresponding to it. Hence, the second-order model is used to design a method which can estimate the initial conditions with line-of-sight measurements.

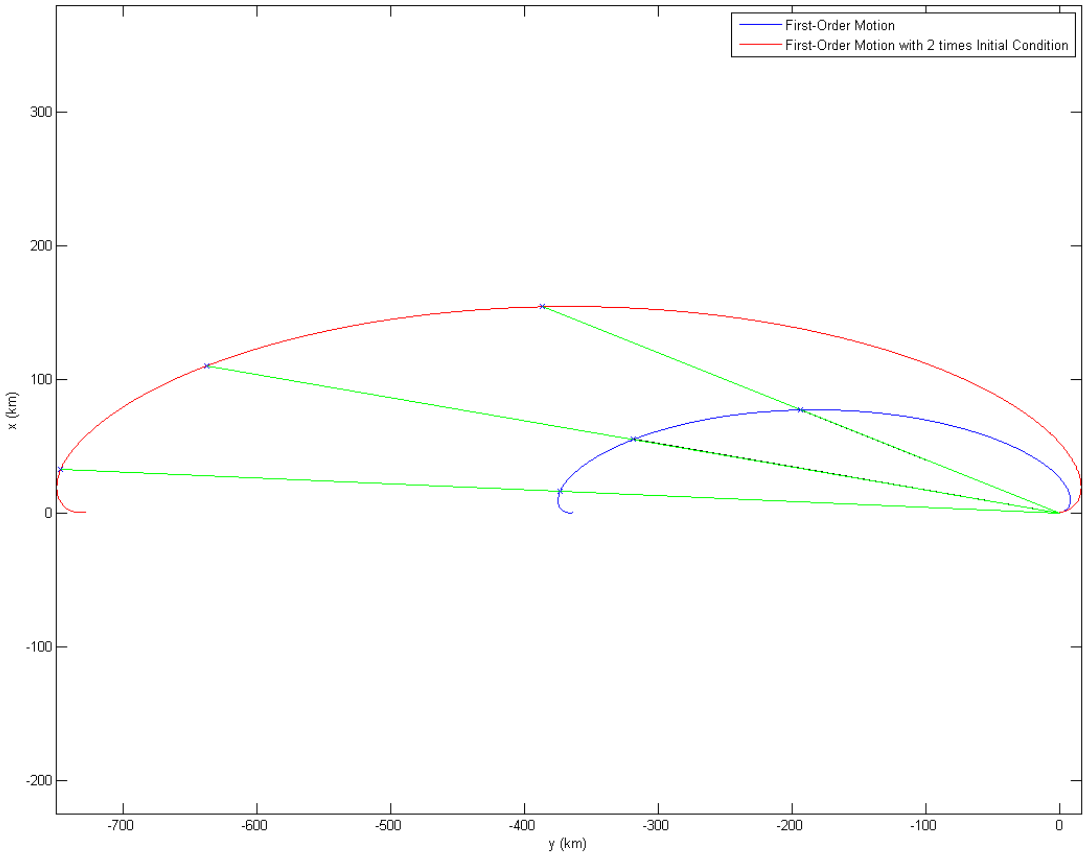

Figure 3. Relative Motion trajectory with First-Order Solution

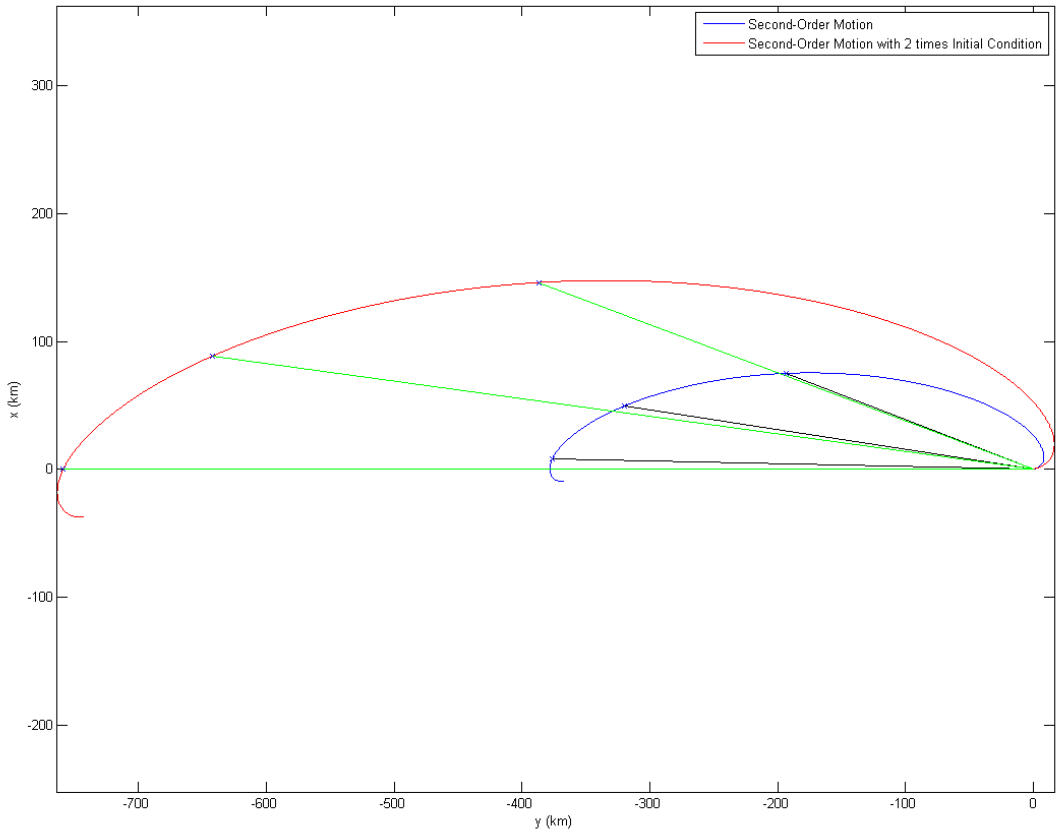

Figure 4. Relative Motion Trajectory with Second-Order Solution

CHAPTER 3

REDUNDANT-MEASUERMENT SOLUTION USING CARTESIAN-COMPONENT FORMULATION

The Cartesian-component formulation has been previously introduced in the literature. As the name suggests, this method determines the Cartesian-components of the initial relative position vector and velocity vector using the second-order dynamics and angle-only observation[8]. The redundant-measurement solution method can be divided into parts. First, the second-order solution is reformulated into a linear homogenous matrix equation using angular measurements, and second, determination of the unique scaling of the computed null vector. The solution is reviewed here, particularly because the second part of this method will be used in later chapters.

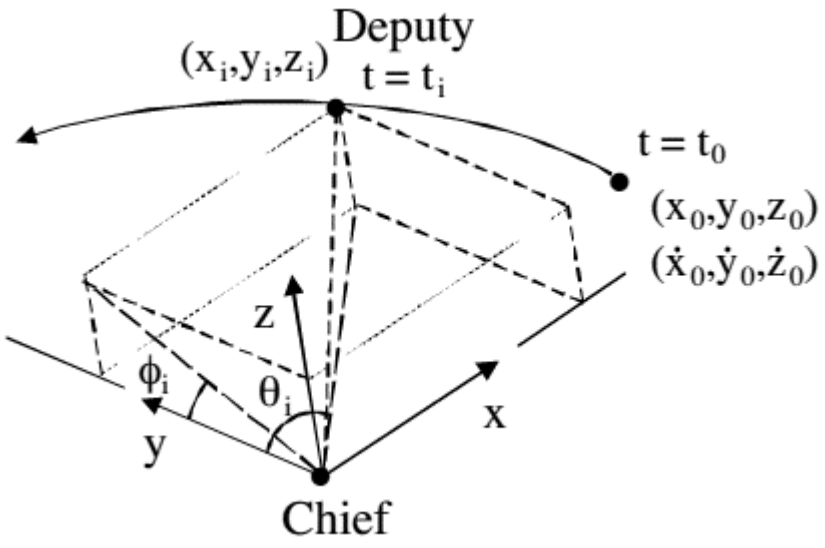

Figure 5. Relative Orbit Determination Geometry[8]

Figure 5 shows the measurement geometry of the line-of-sight from the chief satellite to the deputy satellite. Reference frame xyz is the rotating LVLH frame attached to the chief satellite. An on-board camera on the chief satellite will take the measurement of the azimuth angle and the elevation angle of the deputy satellite to locate its position with respect to the chief satellite. That means, at any observation time, two angles are measured. A series of azimuth angles (θ_i) and elevation angles (Φ_i) at times i = 1, 2, 3 … 13 are measured to locate the deputy satellite. The measurements θ_i is defined as the angle between the y-axis and the projection of line-of-sight vector onto the xy plane, and Φ_i is the angle between the y-axis and the projection of line-of-sight vector onto the yz plane. Notice that only six scalar measurements of angle should be sufficient to determine the six unknown components of initial relative position vector and velocity vector at initial time t_0, but here a total of twenty-six angular observations are required since all the bilinear, quadratic components of the initial relative position vector and velocity vector are treated as an independent elements, as will be seen.

A relation can be established between the relative equation of motions and measured angles. From trigonometric relation, it can be seen:

$$\frac{y(t_i)}{cos(\theta_i)} = \frac{x(t_i)}{sin(\theta_i)} \Rightarrow sin(\theta_i)\, y(t_i) - cos(\theta_i)\, x(t_i) = 0$$

$$\frac{y(t_i)}{cos(\Phi_i)} = \frac{z(t_i)}{sin(\Phi_i)} \Rightarrow sin(\Phi_i)\, y(t_i) - cos(\Phi_i)\, z(t_i) = 0 \qquad (15)$$

$$i = 1, 2, 3 \ldots 13$$

Substitute the nonlinear closed form second-order relative trajectory expression in Eq. (15).

$$F^i_{2x}x_0^2 + F^i_{2y}y_0^2 + F^i_{2z}z_0^2 + F^i_{2\dot{x}}\dot{x}_0^2 + F^i_{2\dot{y}}\dot{y}_0^2 + F^i_{2\dot{z}}\dot{z}_0^2 + F^i_{2xy}x_0y_0 +$$

$$F^i_{2\dot{x}\dot{y}}\dot{x}_0\dot{y}_0 + F^i_{2x\dot{x}}x_0\dot{x}_0 + F^i_{2x\dot{y}}x_0\dot{y}_0 + F^i_{2y\dot{x}}y_0\dot{x}_0 + F^i_{2y\dot{y}}y_0\dot{y}_0 + F^i_{2z\dot{z}}z_0\dot{z}_0 +$$

$$F^i_{1x}x_0 + F^i_{1y}y_0 + F^i_{1\dot{x}}\dot{x}_0 + F^i_{1\dot{y}}\dot{y}_0 = 0$$

$$G^i_{2x}x_0^2 + G^i_{2y}y_0^2 + G^i_{2z}z_0^2 + G^i_{2\dot{x}}\dot{x}_0^2 + G^i_{2\dot{y}}\dot{y}_0^2 + G^i_{2\dot{z}}\dot{z}_0^2 + G^i_{2xy}x_0y_0 + \quad (16)$$

$$G^i_{2xz}x_0z_0 + G^i_{2\dot{x}\dot{y}}\dot{x}_0\dot{y}_0 + G^i_{2\dot{x}\dot{z}}\dot{x}_0\dot{z}_0 + G^i_{2\dot{y}\dot{z}}\dot{y}_0\dot{z}_0 + G^i_{2x\dot{x}}x_0\dot{x}_0 + G^i_{2x\dot{y}}x_0\dot{y}_0 +$$

$$G^i_{2x\dot{z}}x_0\dot{z}_0 + G^i_{2y\dot{x}}y_0\dot{x}_0 + G^i_{2z\dot{x}}z_0\dot{x}_0 + G^i_{2z\dot{y}}z_0\dot{y}_0 + G^i_{2z\dot{z}}z_0\dot{z}_0 + G^i_{1x}x_0 +$$

$$G^i_{1y}y_0 + G^i_{1z}z_0 + G^i_{1\dot{x}}\dot{x}_0 + G^i_{1\dot{y}}\dot{y}_0 + G^i_{1\dot{z}}\dot{z}_0 = 0$$

$$i = 1, 2, 3 \ldots 13$$

$$F^i_{1x} = S_{\theta_i}\{6(\sin(n_0t_i) - n_0t_i)\} - C_{\theta_i}\{4 - 3\cos(n_0t_i)\}$$

$$F^i_{1y} = S_{\theta_i}\{1\}$$

$$F^i_{1\dot{x}} = S_{\theta_i}\{\frac{2}{n_0}(1 - \cos(n_0t_i))\} - C_{\theta_i}\{\frac{1}{n_0}(\sin(n_0t_i)\}$$

$$F^i_{1\dot{y}} = S_{\theta_i}\{\frac{1}{n_0}(4\sin(n_0t_i) - 3n_0t_i)\} - C_{\theta_i}\{\frac{2}{n_0}(1 - \cos(n_0t_i))\}$$

$$F^i_{2x} = S_{\theta_i}\{\frac{3}{4R_0}(40\sin(n_0t_i) + 3\sin(2n_0t_i) - 22n_0t_i - 24n_0t_i\cos(n_0t_i))\}$$

$$- C_{\theta_i}\{\frac{3}{2R_0}(7 - 10\cos(n_0t_i) + 3\cos(2n_0t_i) + 12n_0t_i\sin(n_0t_i)$$

$$- 12n_0^2t_i^2)\}$$

$$F^i_{2y} = S_{\theta_i}\{\frac{3}{R_0}(\sin(n_0t_i) - n_0t_i)\} - C_{\theta_i}\{\frac{3}{2R_0}(1 - \cos(n_0t_i))\}$$

$$F^i_{2z} = S_{\theta_i}\{\frac{1}{4R_0}(4\sin(n_0t_i) + \sin(2n_0t_i) - 6n_0t_i)\} - C_{\theta_i}\{\frac{1}{4R_0}(3 - 2\cos(n_0t_i)$$

$$- \cos(2n_0t_i))\}$$

$$F_{2\dot{x}}^{i} = S_{\theta_i}\{\frac{1}{4n_0^2R_0}(8\sin(n_0t_i) - \sin(2n_0t_i) - 6n_0t_i)\} - C_{\theta_i}\{\frac{1}{2n_0^2R_0}(-3 + 4\cos(n_0t_i) - \cos(2n_0t_i))\}$$

$$F_{2\dot{y}}^{i} = S_{\theta_i}\{\frac{1}{n_0^2R_0}(10\sin(n_0t_i) + \sin(2n_0t_i) - 6n_0t_i - 6n_0t_i\cos(n_0t_i))\} - C_{\theta_i}\{\frac{1}{2n_0^2R_0}(6 - 10\cos(n_0t_i) + 4\cos(2n_0t_i) + 12nt_i\sin(n_0t_i) - 9n_0^2t_i^2)\}$$

$$F_{2\dot{z}}^{i} = S_{\theta_i}\{\frac{1}{4n_0^2R_0}(8\sin(n_0t_i) - \sin(2n_0t_i) - 6n_0t_i)\} - C_{\theta_i}\{\frac{1}{4n_0^2R_0}(3 - 4\cos(n_0t_i) - \cos(2n_0t_i))\}$$

$$F_{2xy}^{i} = S_{\theta_i}\{\frac{3}{R_0}(1 - \cos(n_0t_i))\} - C_{\theta_i}\{\frac{6}{R_0}(-\sin(n_0t_i) + n_0t_i)\}$$

$$F_{2\dot{x}\dot{y}}^{i} = S_{\theta_i}\{\frac{1}{n_0^2R_0}(-3 + 2\cos(n_0t_i) + \cos(2n_0t_i) + 3n_0t_i\sin(n_0t_i))\} - C_{\theta_i}\{\frac{1}{n_0^2R_0}(7\sin(n_0t_i) - 2\sin(2n_0t_i) - 6n_0t_i + 3n_0t_i\cos(n_0t_i))\}$$

$$F_{2x\dot{x}}^{i} = S_{\theta_i}\{\frac{3}{2n_0R_0}(-5 + 4\cos(n_0t_i) + \cos(2n_0t_i) + 4n_0t_i\sin(n_0t_i))\} - C_{\theta_i}\{\frac{3}{n_0R_0}(4\sin(n_0t_i) - \sin(2n_0t_i) - 4n_0t_i + 2n_0t_i\cos(n_0t_i))\}$$

$$F_{2x\dot{y}}^{i} = S_{\theta_i}\{\frac{3}{n_0R_0}(12\sin(n_0t_i) + \sin(2n_0t_i) - 7n_0t_i - 7n_0t_i\cos(n_0t_i))\} - C_{\theta_i}\{\frac{3}{n_0R_0}(4 - 6\cos(n_0t_i) + 2\cos(2n_0t_i) + 7n_0t_i\sin(n_0t_i) - 6n_0^2t_i^2)\}$$

$$F_{2y\dot{x}}^{i} = S_{\theta_i}\{\frac{3}{n_0R_0}(-\sin(n_0t_i) + (n_0t_i))\}$$

$$F_{2y\dot{y}}^{i} = -C_{\theta_i}\{\frac{1}{3n_0R_0}(-\sin(n_0t_i) + n_0t_i)\}$$

$$F^{i}_{2z\dot{z}} = S_{\theta_i}\{\frac{1}{2n_0R_0}(-3 + 4\cos(n_0t_i) - \cos(2n_0t_i))\} - C_{\theta_i}\{\frac{1}{2n_0R_0}(2\sin(n_0t_i) - \sin(2n_0t_i))\}$$

$$G^{i}_{1x} = S_{\phi_i}\{6(\sin(n_0t_i) - n_0t_i)\}$$

$$G^{i}_{1\dot{x}} = C_{\phi_i}\{\frac{2}{n_0}(-1 + \cos(n_0t_i))\}$$

$$G^{i}_{1y} = S_{\phi_i}\{1\}$$

$$G^{i}_{1\dot{y}} = S_{\phi_i}\{\frac{1}{n_0}(4\sin(n_0t_i) - 3n_0t_i)\}$$

$$G^{i}_{1z} = -C_{\phi_i}\{\cos(n_0t_i)\}$$

$$G^{i}_{1\dot{z}} = -C_{\phi_i}\{\frac{1}{n_0}\sin(n_0t_i)\}$$

$$G^{i}_{2x} = S_{\phi_i}\{\frac{3}{4R_0}(40\sin(n_0t_i) + 3\sin(2n_0t_i) - 22n_0t_i - 24n_0t_i\cos(n_0t_i))$$

$$G^{i}_{2\dot{x}} = S_{\phi_i}\{\frac{1}{4n_0^2R_0}(8\sin(n_0t_i) - \sin(2n_0t_i) - 6n_0t_i)\}$$

$$G^{i}_{2y} = S_{\phi_i}\{\frac{3}{R_0}(\sin(n_0t_i) - n_0t_i)\}$$

$$G^{i}_{2\dot{y}} = S_{\phi_i}\{\frac{1}{n_0^2R_0}(10\sin(n_0t_i) + \sin(2n_0t_i) - 6n_0t_i - 6n_0t_i\cos(n_0t_i))\}$$

$$G^{i}_{2z} = S_{\phi_i}\{\frac{1}{4R_0}(4\sin(n_0t_i) + \sin(2n_0t_i) - 6n_0t_i)\}$$

$$G^{i}_{2\dot{z}} = S_{\phi_i}\{\frac{1}{4n_0^2R_0}(8\sin(n_0t_i) - \sin(2n_0t_i) - 6nt_i)\}$$

$$G^{i}_{2xy} = S_{\phi_i}\{\frac{3}{R_0}(1 - \cos(n_0t_i))\}$$

$$G^{i}_{2xz} = -C_{\phi_i}\{\frac{3}{2R_0}(-3 + 2\cos(n_0t_i) + \cos(2n_0t_i) + 4n_0t_i\sin(n_0t_i))\}$$

$$G^i_{2\dot{x}\dot{y}} = S_{\phi_i}\{\frac{1}{n_0^2 R_0}(-3 + 2\cos(n_0 t_i) + \cos(2n_0 t_i) + 3n_0 t_i \sin(n_0 t_i))\}$$

$$G^i_{2\dot{x}\dot{z}} = -C_{\phi_i}\{\frac{1}{2n_0^2 R_0}(3 - 4\cos(n_0 t_i) + \cos(2n_0 t_i))\}$$

$$G^i_{2\dot{y}\dot{z}} = -C_{\phi_i}\{\frac{1}{n_0^2 R_0}(\sin(n_0 t_i) + \sin(2n_0 t_i) - 3n_0 t_i \cos(n_0 t_i))\}$$

$$G^i_{2x\dot{x}} = S_{\phi_i}\{\frac{3}{2n_0 R_0}(-5 + 4\cos(n_0 t_i) + \cos(2n_0 t_i) + 4n_0 t_i \sin(n_0 t_i))\}$$

$$G^i_{2y\dot{x}} = S_{\phi_i}\{\frac{3}{n_0 R_0}(-\sin(n_0 t_i) + (n_0 t_i))\}$$

$$G^i_{2x\dot{y}} = S_{\phi_i}\{\frac{3}{n_0 R_0}(12\sin(n_0 t_i) + \sin(2n_0 t_i) - 7n_0 t_i - 7n_0 t_i \cos(n_0 t_i))\}$$

$$G^i_{2x\dot{z}} = -C_{\phi_i}\{\frac{3}{2n_0 R_0}(2\sin(n_0 t_i) + \sin(2n_0 t_i) - 4n_0 t_i \cos(n_0 t_i))\}$$

$$G^i_{2z\dot{x}} = -C_{\phi_i}\{\frac{3}{2n_0 R_0}(2\sin(n_0 t_i) - \sin(2n_0 t_i))\}$$

$$G^i_{2z\dot{y}} = -C_{\phi_i}\{\frac{1}{n_0 R_0}(-3 + 2\cos(n_0 t_i) + \cos(2n_0 t_i) + 3n_0 t_i \sin(n_0 t_i))\}$$

$$G^i_{2z\dot{z}} = S_{\phi_i}\{\frac{1}{2n_0 R_0}(-3 + 4\cos(n_0 t_i) - \cos(2n_0 t_i))\}$$

Here, S" = sin("), C" = cos("). The measurement equations can be expressed as Eq. (16) with the support from Eq. (17). Eq. (16) represents a set of nonlinear algebraic equations, more specifically, six coupled quadratic polynomial equations, for the six deputy initial positions and velocities. Coefficient $F_{np}{}^i$, $F_{npq}{}^i$, $G_{np}{}^i$, $G_{npq}{}^i$ appearing in these equations are known functions of the measurement angles, measurement times, and the chief orbital elements. In these coefficients, note $t = t_i - t_0$.

Since at each observation time i = 1, 2, 3 … 13, two angles are measured, it will constitute a total of twenty-six equations. These can be reformulated into a linear

homogenous matrix equation involving an unknown vector $\boldsymbol{\chi}_0$ which contains the linear, bilinear and quadratic terms of components of the initial relative positon vector and the velocity vector. These nonlinear terms are considered to be independent elements of vector $\boldsymbol{\chi}_0$.

$$\mathbf{A}\,\boldsymbol{\chi}_0 = \mathbf{0}$$

Where

$$\begin{aligned}
\boldsymbol{\chi}_0 &= [x_0\ \ y_0\ \ z_0\ \ \dot{x}_0\ \ \dot{y}_0\ \ \dot{z}_0\ \ x_0^2\ \ \ y_0^2\ \ \ z_0^2\ \ x_0y_0\ \ x_0z_0\ \ \dot{x}_0^2\ \ \dot{y}_0^2\ \ \dot{z}_0^2\ \ \dot{x}_0\dot{y}_0\ \ \dot{x}_0\dot{z}_0 \\
&\quad\ \dot{y}_0\dot{z}_0\ x_0\dot{x}_0\ \ x_0\dot{y}_0\ \ x_0\dot{z}_0\ \ y_0\dot{x}_0\ \ y_0\dot{y}_0\ \ z_0\dot{x}_0\ z_0\dot{y}_0\ \ z_0\dot{z}_0]^T \\
r_i &= [F^i_{1x}\ F^i_{1y}\ 0\ F^i_{1\dot{x}}\ F^i_{1\dot{y}}\ 0\ F^i_{2x}\ F^i_{2y}\ F^i_{2z}\ F^i_{2xy}\ 0\ F^i_{2\dot{x}}\ F^i_{2\dot{y}}\ F^i_{2\dot{z}}\ F^i_{2\dot{x}\dot{y}}\ 0\ 0 \\
&\quad\ F^i_{2x\dot{x}}\ F^i_{2x\dot{y}}\ 0\ F^i_{2y\dot{x}}\ F^i_{2y\dot{y}}\ 0\ 0\ F^i_{2z\dot{z}}] \\
r_{i+12} &= [G^i_{1x}\ G^i_{1y}\ G^i_{1z}\ G^i_{1\dot{x}}\ G^i_{1\dot{y}}\ G^i_{1\dot{z}}\ G^i_{2x}\ G^i_{2y}\ G^i_{2z}\ G^i_{2xy}\ G^i_{2xz}\ G^i_{2\dot{x}}\ G^i_{2\dot{y}}\ G^i_{2\dot{z}}\ G^i_{2\dot{x}\dot{y}} \\
&\quad\ G^i_{2\dot{x}\dot{z}}\ G^i_{2\dot{y}\dot{z}}\ G^i_{2x\dot{x}}\ G^i_{2x\dot{y}}\ G^i_{2x\dot{z}}\ G^i_{2y\dot{x}}\ 0\ G^i_{2z\dot{x}}\ G^i_{2z\dot{y}}\ G^i_{2z\dot{z}}] \\
&\quad\ i = 1,2,\ldots,12 \\
r_{25} &= [F^{13}_{1x} + G^{13}_{1x}\ \ F^{13}_{1y} + G^{13}_{1y}\ \ G^{13}_{1z}\ \ F^{13}_{1\dot{x}} + G^{13}_{1\dot{x}}\ \ F^{13}_{1\dot{y}} + G^{13}_{1\dot{y}}\ \ G^{13}_{1\dot{z}}\ \ F^{13}_{2x} + G^{13}_{2x} \\
&\quad\ F^{13}_{2y} + G^{13}_{2y}\ \ F^{13}_{2z} + G^{13}_{2z}\ \ F^{13}_{2xy} + G^{13}_{2xy}\ \ G^{13}_{2xz}\ \ F^{13}_{2\dot{x}} + G^{13}_{2\dot{x}}\ \ F^{13}_{2\dot{y}} + G^{13}_{2\dot{y}} \\
&\quad\ F^{13}_{2\dot{z}} + G^{13}_{2\dot{z}}\ \ F^{13}_{2\dot{x}\dot{y}} + G^{13}_{2\dot{x}\dot{y}}\ \ G^{13}_{2\dot{x}\dot{z}}\ \ G^{13}_{2\dot{y}\dot{z}}\ \ F^{13}_{2x\dot{x}} + G^{13}_{2x\dot{x}}\ \ F^{13}_{2x\dot{y}} + G^{13}_{2x\dot{y}} \\
&\quad\ G^{13}_{2\dot{x}\dot{z}}\ \ F^{13}_{2y\dot{x}} + G^{13}_{2y\dot{x}}\ F^{13}_{2y\dot{y}}\ \ G^{13}_{2z\dot{x}}\ \ G^{13}_{2z\dot{y}}\ \ F^{13}_{2z\dot{z}} + G^{13}_{2z\dot{z}}]
\end{aligned} \tag{18}$$

Reformulated relations are given in Eq. (18) where r_i denotes the i^{th} row of matrix **A**. Assuming all initial state combinations are independent, Eq. (18) represents a homogenous set of twenty-five equations in twenty five unknowns where square matrix **A** has dimension of 25×25. Since the angle measurements are in pairs, one excess measurement equation is available. Instead of discarding that measurement equation, note the last row in Eq. (18) consists of the sum of i = 13 azimuth and elevation measurement equations[8]. Since all

elements are considered to be independent, it is possible that the solution of the vector $\boldsymbol{\chi_0}$ may not satisfy the original nonlinear relations because connections between the last nineteen variables and the first six variables has been severed. So an additional nineteen constraint equations are needed to get the precise results.

A Non-trivial vector $\boldsymbol{\chi}_0$ which satisfies Eq. (18), or eigenvectors corresponding to zero eigenvalues of the matrix **A**, are sought. Based on physical arguments and assuming zero plant noise, at least one zero eigenvalue and associated eigenvector exist corresponding to the unknown initial conditions[8]. The eigen value-vector decomposition of matrix **A**, denoted by λ_i and $\boldsymbol{\phi}_i$ for i = 1, 2, 3 … 25 is calculated.

$$\mathbf{A}\,\boldsymbol{\phi}_i = \lambda_i\,\boldsymbol{\phi}_i \text{ where } |\lambda_1| \le |\lambda_2| \le \ldots \le |\lambda_{25}| \tag{19}$$

Discard Method for Calculating the Scalar Ambiguity

The null vector $\boldsymbol{\phi}_1$ will be the non-unique solution of unknown vector $\boldsymbol{\chi}_0$. To remove the ambiguity, an unknown scaling factor α must be included to scale the computed eigenvector. The uniform scaling of all vector components does not allow determination of α, since upon back substitution into any measurement equation, α will cancel from each term. Hence, a non-uniform scaling is essential. It is obtained by enforcing the neglected constraints from the original nonlinear formulation. To implement the constraints, the last nineteen quadratic and bilinear elements of the scaled null vector ($\alpha\boldsymbol{\phi}$) are discarded, and then reformed again using the retained first six linear elements of the scaled null vector.

The vector $\boldsymbol{\chi_0}$ is:

$$\begin{aligned}\boldsymbol{\chi}_0 = [&x_0\ y_0\ z_0\ \dot{x}_0\ \dot{y}_0\ \dot{z}_0\ x_0^2\ y_0^2\ z_0^2\ x_0y_0\ x_0z_0\ \dot{x}_0^2\ \dot{y}_0^2\ \dot{z}_0^2\ \dot{x}_0\dot{y}_0\ \dot{x}_0\dot{z}_0\\ &\dot{y}_0\dot{z}_0\ x_0\dot{x}_0\ x_0\dot{y}_0\ x_0\dot{z}_0\ y_0\dot{x}_0\ y_0\dot{y}_0\ z_0\dot{x}_0\ z_0\dot{y}_0\ z_0\dot{z}_0]^T\end{aligned} \tag{20}$$

Suppose eigenvector $\boldsymbol{\phi}_1$ is given as:

$$\boldsymbol{\phi}_1 = [\phi_{01} \quad \phi_{02} \quad \phi_{03} \quad \phi_{04} \quad \phi_{05} \quad \phi_{06} \quad \phi_{07} \quad \phi_{08} \quad \phi_{09} \quad \phi_{10} \quad \phi_{11} \quad \phi_{12} \quad \phi_{13} \quad \phi_{14} \quad \phi_{15} \quad \phi_{16} \quad \phi_{17} \quad \phi_{18} \quad \phi_{19} \quad \phi_{20} \quad \phi_{21} \quad \phi_{22} \quad \phi_{23} \quad \phi_{24} \quad \phi_{25}]^T \tag{22}$$

According to this method, last nineteen elements of constraints are discarded from the original null vector $\boldsymbol{\phi}_1$ and replaced by the combinations of scaled linear terms.

The last nineteen nonlinear terms are replaced with combinations of linear terms as shown below:

$$\begin{aligned}
&(\phi_{07}) = (\alpha\phi_{01})^2; \quad (\phi_{08}) = (\alpha\phi_{02})^2; \quad (\phi_{09}) = (\alpha\phi_{03})^2; \quad (\phi_{10}) = (\alpha\phi_{01})(\alpha\phi_{02}) \\
&(\phi_{11}) = (\alpha\phi_{01})\,(\alpha\phi_{03}); \quad (\phi_{12}) = (\alpha\phi_{04})^2; \quad (\phi_{13}) = (\alpha\phi_{05})^2; \quad (\phi_{14}) = (\alpha\phi_{06})^2; \\
&(\phi_{15}) = (\alpha\phi_{04})\,(\alpha\phi_{05}); \quad (\phi_{1\text{-}16}) = (\alpha\phi_{04})\,(\alpha\phi_{06}); \quad (\phi_{17}) = (\alpha\phi_{05})\,(\alpha\phi_{06}); \\
&(\phi_{18}) = (\alpha\phi_{01})\,(\alpha\phi_{04}); \quad (\phi_{19}) = (\alpha\phi_{01})\,(\alpha\phi_{05}); \quad (\phi_{20}) = (\alpha\phi_{01})\,(\alpha\phi_{06}); \\
&(\phi_{21}) = (\alpha\phi_{02})\,(\alpha\phi_{04}); \quad (\phi_{22}) = (\alpha\phi_{02})\,(\alpha\phi_{06}); \quad (\phi_{23}) = (\alpha\phi_{03})\,(\alpha\phi_{01}); \\
&(\phi_{24}) = (\alpha\phi_{03})\,(\alpha\phi_{02}); \quad (\phi_{25}) = (\alpha\phi_{03})\,(\alpha\phi_{06});
\end{aligned} \tag{22}$$

Hence, the transformed scaled null vector ($\alpha\boldsymbol{\phi}_1$) which satisfy the constraints is written as:

$$\begin{aligned}
&[\alpha\phi_{01} \quad \alpha\phi_{02} \quad \alpha\phi_{03} \quad \alpha\phi_{04} \quad \alpha\phi_{05} \quad \alpha\phi_{06} \quad (\alpha\phi_{01})^2 \quad (\alpha\phi_{02})^2 \quad (\alpha\phi_{03})^2 \quad (\alpha\phi_{01})(\alpha\phi_{02}) \\
&(\alpha\phi_{01})(\alpha\phi_{03}) \quad (\alpha\phi_{04})^2 \quad (\alpha\phi_{05})^2 \quad (\alpha\phi_{06})^2 \quad (\alpha\phi_{04})(\alpha\phi_{05}) \quad (\alpha\phi_{04})(\alpha\phi_{06}) \quad (\alpha\phi_{05})(\alpha\phi_{06}) \\
&(\alpha\phi_{01})(\alpha\phi_{04}) \quad (\alpha\phi_{01})(\alpha\phi_{05}) \quad (\alpha\phi_{01})(\alpha\phi_{06}) \quad (\alpha\phi_{02})(\alpha\phi_{04}) \quad (\alpha\phi_{02})(\alpha\phi_{06}) \quad (\alpha\phi_{03})(\alpha\phi_{01}) \\
&(\alpha\phi_{03})(\alpha\phi_{02}) \quad (\alpha\phi_{03})(\alpha\phi_{06})]
\end{aligned} \tag{23}$$

This new scaled null vector is substituted into the linear homogenous matrix equation to solve for the value of scalar ambiguity.

$$\begin{gathered}
A(i,1{:}6)\ \alpha\boldsymbol{\phi}_1(1{:}6) + A(i,7{:}25)\ \alpha^2\boldsymbol{\phi}_1(7{:}25) = 0 \\
i = 1, 2, 3 \ldots 25
\end{gathered} \tag{24}$$

In a case with no process noise, i.e. the measurements are generated using the second-order dynamics solution, and no measurement noise, each of the measurement equation yields an identical value of α, and the true initial conditions are recovered precisely. In a case with process noise and/or measurement noise, each of the measurement equation yields a different value of α. It is then suggested to compute the mean of these different values of α as the appropriate scale factor[8].

It has been shown that this method of determining the initial relative state vector of the deputy satellite with respect to the chief satellite is very effective in results[8]. The method is evaluated in presence of varying noise types, noise levels, and sample periods. In summary, the Cartesian-component formulation uses a total of thirteen observations, each observation includes measurement of two angles, so a total of twenty-six angle measurements which generate a square matrix of dimension 25 × 25. By comparison, the method proposed in the next chapter will need a total of eight unit-direction-vector observations, generating a square matrix of 21 × 21, therefore requiring fewer observations and lower computational expense.

CHAPTER 4

REDUNDANT-MEASUREMENT SOLUTION USING SEPARATION-MAGNITUDE FORMULATION

The main aim of the IROD problem is to determine the initial relative position vector and the velocity vector of the deputy satellite with respect to the chief satellite using unit-direction-vector observations. A camera on-board the chief satellite will observe the location of the deputy satellite relative to the chief. The initial time can arbitrarily be chosen as the time of the first observation. This observation means the initial direction of the deputy satellite with respect to the chief satellite is already known, and it is only the relative magnitude that needs to be computed for complete knowledge of relative position vector.

$$\mathbf{u}(t) = \mathbf{r}(t)/||r(t)| \tag{25}$$

The problem is reduced with the remaining unknowns being the relative magnitude of position vector and relative-velocity vector of the deputy satellite with respect to the chief satellite.

In general, the Cartesian-component formulation was a two-step method: first, to reformulate the second-order dynamics solution as a linear matrix homogenous equation with the total of 13 observations; second, calculation of scalar ambiguity to remove the unobservability problem using discard method. Similar to this, the Separation-Magnitude formulation is also a two-step method: first, use the second-order dynamics model of relative motion with the total of eight observation measurements to form a linear homogenous matrix equation; second, calculate the scalar ambiguity. A new, constraint-

enforcement method is also proposed for the scalar-ambiguity calculation, which as will be seen, proved ineffective in estimating the true initial conditions.

To begin with, the second-order dynamics model can be expressed in matrix notation as:

$$\begin{bmatrix} x_t \\ y_t \\ z_t \end{bmatrix} = \phi_{rr} \begin{bmatrix} x_0 \\ y_0 \\ z_0 \end{bmatrix} + \phi_{rv} \begin{bmatrix} \dot{x}_0 \\ \dot{y}_0 \\ \dot{z}_0 \end{bmatrix} + \phi_1 \begin{bmatrix} x_0 x_0 \\ y_0 y_0 \\ z_0 z_0 \end{bmatrix} + \phi_2 \begin{bmatrix} y_0 x_0 \\ y_0 y_0 \\ y_0 z_0 \end{bmatrix} + \phi_3 \begin{bmatrix} z_0 x_0 \\ z_0 y_0 \\ z_0 z_0 \end{bmatrix} + \phi_4 \begin{bmatrix} \dot{x}_0^2 \\ \dot{y}_0^2 \\ \dot{z}_0^2 \end{bmatrix} + \phi_5 \begin{bmatrix} x_0 \dot{x}_0 \\ x_0 \dot{y}_0 \\ x_0 \dot{z}_0 \end{bmatrix} + \phi_6 \begin{bmatrix} y_0 \dot{x}_0 \\ y_0 \dot{y}_0 \\ y_0 \dot{z}_0 \end{bmatrix} + \phi_7 \begin{bmatrix} z_0 \dot{x}_0 \\ z_0 \dot{y}_0 \\ z_0 \dot{z}_0 \end{bmatrix} + \phi_8 \begin{bmatrix} \dot{x}_0 \dot{y}_0 \\ \dot{y}_0 \dot{z}_0 \\ \dot{z}_0 \dot{x}_0 \end{bmatrix} \tag{26}$$

The following 3×3 matrices are functions of the known parameters, the chief's mean motion, n_0, and the distance of the chief satellite from the center of Earth, R_0. Both of these parameters are constant since the chief satellite is in a circular orbit.

$$\phi_{rr}(t) = \begin{bmatrix} 4 - 3\cos(n_0 t) & 0 & 0 \\ 6\{\sin(n_0 t) - n_0 t\} & 1 & 0 \\ 0 & 0 & \cos(n_0 t) \end{bmatrix}$$

$$\phi_{rv}(t) = \begin{bmatrix} \frac{1}{n_0}\sin(n_0 t) & \frac{2}{n_0}\{1 - \cos(n_0 t)\} & 0 \\ \frac{2}{n_0}\{-1 + \cos(n_0 t)\} & \frac{1}{n_0}\{4\sin(n_0 t) - 3n_0 t\} & 0 \\ 0 & 0 & \frac{1}{n_0}\sin(n_0 t) \end{bmatrix}$$

$$\phi_1(t)=\begin{bmatrix} \frac{3}{2R_0}\{7-10\cos(n_0t)+3\cos(2n_0t) & \frac{6}{2R_0}\{\sin(n_0t)+n_0t\} & 0 \\ +2n_0t+12n_0t\sin(n_0t)-12n_0^2t^2\} & & \\ \frac{3}{4R_0}\{40\sin(n_0t)+3\sin(2n_0t) & \frac{3}{R_0}\{1-\cos(n_0t)\} & 0 \\ -22n_0t-24n_0t\cos(n_0t)\} & & \\ 0 & 0 & \frac{3}{2R_0}\{-3+2\cos(2n_0t) \\ & & +\cos(2n_0t)+4n_0t\sin(n_0t)\} \end{bmatrix}$$

$$\phi_2(t)=\begin{bmatrix} 0 & \frac{3}{2R_0}\{1-\cos(n_0t)\} & 0 \\ 0 & \frac{3}{2R_0}\{\sin(n_0t)-n_0t\} & 0 \\ 0 & 0 & 0 \end{bmatrix}$$

$$\phi_3(t)=\begin{bmatrix} 0 & 0 & \frac{1}{4R_0}\{3-2\cos(2n_0t)-\cos(2n_0t)\} \\ 0 & 0 & \frac{1}{4R_0}\{4\sin(n_0t)+\sin(2n_0t)-6n_0t\} \\ 0 & 0 & 0 \end{bmatrix}$$

$$\phi_4(t)=\begin{bmatrix} \frac{1}{2n_0^2R_0}\{-3+4\cos(n_0t) & \frac{1}{2n_0^2R_0}\{6-10\cos(n_0t) & \frac{1}{4n_0^2R_0}\{3-4\cos(n_0t) \\ -\cos(2n_0t)\} & +4\cos(2n_0t)+12n_0t\sin(n_0t)-9n_0^2t^2\} & -\cos(2n_0t)\} \\ \frac{1}{4n_0^2R_0}(8\sin(n_0t)-\sin(2n_0t) & \frac{1}{n_0^2R_0}(10\sin(n_0t)+\sin(2n_0t) & \frac{1}{4n_0^2R_0}\{8\sin(n_0t) \\ -6n_0t) & -6n_0t-6n_0t\cos(n_0t) & -\sin(2n_0t)-6n_0t\} \\ 0 & 0 & 0 \end{bmatrix}$$

$$\phi_5(t)=\begin{bmatrix} \frac{3}{nR_0}\{4\sin(n_0t)-\sin(2n_0t) & \frac{3}{n_0R_0}\{4-6\cos(n_0t)+2\cos(2n_0t) & 0 \\ -4n_0t+2n_0t\cos(n_0t)\} & +7n_0t\sin(n_0t)-6n_0^2t^2\} & \\ \frac{3}{2n_0R_0}\{-5+4\cos(n_0t) & \frac{3}{n_0R_0}\{12\sin(n_0t)+\sin(2n_0t) & 0 \\ +\cos(2n_0t)+4n_0t\sin(n_0t)\} & -7n_0t-7n_0t\cos(n_0t)\} & \\ 0 & 0 & \frac{3}{2n_0R_0}\{2\sin(2n_0t) \\ & & +\sin(2n_0t)-4n_0t\cos(n_0t)\} \end{bmatrix}$$

$$\phi_6(t)=\begin{bmatrix} 0 & \frac{3}{n_0R_0}\{-\sin(n_0t)+n_0t\} & 0 \\ \frac{3}{n_0R_0}\{-\sin(n_0t)+n_0t\} & 0 & 0 \\ 0 & 0 & 0 \end{bmatrix}$$

$$\phi_7(t)=\begin{bmatrix} 0 & 0 & \frac{1}{2n_0R_0}\{2\sin(n_0t) \\ & & -\sin(2n_0t)\} \\ 0 & 0 & \frac{1}{2n_0R_0}\{-3+ \\ & & 4\cos(n_0t)-\cos(2n_0t)\} \\ \frac{1}{2n_0R_0}\{2\sin(n_0t)-\sin(2n_0t)\} & \frac{1}{n_0R_0}\{-3+2\cos(n_0t) & 0 \\ & +\cos(2n_0t)+3n_0t\sin(n_0t)\} & \end{bmatrix}$$

$$\phi_8(t) = \begin{bmatrix} \frac{1}{n_0^2 R_0}\{7\sin(n_0 t) - 2\sin(2n_0 t) & 0 & 0 \\ -6n_0 t + 3n_0 t\cos(n_0 t)\} & & \\ \frac{1}{n_0^2 R_0}\{-3 + 2\cos(n_0 t) & 0 & 0 \\ +\cos(2n_0 t) + 3n_0 t\sin(n_0 t)\} & & \\ 0 & \frac{1}{n_0^2 R_0}\{\sin(n_0 t) + \sin(2n_0 t) & \frac{1}{2n_0^2 R_0}\{-3 - 4\cos(n_0 t) \\ & -3n_0 t\cos(n_0 t)\} & +\cos(2n_0 t)\} \end{bmatrix}$$

Equation (26) can be further transformed using the fact that the directions of the relative position vector at the initial time and subsequent measurement times are known.

$$\begin{bmatrix} x_0 \\ y_0 \\ z_0 \end{bmatrix} = \begin{bmatrix} r_0 u_{01} \\ r_0 u_{02} \\ r_0 u_{03} \end{bmatrix} = r_0 \begin{bmatrix} u_{01} \\ u_{02} \\ u_{03} \end{bmatrix} = r_0 \hat{\mathbf{u}}_0$$
$$\begin{bmatrix} x \\ y \\ z \end{bmatrix} = r_t \hat{\mathbf{u}}_t \tag{27}$$

Where $\hat{\mathbf{u}}_0$ and $\hat{\mathbf{u}}_\mathbf{t}$ are the measured line-of-sight unit-direction-vectors. It is the magnitude of the relative position of the deputy satellite with respect to the chief satellite at initial time that needs to be computed. Substitute Eq. (27) into Eq. (26) and collect the terms, the Eq. (26) can now be arranged in the form shown below:

$$\begin{bmatrix} -\phi_{rr}\hat{\boldsymbol{u}}_0 & \hat{\boldsymbol{u}}_t & -\phi_{rv}\vec{\boldsymbol{v}}_0 & -\phi_1' & -\phi_4 & -\phi_2' & -\phi_8 \end{bmatrix} \begin{bmatrix} r_0 \\ r_t \\ \vec{\boldsymbol{v}}_0 \\ r_0^2 \\ \vec{\boldsymbol{A}} \\ \vec{\boldsymbol{B}} \\ \vec{\boldsymbol{C}} \end{bmatrix} = 0 \tag{28}$$

Where $\vec{\mathbf{A}} = \begin{bmatrix} \dot{x}_0^2 \\ \dot{y}_0^2 \\ \dot{z}_0^2 \end{bmatrix}$ $\vec{\mathbf{B}} = \begin{bmatrix} r_0\dot{x}_0 \\ r_0\dot{y}_0 \\ r_0\dot{z}_0 \end{bmatrix}$ $\vec{\mathbf{C}} = \begin{bmatrix} \dot{x}_0\dot{y}_0 \\ \dot{y}_0\dot{z}_0 \\ \dot{z}_0\dot{x}_0 \end{bmatrix}$, and ϕ_1', ϕ_2' are linear combinations of the previously introduced ϕ matrices and the measured initial unit-direction-vector.

$$\phi_1' = \phi_1 \begin{bmatrix} u_{01}u_{01} \\ u_{01}u_{02} \\ u_{01}u_{03} \end{bmatrix} + \phi_2 \begin{bmatrix} u_{02}u_{01} \\ u_{02}u_{02} \\ u_{02}u_{03} \end{bmatrix} + \phi_3 \begin{bmatrix} u_{03}u_{01} \\ u_{03}u_{02} \\ u_{03}u_{03} \end{bmatrix}$$

$$\phi_2' = \phi_5 u_{01} + \phi_6 u_{02} + \phi_7 u_{03}$$

With the help of six more unit-direction-vector measurements, Eq. (28) can be transformed into a linear homogenous matrix equation as shown:

$$\mathbf{Mx} = \mathbf{0}$$

$$\mathbf{M} = [\mathbf{M1} \quad \mathbf{M2}]$$

$$\mathbf{M1} = \begin{bmatrix} -\phi_{rr}(t_1)\hat{\mathbf{u}}_0 & \hat{\boldsymbol{u}}_1 & 0 & 0 & 0 & 0 & 0 & 0 & -\phi_{rv}(t_1)\vec{\mathbf{v}}_0 \\ -\phi_{rr}(t_2)\hat{\mathbf{u}}_0 & 0 & \hat{\boldsymbol{u}}_2 & 0 & 0 & 0 & 0 & 0 & -\phi_{rv}(t_2)\vec{\mathbf{v}}_0 \\ -\phi_{rr}(t_3)\hat{\mathbf{u}}_0 & 0 & 0 & \hat{\boldsymbol{u}}_3 & 0 & 0 & 0 & 0 & -\phi_{rv}(t_3)\vec{\mathbf{v}}_0 \\ -\phi_{rr}(t_4)\hat{\mathbf{u}}_0 & 0 & 0 & 0 & \hat{\boldsymbol{u}}_4 & 0 & 0 & 0 & -\phi_{rv}(t_4)\vec{\mathbf{v}}_\mathbf{0} \\ -\phi_{rr}(t_5)\hat{\mathbf{u}}_0 & 0 & 0 & 0 & 0 & \hat{\boldsymbol{u}}_5 & 0 & 0 & -\phi_{rv}(t_5)\vec{\mathbf{v}}_\mathbf{0} \\ -\phi_{rr}(t_6)\hat{\mathbf{u}}_0 & 0 & 0 & 0 & 0 & 0 & \hat{\boldsymbol{u}}_6 & 0 & -\phi_{rv}(t_6)\vec{\mathbf{v}}_\mathbf{0} \\ -\phi_{rr}(t_7)\hat{\mathbf{u}}_0 & 0 & 0 & 0 & 0 & 0 & 0 & \hat{\boldsymbol{u}}_7 & -\phi_{rv}(t_7)\vec{\mathbf{v}}_\mathbf{0} \end{bmatrix} \tag{29}$$

$$\mathbf{M2} = \begin{bmatrix} -\phi_1'(t_1) & -\phi_4(t_1) & -\phi_2'(t_1) & -\phi_8(t_1) \\ -\phi_1'(t_2) & -\phi_4(t_2) & -\phi_2'(t_2) & -\phi_8(t_2) \\ -\phi_1'(t_3) & -\phi_4(t_3) & -\phi_2'(t_3) & -\phi_8(t_3) \\ -\phi_1'(t_4) & -\phi_4(t_4) & -\phi_2'(t_4) & -\phi_8(t_4) \\ -\phi_1'(t_5) & -\phi_4(t_5) & -\phi_2'(t_5) & -\phi_8(t_5) \\ -\phi_1'(t_6) & -\phi_4(t_6) & -\phi_2'(t_6) & -\phi_8(t_6) \\ -\phi_1'(t_7) & -\phi_4(t_7) & -\phi_2'(t_7) & -\phi_8(t_7) \end{bmatrix}$$

$$\mathbf{x} = \begin{bmatrix} r_0 & r_1 & r_2 & r_3 & r_4 & r_5 & r_6 & r_7 & \vec{\mathbf{v}}_0^{\,\mathbf{T}} & r_0^2 & \vec{\mathbf{A}}^{\mathbf{T}} & \vec{\mathbf{B}}^{\mathbf{T}} & \vec{\mathbf{C}}^{\mathbf{T}} \end{bmatrix}^{\mathbf{T}}$$

The square matrix M has dimension of 21×21. It is a function of the ϕ matrices and measured unit-direction-vectors. The elements of unknown vector $\mathbf{x}$ includes the magnitude of the relative position of the deputy satellite with respect to the chief satellite along with

linear and quadratic combinations of the initial relative position magnitude and the relative velocity vector. These nonlinear terms are initially considered to be independent elements of the vector **x**. Later, these nonlinear terms will help in determining the scalar ambiguity and hence the initial state vector. The vector **x** has twenty-one unknowns of which the first eleven terms are linear and rest of the ten terms are quadratic and bilinear combinations of the first eleven terms.

A non-trivial vector which satisfies Eq. (29), or eigenvector corresponding to a zero eigenvalue of **M**, is calculated. As mentioned earlier, based on physical arguments and assuming zero plant noise, at least one zero eigenvalue and associated eigenvector exist corresponding to the unknown initial conditions. The eigen decomposition of matrix **M**, denoted by λ_i and μ_i for i = 1, 2, 3… 21, can be produced.

$$\mathbf{M}\ \boldsymbol{\mu}_i = \lambda_i\ \boldsymbol{\mu}_i \text{ where } |\lambda_1| \leq |\lambda_2| \leq \ldots \leq |\lambda_{21}| \tag{30}$$

Similar to the Cartesian-component formulation, the null-vector in Eq. (30) provides a magnitude-ambiguous solution for vector **μ.** A second step must be performed to solve for the magnitude.

Constraint-Enforcement method for calculating scalar ambiguity

An alternative to the discard method is proposed here to calculate the scalar ambiguity. The previously mentioned method discards the non-linear terms, hence losing the information stored in those non-linear terms. The alternative concept is motivated by the idea that if optimal use of the measurements had been made, then it would not be possible to extract additional information by discarding the non-linear terms and back substituting them while reforming with linear terms. Instead, the solution for the eigenvector has extracted information from the measurements while neglecting the relations between linear and quadratic components of the unknown vector. A solution for α can now be extracted by

simply enforcing these relations without making further use of the measurements. The constraint-enforcement method calculates the least square best fit solution of the constraint equations applied to both the linear and non-linear terms in the unknown vector **x**.

To obtain the unique solution for vector **x**, an unknown scaling factor α is used to scale the computed eigenvector, $\boldsymbol{\mu}_1$, corresponding to the zero eigenvalue, λ_1 to generate a corrected initial vector **x**.

$$\mathbf{x} = \alpha\boldsymbol{\mu}_1$$

The extended **x** vector is given as:

$$\mathbf{x} = [r_0 \quad r_1 \quad r_2 \quad r_3 \quad r_4 \quad r_5 \quad r_6 \quad r_7 \quad \dot{x}_0 \quad \dot{y}_0 \quad \dot{z}_0 \quad r_0^2 \quad \dot{x}_0^2 \quad \dot{y}_0^2 \quad \dot{z}_0^2 \quad r_0\dot{x}_0 \quad r_0\dot{y}_0 \quad r_0\dot{z}_0 \quad \dot{x}_0\dot{y}_0 \quad \dot{y}_0\dot{z}_0 \quad \dot{z}_0\dot{x}_0]^T \tag{31}$$

Based on this definition, the components of the solution of $\alpha\boldsymbol{\mu}_1$ must satisfy the following constraints (with the trivial solution $\alpha = 0$ discarded).

$$\begin{aligned} &\mu_{12} = \alpha\mu_{01}^2; \quad \mu_{13} = \alpha\mu_{09}^2; \quad \mu_{14} = \alpha\mu_{10}^2; \quad \mu_{15} = \alpha\mu_{11}^2; \\ &\mu_{16} = \alpha\mu_{01}\,\mu_{09}; \quad \mu_{17} = \alpha\mu_{01}\,\mu_{10}; \quad \mu_{18} = \alpha\mu_{01}\,\mu_{11}; \quad \mu_{19} = \alpha\mu_{09}\,\mu_{10}; \\ &\mu_{20} = \alpha\mu_{10}\,\mu_{11}; \quad \mu_{21} = \alpha\mu_{09}\,\mu_{11} \end{aligned} \tag{32}$$

All ten constraint equations can be written in vector form as

$$\mathbf{c}\alpha = \mathbf{d} \tag{33}$$

Where, $\mathbf{c} = [\mu_{01}^2 \quad \mu_{09}^2 \quad \mu_{110}^2 \quad \mu_{11}^2 \quad \mu_{01}\mu_{09} \quad \mu_{01}\mu_{10} \quad \mu_{01}\mu_{11} \quad \mu_{09}\mu_{10} \quad \mu_{10}\mu_{11} \quad \mu_{09}\,\mu_{11}]^T$ and $\mathbf{d} = [\mu_{12} \quad \mu_{13} \quad \mu_{14} \quad \mu_{15} \quad \mu_{16} \quad \mu_{17} \quad \mu_{18} \quad \mu_{19} \quad \mu_{20} \quad \mu_{21}]^T$. The least square solution for the scaling factor α can be found as

$$\alpha = (\mathbf{c}^T\,\mathbf{c})^{-1}\,\mathbf{c}^T\,\mathbf{d} \tag{34}$$

However, as will be seen, this method proves to be ineffective.

Numerical Example

The effectiveness of this method is checked under a test run. A two-dimensional relative motion resulting from coplanar orbits is considered. Initial state conditions are estimated with noise included in the system. The linear equation **Mx** = **0** contains an 18 × 18 square matrix **M** for the two-dimensional case.

$$\mathbf{x} = [r_0 \quad r_1 \quad r_2 \quad r_3 \quad r_4 \quad r_5 \quad r_6 \quad r_7 \quad r_8 \quad r_9 \quad \dot{x}_0 \quad \dot{y}_0 \quad r_0^2 \quad \dot{x}_0^2 \quad \dot{y}_0^2 \quad r_0\dot{x}_0 \quad r_0\dot{y}_0 \quad \dot{x}_0\dot{y}_0]^T$$

The matrix **M** of size 18 × 18 can be formulated using the steps shown in the separation-magnitude formulation. For the three dimensional case, eight observations of line-of-sight unit vectors were required; however for the two dimensional case, ten measurements of line-of-sight unit vectors are required to estimate the initial conditions.

Two types of noises are used to test the method: process noise and measurement noise. Process noise means estimating the initial state vectors with second-order dynamics but measurements are generated using a higher-fidelity model. Here, the measurements are generated with the full non-linear relative equation of motion. Since, for testing purposes, the true initial conditions are known, they are used to generate the measurements. While keeping the same time interval between each measurement, the true initial state vector is propagated forward in time using the full non-linear relative dynamics, and the obtained position vector at each measurement time is normalized to get a unit direction vector. Here, a constant time interval between each measurement time is used; however, variable time intervals between each measurement can also be used. Zero mean, Gaussian measurement noise with standard deviation of 10^{-6} rad is also added. It is added to the azimuth and elevation angle obtained from the true unit-direction-vector measurement and the corrupted

measurement vector is reformed again from these noise added angles. Hence, the noisy observation vector is reamins a unit vector. An example is given considering the coplanar orbits of the chief and deputy satellite. Measurements are sampled at equal time interval of 1000 s, with $\mu = 398600.436\ km^3/s^2$. In these equations, the subscript '0' denotes the value of a quantity at the initial time (t_0).

Table 1. Solved Initial Conditions

	Plant Noise	Plant Plus Measurement Noise
x_0 (km)	-3.14034924011524	-3.39075176606197
y_0 (km)	0.157017462005762	0.169536504747181
$\dot{x}_0$ (km/s)	5.50685419032298	5.94591466667296
$\dot{y}_0$ (km/s)	0.314543307572514	0.339620117749289

Chief: Deputy:

$R_0 = 7100$ km, $i_0 = 70$ deg $x_0 = -0.02$ km, $\dot{x}_0 = 0.035$ km/s

$\Omega_0 = 45$ deg, $\theta_0 = 0$ deg $y_0 = 0.001$ km, $\dot{y}_0 = 0.002$ km/s (35)

The constraint-enforcement method computes the correct estimate of the initial conditions under ideal situation where second-order dynamics is used to generate error-free measurements. But, from Table 1, it is evident that this method fails when noises are present. This failure can be understood from more detailed investigation of the intermediate solution steps, described in the following paragraphs.

Since in simuation, the initial conditions are known, the unknown vector **x** is formed by true initial conditions (say, $\mathbf{X}_0$) and is compared with the scaled null vector. If the value obtained for ambiguity α is correct, then the scaled null vector should be similar to the unknown vector formed by true initial condition ($\mathbf{X}_0$). The original null vector obtained for above mentioned example with plant and measurement noise is:

$\boldsymbol{\mu}_1$ = [-5.6508×10^{-5} -1.2746×10^{-1} -3.1432×10^{-1} -4.2789×10^{-1} -3.7162×10^{-1} -2.0695×10^{-1}
-1.0314×10^{-1} -2.2265×10^{-1} -4.2134×10^{-1} -5.3215×10^{-1} -9.8966×10^{-5} -5.653×10^{-6}
-2.5480×10^{-3} -3.4885×10^{-6} -5.2385×10^{-8} -1.8924×10^{-5} -1.2201×10^{-5} -2.3758×10^{-7}]^{T}

The least square solution obtained for scalar factor using constraint-enforcement method is α = -60080.1999. So the scaled null vector will be given by:

$\alpha\boldsymbol{\mu}_1$= [3.3950 7.6576×10^{3} 1.8884×10^{4} 2.5707×10^{4} 2.2327×10^{4} 1.2434×10^{4}
6.1972×10^{3} 1.3377×10^{4} 2.5314×10^{4} 3.1972×10^{4} 5.9459 3.3962×10^{-1}
1.5308×10^{2} 2.0959×10^{-1} 3.1472×10^{-3} 1.1370 7.3305×10^{-1} 1.4274×10^{-2}]^{T}

However, the true solution vector is:

$\mathbf{X}_0$ = [2.0025×10^{-2} 4.5076×10^{1} 1.1116×10^{2} 1.5133×10^{2} 1.3143×10^{2} 7.3190×10^{1}
3.6470×10^{1} 7.8732×10^{1} 1.4900×10^{2} 1.8819×10^{2} 3.5000×10^{-2} 2.0000×10^{-3}
4.0100×10^{-4} 1.225×10^{-3} 4.0000×10^{-6} 7.0087×10^{-4} 4.0050×10^{-5} 7.0000×10^{-5}]^{T}

As it can be seen, the scaled null vector and the true vector have very different values.

Further, different values of scalar ambiguities are calculated from the constraint relations, i.e. Eq. (32), and is compared with the value of scalar ambiguity obtained from least square technique, i.e. Eq. (34). Following are the values of scalar ambiguity obtained from solving individual constraint relations given in Eq. (32):

[-7.9796×10^{5} -3.5618×10^{2} -1.6394×10^{3} -1.2713 -9.8520×10^{-1} -1.0953×10^{-2}]

And as mentioned earlier, the value of the scalar ambiguity from the least square technique is -60080.1999. As it can be seen, there is wide variation in the values of scalar ambiguity, so there is not a single solution that provides a good satisfaction of all the constraint relations.

Another point that can provide the reason for the failure of constraint-enforcement method for calculating the correct value of scalar ambiguity is to check if the given value of scalar ambiguity is able to satisfy the constraint relations in Eq. (32). As per the constraints relations in Eq. (32), the thirteenth element of the scaled null vector should be equal to the square of the first element.

$(\alpha\boldsymbol{\mu}_1)_1 = 3.3950$

$\Rightarrow \quad (\alpha\boldsymbol{\mu}_1)_1^2 = 11.5260$

$(\alpha\boldsymbol{\mu}_1)_{13} = 153.0822$

$\Rightarrow \quad (\alpha\boldsymbol{\mu}_1)_{13} \neq (\alpha\boldsymbol{\mu}_1)_1^2$

However, they are not. Similar is the case with the rest of constraints equations, i.e. the constraint-enforcement method was not able to estimate the correct value of scalar ambiguity.

Further investigation shows that the null vector obtained for the linear homogenous matrix **M** is a non-physical model. The normalized true vector is given by:

$$\frac{\mathbf{X}_0}{||\mathbf{X}_0||} = [5.6624\times10^{-5} \;\; 1.2746\times10^{-1} \;\; 3.1434\times10^{-1} \;\; 4.2790\times10^{-1} \;\; 3.7163\times10^{-1} \;\; 2.0696\times10^{-1}$$

$$1.0312\times10^{-1} \;\; 2.2263\times10^{-1} \;\; 4.2134\times10^{-1} \;\; 5.3215\times10^{-1} \;\; 9.8969\times10^{-5} \;\; 5.6554\times10^{-6}$$

$$1.1339\times10^{-6} \;\; 3.44639\times10^{-6} \;\; 1.1311\times10^{-8} \;\; 1.9819\times10^{-6} \;\; 1.1325\times10^{-7} \;\; 1.9794\times10^{-7}]^T$$

This vector's linear terms are almost similar to the null vector's ($\boldsymbol{\mu}_1$) linear term, but the quadratic terms are very different. Also, the true vector formed by true values provides a satisfactory result of the measurement equations, $||\mathbf{M}\mathbf{X}_0|| = 1.997\times10^{-4}$, but the null vector provides an even better result of the measurement equations, $||\mathbf{M}\boldsymbol{\mu}_1|| = 1.6510\times10^{-5}$. The null vector is able to achieve this improved satisfaction by taking advantage of the non-physical

degrees of freedom in the quadratic components of the unknown vector. But this results in a non-physical solution.

Hence, to implement the constraint relations the discard method will be a good choice for calculating the scalar ambiguity, where the null-vector is forced to maintain the physical model by initially discarding the bilinear and quadratic combinations and then forming them again using scaled initial vector, Eq. (22). Constraint-enforcement method works only in ideal conditions when there is no noise, but for practical purposes, when noises are there, constraint-enforcement method will fail.

Applying Discard method to Separation-Magnitude Formulation

From the previous discussion, the eigenvector obtained from the linear homogenous matrix equation was a non-physical solution and the constraint-enforcement method failed in estimating an accurate scalar ambiguity. Hence, to force the physical solution on the eigenvector, the discard method is used with separation-magnitude formulation. The measurement equations are set up by the separation-magnitude method and the discard method is used for calculating the scalar ambiguity α.

As discussed earlier, according to the discard method, all the elements of the unknown vector (**x**) are considered to be independent. It has both linear terms and non-linear terms. The non-linear terms helps in calculating the scalar ambiguity. The extended **x** vector is:

$$\mathbf{x} = [\mathrm{r}_0 \quad \mathrm{r}_1 \quad \mathrm{r}_2 \quad \mathrm{r}_3 \quad \mathrm{r}_4 \quad \mathrm{r}_5 \quad \mathrm{r}_6 \quad \mathrm{r}_7 \quad \dot{\mathrm{x}}_0 \quad \dot{\mathrm{y}}_0 \quad \dot{\mathrm{z}}_0 \quad \mathrm{r}_0^2 \quad \dot{\mathrm{x}}_0^2 \quad \dot{\mathrm{y}}_0^2 \quad \dot{\mathrm{z}}_0^2 \quad \mathrm{r}_0\dot{\mathrm{x}}_0 \quad \mathrm{r}_0\dot{\mathrm{y}}_0 \quad \mathrm{r}_0\dot{\mathrm{z}}_0 \quad \dot{\mathrm{x}}_0\dot{\mathrm{y}}_0 \quad \dot{\mathrm{y}}_0\dot{\mathrm{z}}_0 \quad \dot{\mathrm{z}}_0\dot{\mathrm{x}}_0]^{\mathrm{T}}$$

Suppose eigenvector $\boldsymbol{\mu}_1$ corresponding to matrix **M** is given as:

$[\mu_{01}\ \ \mu_{02}\ \ \mu_{03}\ \ \mu_{04}\ \ \mu_{05}\ \ \mu_{06}\ \ \mu_{07}\ \ \mu_{08}\ \ \mu_{09}\ \ \mu_{10}\ \ \mu_{11}\ \ \mu_{12}\ \ \mu_{13}\ \ \mu_{14}\ \ \mu_{15}\ \ \mu_{16}\ \ \mu_{17}\ \ \mu_{18}\ \mu_{19}\ \ \mu_{20}\ \ \mu_{21}]^T$

Since $\boldsymbol{\mu}_1$ is a non-unique vector, a scalar factor is calculated to obtain a unique scaled null-vector. The constraint relations which were severed earlier will be used to calculate a unique scaled null-vector ($\alpha\boldsymbol{\mu}_1$). First, the last ten non-linear elements of scaled null-vector are discarded, and then reformed again by linear and bilinear combinations of the first eleven linear terms using the method described in the chapter of Cartesian-component formulation. The reformed bilinear and quadratic components can be written as:

$$\mu_{12} = \alpha^2\mu_{01}^2;\quad \mu_{13} = \alpha^2\mu_{09}^2;\quad \mu_{14} = \alpha^2\mu_{10}^2;\quad \mu_{15} = \alpha^2\mu_{11}^2;\quad \mu_{16} = \alpha^2\mu_{01}\,\mu_{09}$$
$$\mu_{17} = \alpha^2\mu_{01}\,\mu_{10};\ \ \mu_{18} = \alpha^2\mu_{01}\,\mu_{11};\ \ \mu_{19} = \alpha^2\mu_{09}\,\mu_{10};\ \ \mu_{20} = \alpha^2\mu_{10}\,\mu_{11};\ \ \mu_{21} = \alpha^2\mu_{09}\,\mu_{11} \tag{3}$$

Hence, the reformed null-vector will be given as:

$$[\alpha\mu_{01}\ \ \alpha\mu_{02}\ \ \alpha\mu_{03}\ \ \alpha\mu_{04}\ \ \alpha\mu_{05}\ \ \alpha\mu_{06}\ \ \alpha\mu_{07}\ \ \alpha\mu_{08}\ \ \alpha\mu_{09}\ \ \alpha\mu_{10}\ \ \alpha\mu_{11}\ \ (\alpha\mu_{01})^2\ \ (\alpha\mu_{09})^2$$
$$(\alpha\mu_{10})^2\ (\alpha\mu_{11})^2\ \ (\alpha\mu_{01})(\alpha\mu_{09})\ \ (\alpha\mu_{01})(\alpha\mu_{10})\ \ (\alpha\mu_{01})(\alpha\mu_{11})\ \ (\alpha\mu_{09})(\alpha\mu_{10})\ \ (\alpha\mu_{10})(\alpha\mu_{11}) \tag{37}$$
$$(\alpha\mu_{09})(\alpha\mu_{11})]^T$$

The transformed null-vector is now substituted back into the linear homogenous matrix equation, Eq. (29), and solved for the values of scalar ambiguity, similar to Eq. (24), while discarding the trivial solution. If there is no noise in the system, the obtained values of α is similar but on adding noise, the variation in different values of α will increase. In that case, the mean value of all different values of α will be used as the scaling factor. This method proves to be effective as it will be shown via numerical example.

Performance Analysis

Several numerical examples are considered to test the IROD performance and to estimate the initial state vector. One considered performance metric is to simply compare the known initial state test values with the computed initial states. The quantity used to

evaluate the performance is root-mean-square (RMS) of the angle residual. Angle residual is the difference of the computed line-of-sight angle obtained from the propagation of computed initial states to the measurement time using the second-order dynamics solution and the true measurement angle obtained from the propagation of true initial states with the full non-linear equations. A root-mean-square value of the angle residual that is close to zero indicates that the predicted angles are close to the originally collected measurement angles. The largest and worst possible RMS error value is equal to π radians away from its corresponding true line-of-sight measurement. This RMS error metric is valuable because in a real-world application of this problem, the true initial states would be unknown and therefore not available to compare against the calculated initial states.

Another way to evaluate the performance of this method is to calculate the range ratio RMS. It is calculated by taking the root-mean-square of the ratio of the chief-deputy separation distance predicted by the propagation of the computed initial conditions with the second-order dynamics solution over the true separation distance obtained from the full nonlinear equations at all measurement times. A value near one indicates the predicted ranges are close to the true ranges. Range ratio RMS helps in establishing the validity of the application of the initial relative orbit determination method during numerical simulation. In a real-world application, the collected observations are angles-only measurements and the range data is unknown. Thus, the predicted range values have no basis for comparison in a real-time in-flight situation using angles-only observations.

Several factors including noise type and level, sample rate, and deputy drift rate are varied to explore certain aspects of the IROD performance. Two types of noise are used to test this IROD technique: process noise and process plus the measurement noise. As

mentioned earlier, the term process noise refers to generating the measurements with a higher fidelity model than the model on which the estimation solution is based, i.e. the second-order model. Measurement noise level is considered across the range 10^{-8} to 10^{-3} radians. Measurement sample rate is varied across a wide range of cases from 150 seconds to 10000 seconds to show dependency on temporal distribution of the measurements.

Estimating initial conditions with process noise and measurement noise

The IROD solution reformulated using the separation-magnitude formulation and the discard method is tested and validated here. A two-dimensional coplanar orbit is considered again. For the nonlinear simulation, the true measurements are generated by choosing a set of initial conditions and propagating them forward using two-body dynamics and a fourth order Runge-Kutta numerical integrator with time step equal to one second. Both process noise and process plus measurement noise cases are considered. Process noise is introduced by using the second-order dynamics solution to estimate the initial conditions. In the case with measurement corruption, Gaussian noise with a standard deviation of $\sigma = 10^{-6}$ rad is added to each measurement. For simplicity, measurements are taken at equal time steps. It is not necessary that measurements always be taken at equal time increments, but the time at which a measurement is taken must be recorded. Measurements for this case are sampled at equal time step increments of 1000 s. The initial conditions for this case are given below, in terms of circular chief orbit elements and the deputy's relative states with $\mu = 398600.436\ km^3/s^2$.

Chief:	Deputy:	
$R_0 = 7100$ km, $i_0 = 70$ deg	$x_0 = -0.02$ km,	$\dot{x}_0 = 0.035$ km/s
$\Omega_0 = 45$ deg, $\theta_0 = 0$ deg	$y_0 = 0.001$ km,	$\dot{y}_0 = 0.002$ km/s

Table 2 shows the calculated initial conditions with both noise included in the system. It can be seen that the computed initial state vector are close to the true initial conditions.

Table 2. Estimated Initial Conditions

	Process noise	Process plus Measurement Noise
x_0 (km)	-0.0201	-0.0201
y_0 (km)	0.0010	0.0010
$\dot{x}_0$ (km/s)	0.0352	0.0353
$\dot{y}_0$ (km/s)	0.0020	0.0020

Table 3 shows the RMS error of the angle residual and of range ratio with both types of noise. As mentioned earlier, RMS error of angle residual will help in determining how close the computed solution is in comparison with the true solution.

Table 3. RMS Error of Angle Residual & of Range Ratio

	Process Noise	Process plus Measurement Noise
RMS Angle	6.370559479397730e-04	6.373936322672941e-04
RMS Range	1.007713574870067	1.007677503474768

The range ratio RMS, close to one, indicates that the predicted separation distance between the chief and deputy satellite is very close to the true separation distance at each measurement time. This helps in confirming that predicted flight path is in proximity to the true flight path rather than the IROD method simply generating predicted line-of-sight angles close to the true line-of-sight angles at the appropriate measurement times.

Figure 6 shows the trajectory of relative motion between the chief and deputy satellite till the last measurement time (i.e. 9000 s) when the system has both process plus measurement noise. The trajectory generated using the true state vector with the full

nonlinear equation is labelled as “True IC/Nonlinear”. The trajectory generated using the computed state vector with the second-order dynamics is labeled as “Computed IC/2nd Order”. And, the line-of-sight direction vectors are labelled as “LOS direction. It is clear from the figure and the table that the separation-magnitude method is performing well under these conditions.

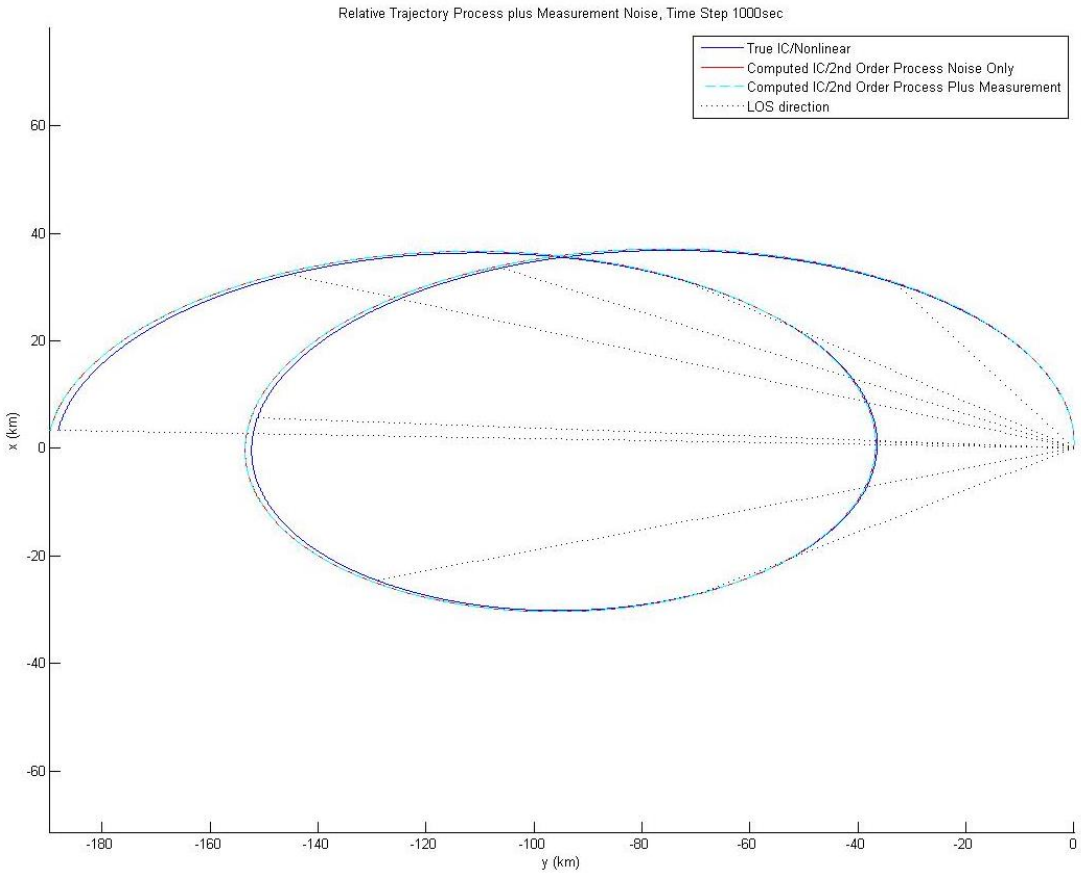

Figure 6. Relative Orbit with Process plus Measurement Noise, Time Step of 1000 s

Effect of varying the measurement noise on estimation of initial conditions

In order to determine how the separation-magnitude formulation will work with the varying noise level, the same initial conditions are run with six different levels of measurement noise added to the process noise. The initial conditions are held constant at each run and the standard deviation of Gaussian noise is changed. From Table 4, it can be seen, the largest level of the measurement noise ($\sigma = 10^{-3}$ rad) produces the highest error as expected, hence it hinders the ability of the IROD method. So it is desirable that the camera should take high precision measurements to reduce the corruption of measurements.

Table 4. Estimated Initial Conditions with Process Noise & Varying Level of Measurement Noise

	$\sigma = 10^{-8}$ rad	$\sigma = 10^{-7}$ rad	$\sigma = 10^{-6}$ rad	$\sigma = 10^{-5}$ rad	$\sigma = 10^{-4}$ rad	$\sigma = 10^{-3}$ rad
x_0 (km)	-0.020113	-0.020113	-0.020112	-0.020122	-0.019764	-0.014171
y_0 (km)	0.0010056	0.0010056	0.0010056	0.0010064	0.0009868	0.0007114
$\dot{x}_0$ (km/s)	0.0352701	0.0352697	0.0352689	0.0353201	0.0351291	0.0384805
$\dot{y}_0$ (km/s)	0.0020145	0.0020145	0.0020145	0.0020178	0.0020041	0.0022004

Table 5 shown below represents the RMS error associated with range ratio and angle residual when system has process noise and varying level of measurement noise. It can be seen from the table that as the standard deviation of measurement noise increases from 10^{-8} rad to 10^{-3} rad, the error also keeps on increasing as expected.

Table 5. RMS with Process Noise & Varying Level of Measurement Noise

	$\sigma = 10^{-8}$ rad	$\sigma = 10^{-7}$ rad	$\sigma = 10^{-6}$ rad	$\sigma = 10^{-5}$ rad	$\sigma = 10^{-4}$ rad	$\sigma = 10^{-3}$ rad
Angle	6.3707e-04	6.3687e-04	6.3802e-04	6.4248e-04	4.1686e-03	9.9039e-03
Range	1.0077e+00	1.0077e+00	1.0076e+00	1.0074e+00	1.0433e+00	8.4809e-01

Figure 7 shows the relative trajectory of the deputy satellite with respect to the chief satellite for the period of 9000 s when the system has process plus measurement noise. The trajectory generated using the true state vector with the full nonlinear equation is labelled as “True IC/Nonlinear”. The trajectory generated using the computed state vector with the second-order dynamics is labeled as “Computed IC/2nd Order”. And, the line-of-sight direction vectors are labelled as “LOS direction”. In Figure 7 the estimated relative trajectory generated with the process plus measurement noise having 10^{-3} rad of standard deviation is compared with the estimated relative trajectory generated with the process plus measurement noise having 10^{-8} rad of standard deviation in the system and also with the true relative trajectory. It is clear from the figure and the tables that the separation-magnitude method is performing well when the measurements are less corrupted.

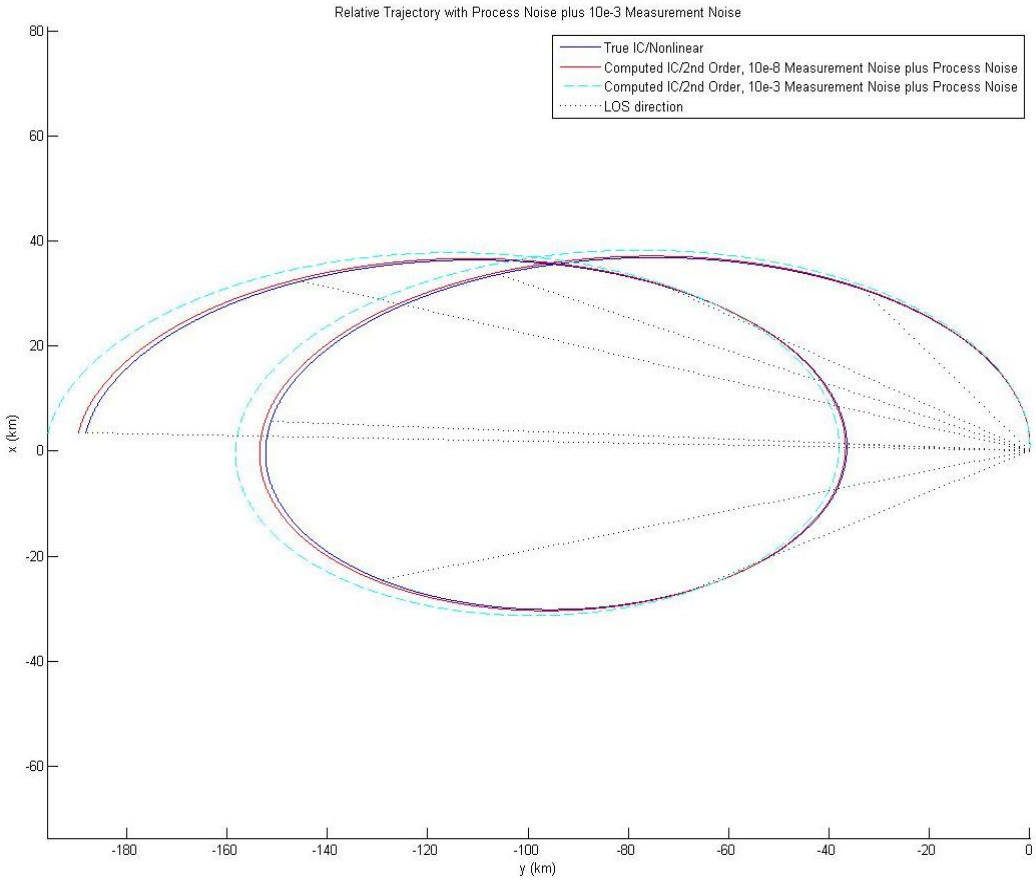

Figure 7. Relative Orbit with Process plus Measurement Noise

(10^{-8} rad and 10^{-3} rad)

Time Step of 1000 s

Effect of varying sample time period on estimation of initial conditions

To present the potential of this method with varying sample time period, the same initial conditions are run with five different sample time periods. Each run is made with the process noise plus Gaussian measurement noise with a standard deviation of $\sigma = 10^{-6}$ rad. The initial state vector is estimated using the time interval of 2000 s, 3000 s, 4000 s and 5000 s.

Tables 6 and 7 show the estimated initial conditions and the RMS associated with angle residual and range ratio estimation for different sample time period respectively. It can be noticed from both the tables that with the time period of 1000 s and 2000 s the results are accurate. RMS value associated with angle residual is almost zero and the range ratio RMS value is almost equal to one. But with the time period of 3000 s, estimated results are especially poor in comparison to any other sample time period. RMS error in angle residual and range ratio is very high, i.e. 177 and 4.5 respectively. The time period of chief satellite is approximately 5954 s, which means the measurements are taken approximately at the starting point and at the halfway point of the orbit. This sequence leads to a loss of observability since every other line-of-sight is pointing in approximately the same direction[6]. The sampling period of 4000 s also encounters the same problem, but to a lesser extent, because the sample period is almost two-thirds of the chief orbital period. Although the estimation of the relative position vector is very poor as the sample time period is increased, the estimated velocity vector is still accurate except for the sample time period of 3000 s. Therefore, the performance of the IROD method can be sensitive to a uniform sample rate and thus should be given careful consideration.

Table 6. Estimated Initial Conditions with Varying Time Interval

	t = 1000 s	t = 2000 s	t = 3000 s	t = 4000 s	t = 5000 s
x_0 (km)	-2.0112e-02	-1.9486e-02	7.7161e-02	-1.4286e-02	-5.4654e-02
y_0 (km)	1.0056e-03	9.7425e-04	-3.8582e-03	7.1428e-04	2.7327e-03
$\dot{x}_0$ (km/s)	3.5268e-02	3.4619e-02	-1.3501e-01	3.1563e-02	3.5711e-02
$\dot{y}_0$ (km/s)	2.0145e-03	1.9858e-03	-1.1083e-02	1.8190e-03	2.1169e-03

Table 7. RMS with Varying Sample Time Period

	t = 1000 s	t = 2000 s	t = 3000 s	t = 4000 s	t = 5000 s
Angle	6.3761e-04	7.3165e-04	1.7727e+02	1.7339e-03	1.8527e-03
Range	1.0077e+00	9.9108e-01	4.4547e+00	9.0698e-01	1.0224e+00

Figures 8 - 12 show the trajectory of the relative motion between the deputy satellite and the chief satellite for the sample time period of 1000 s, 2000 s, 3000 s, 4000 s, and 5000 s. The trajectory generated using the true state vector with the full nonlinear equation is labelled as “True IC/Nonlinear”. The trajectory generated using the computed state vector with the second-order dynamics is labeled as “Computed IC/2nd Order”. And, the line-of-sight direction vectors are labelled as “LOS direction”. As expected after observing the above tables, the relative trajectory propagated with the estimated initial state vector using the second-order dynamics is following the true relative trajectory for the sample time period of 1000 s and 2000 s. As the sample time period is increased, the computed relative trajectory is going way off in comparison with the true relative trajectory. For the sample period of 3000 s, the computed relative trajectory plot is completely opposite in direction to

the true relative trajectory. Hence, it is required that special attention should be given to the sample period.

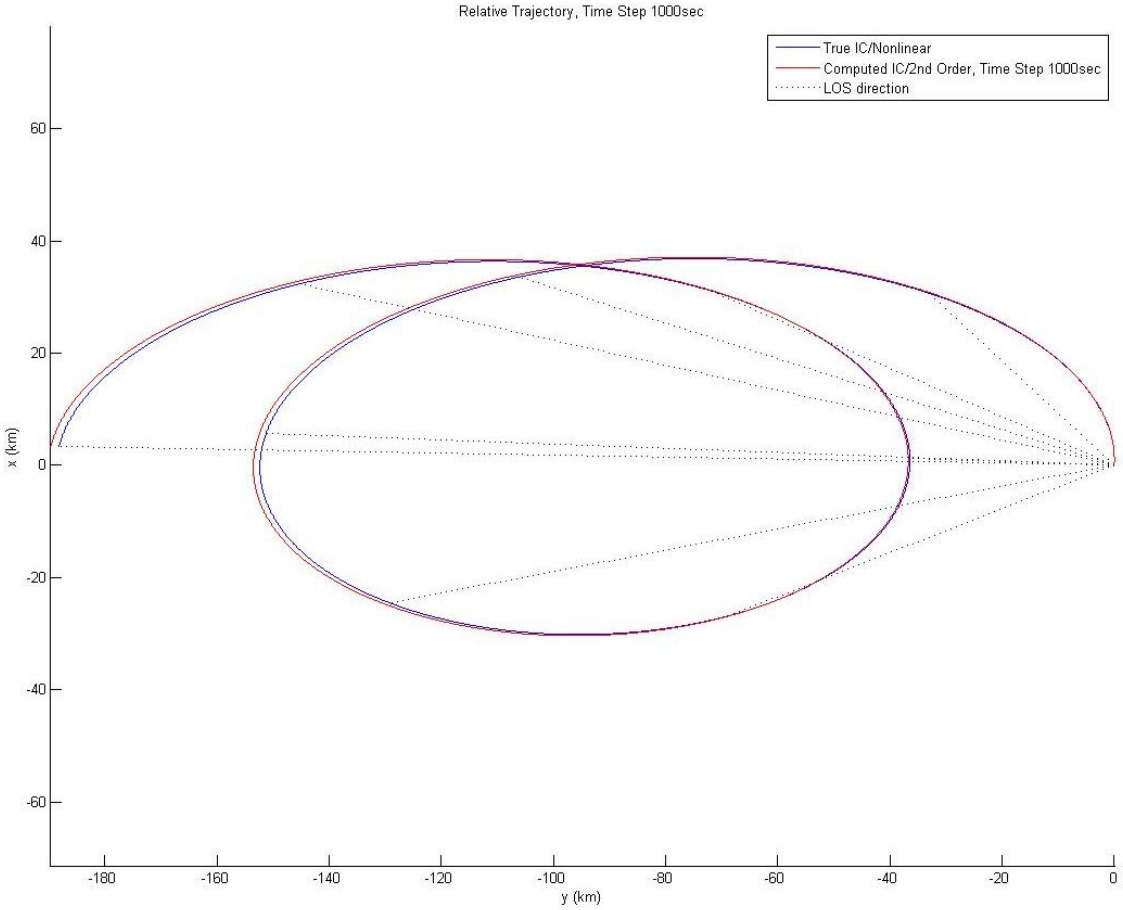

Figure 8. Relative Orbit with Process plus Measurement Noise, Time Step of 1000 s

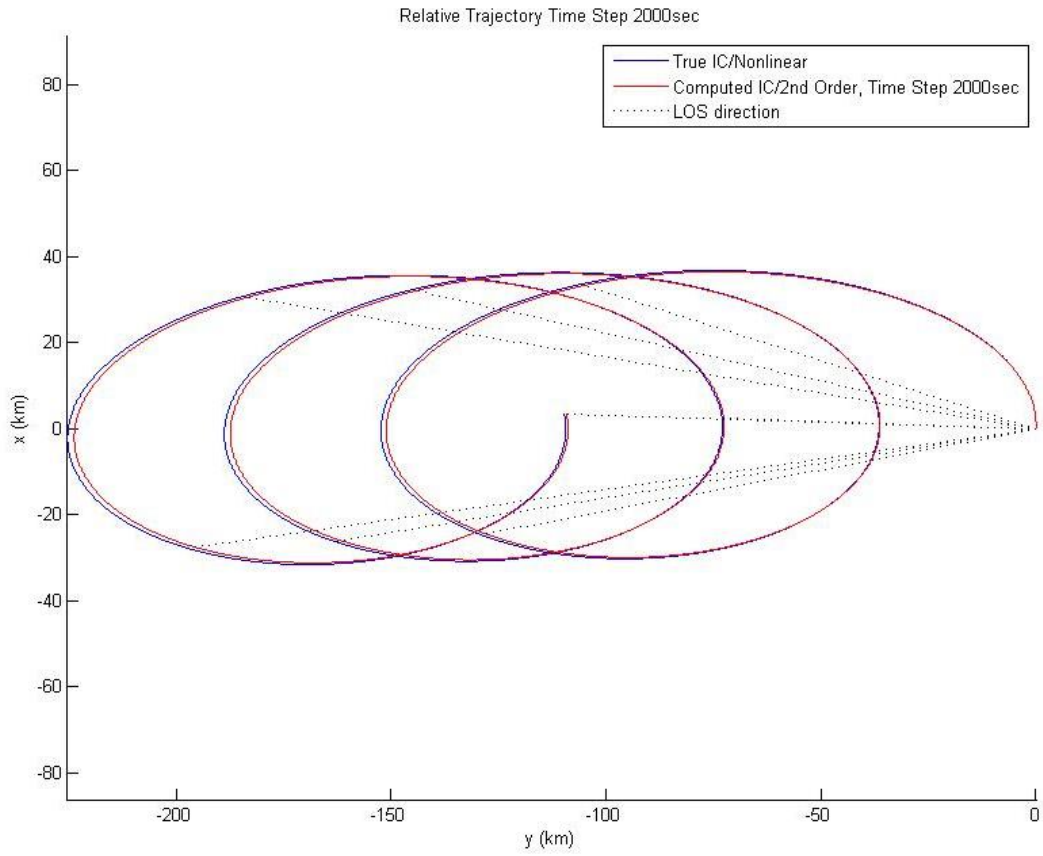

Figure 9. Relative Orbit with Process plus Measurement Noise, Time Step of 2000 s

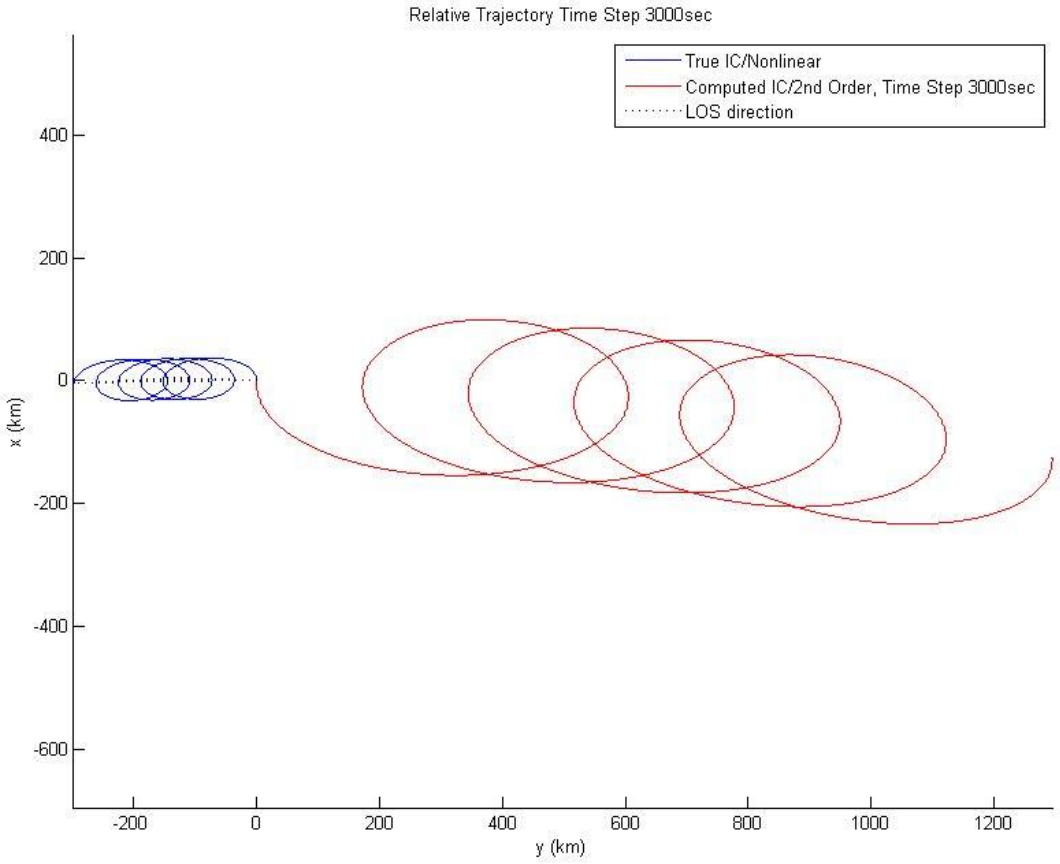

Figure 10. Relative Orbit with Process plus Measurement Noise, Time Step of 3000 s

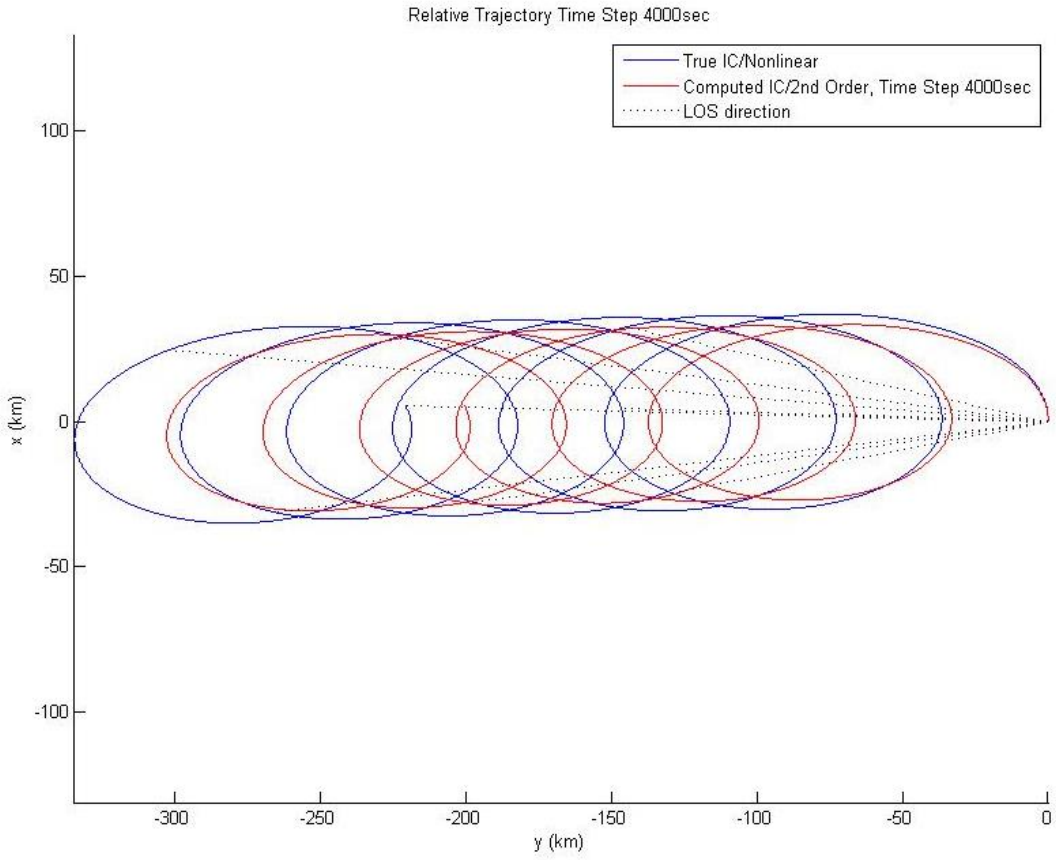

Figure 11. Relative Orbit with Process plus Measurement Noise, Time Step of 4000 s

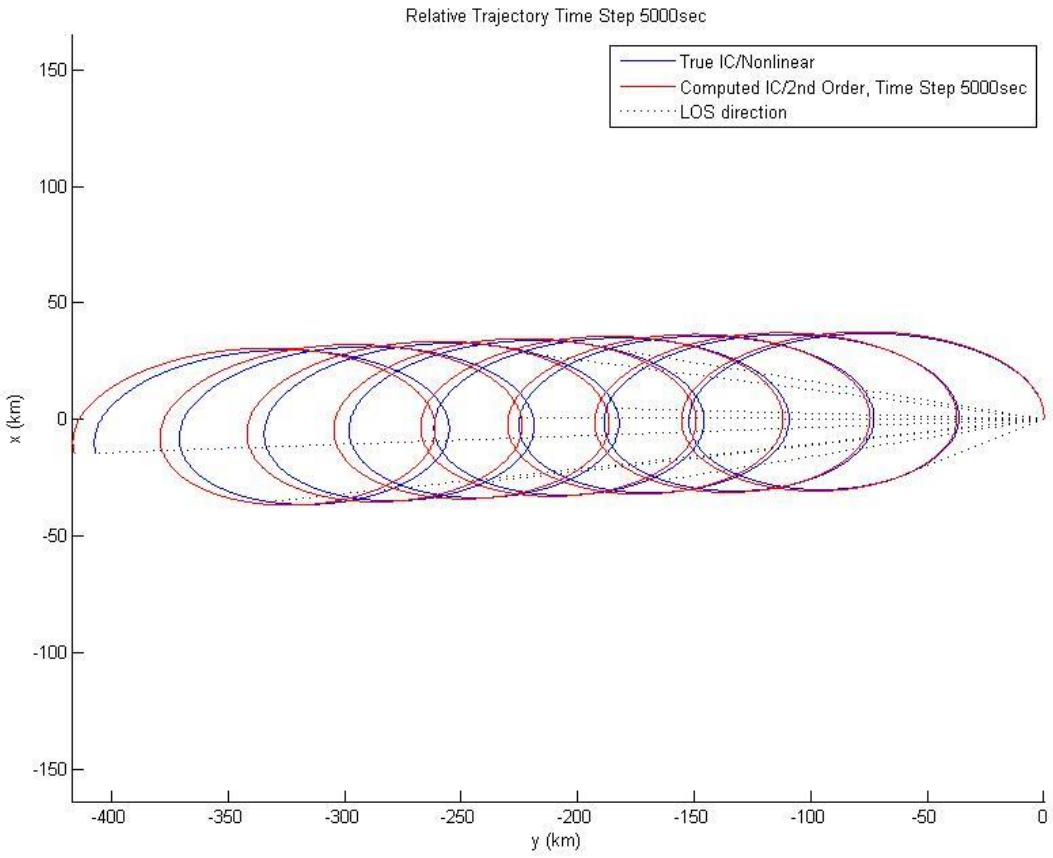

Figure 12. Relative Orbit with Process plus Measurement Noise, Time Step of 5000 s

Zero-Drift Orbit

The performance of this method is further tested using non-drifting orbits. The given data, with a sample period of 1000 s, is used to estimate the initial conditions with process noise and measurement noise included in the system. The measurement noise is Gaussian with 10^{-6} rad of standard deviation.

Chief:	Deputy
R_0 = 7100 km, i_0 = 70 deg	x_0 = -0.7100000000000364 km, $\dot{x}_0$ = 0.00001 km/s
Ω_0 = 45 deg, θ_0 = 0 deg	y_0 = 0.000001 km, $\dot{y}_0$ = 0.00149858136153523 km/s

The IROD method is still able to recover the true initial conditions with minimal error. Table 8 shows the solved initial conditions with both categories of noise. The capability of this method to find the proper scaling of the null-vector despite the trajectory having practically zero drift is quite significant.

Table 8. Estimated Initial Conditions for Non-drifting Orbit

	Process noise	Process plus Measurement noise
x_0 (km)	-7.1047e-01	-6.8358e-01
y_0 (km)	1.0007e-06	1.8567e-06
$\dot{x}_0$ (km/s)	1.0007e-05	9.6274e-06
$\dot{y}_0$ (km/s)	1.4996e-03	1.4428e-03

The calculated RMS angle residual for both types of noise are given in Table 9. It can be seen, the RMS angle residual is close to zero and RMS range ratio is close to one.

Table 9. RMS for Non-drifting orbit

	Process Noise	Process plus Measurement Noise
RMS Angle	9.8815e-06	3.2818e-04
RMS Range	1.0007e+00	9.6279e-01

Figure 13 shows the relative trajectory plot with the process plus measurement noise respectively. The trajectory generated using the true state vector with the full nonlinear equation is labelled as "True IC/Nonlinear". The trajectory generated using the computed state vector with the second-order dynamics is labeled as "Computed IC/2nd Order". And, the line-of-sight direction vectors are labelled as "LOS direction".

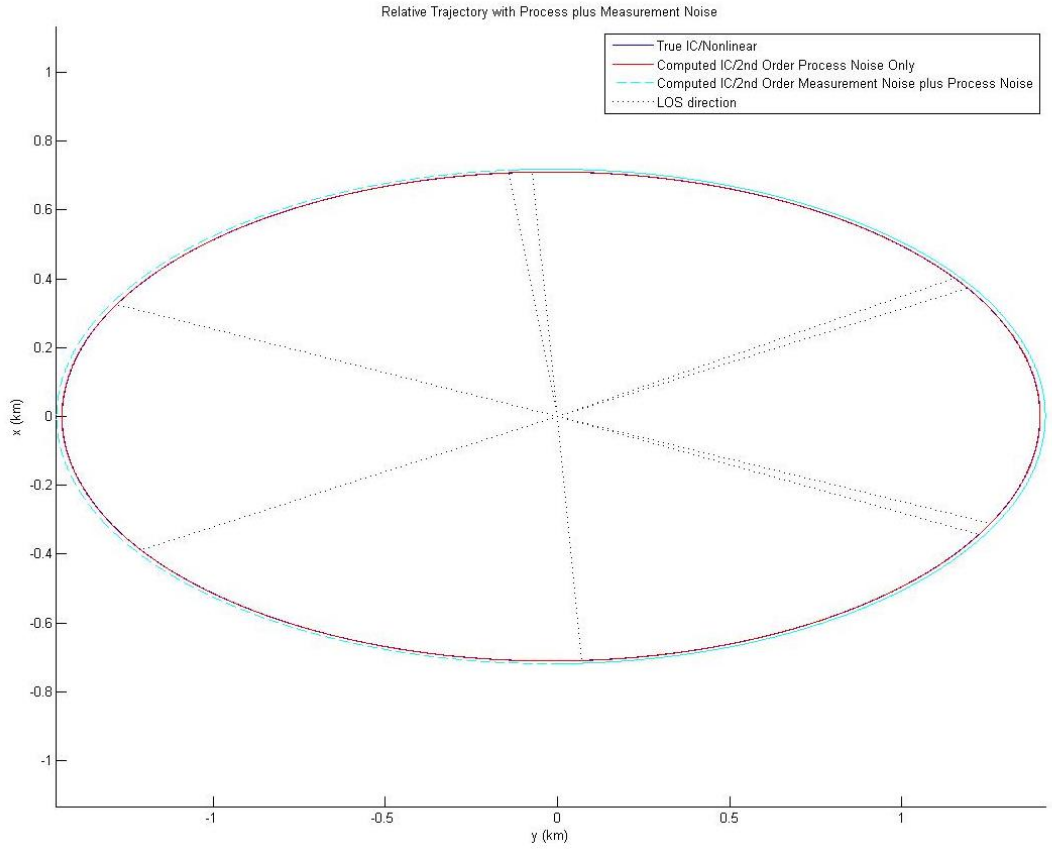

Figure 13. Relative Trajectory of Non-drifting Orbit with Process plus 10^{-6} rad of Measurement Noise

Limitations of the IROD Method

A few factors can limit the success of the IROD method. Poor measurements will adversely affect the result of this method. Obviously extremely noisy measurements will result in the IROD method failing to properly recover the true initial orbit. Also, the measurements must be chosen wisely over time. Measurements that are too close together may result in failure to recover the initial orbit. Taking measurements of the same, or close to the same, line-of-sight angles over multiple orbits will also give poor results. However, the situations can be easily avoided by proper scheduling of observations. For best results, the measurements taken should be a good sampling of the orbit geometry in order to get a good idea of the shape of the orbit.

Fast Sample Rate

In order to show the effect of fast sample rate, the same model parameters are run with sample period of 150 s. The only difference is, the earlier sample time period was 1000 s, but in this case, the sample time period is changed to 150 s. Both process noise and the standard measurement noise of 10^{-6} rad is added to the system.

In Figure 6, the relative orbit and line-of-sight representations were plotted for the sample rate of 1000 s. Similarly, the orbit and line-of-sight measurements for sample period of 150 s are plotted in Figure 14. The longer time step from the original run allows for a good sampling of the entire orbit and its drift behavior. However, Figure 14 shows that the short time step creates measurements which are closely packed and only captures slightly over a quarter of the orbit. Such a small sample does not give much information on the shape and drift behavior of the relative orbit trajectory.

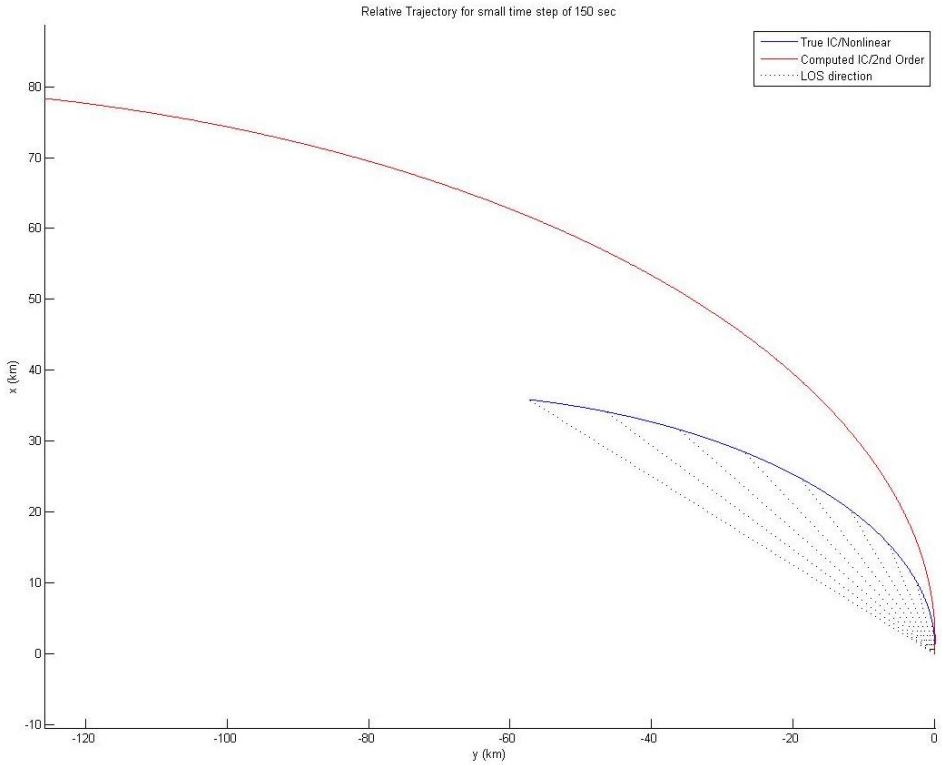

Figure 14. Relative Trajectory of Orbit with Sample Time Period of 150 s

Table 10 gives the estimate of the initial conditions for the small sample rate of 150 s for both types of noise with $\sigma = 10^{-6}$ rad. It is very clear from the table that the IROD method fails in this particular case with poorly chosen measurement time. The solved initial conditions differ from the true initial conditions by several order of magnitude.

Table 10. Estimated Initial Conditions with Time Step of 150 s

	Process noise	Process plus Measurement noise
x_0 (km)	-0.0439612644183993	-0.0440818789050685
y_0 (km)	0.0021980632209199	0.00220401290206098
$\dot{x}_0$ (km/s)	0.0769428592997356	0.0771512998865675
$\dot{y}_0$ (km/s)	0.00439673900811533	0.00440850954455815

Table 11 shows the RMS associated with angle residual and range ratio. Examining this table for fast sample rate confirms the conclusion. The magnitude of RMS range ratio is greater than one, indicating that the estimated relative trajectory is vastly different from the true relative trajectory.

Table 11. RMS for Fast Sample Rate

	Process Noise	Process plus Measurement Noise
RMS Angle	2.0557e-02	2.0706e-02
RMS Range	2.1976e+00	2.2073e+00

Slow Sample Rate

Large separations between the chief and deputy satellites, large time periods between the measurements, and very large drift rates can also prevent the success of the IROD method. The second-order solution is based on the assumption that the deputy is relatively "close" to the chief. The validity of the second-order solution extends to further separation distances than the Clohessy-Wiltshire solution, but it still has its limits. Inside the second-order solution, there are several secular terms, including some terms in which time is squared. Thus, for very large time periods, the secular terms can dominate the solution and cause it to diverge from the true solution. Since the IROD method is fundamentally based on the second-order solution, it ceases to be valid where the second-order solution is no longer suitable.

If the original system model is run again with a sample rate of 10000 s, the results are poor. Table 12 shows the estimated results for the large sample time of 10000 s. Table 13 is of RMS associated with angle residual and range ratio and further provides evidence in the fact that large sample rate hinders the ability of IROD method.

Table 12. Estimated Initial Conditions with Large Time Step of 10000 s

	Process noise	Process plus Measurement noise
x_0 (km)	0.0333123690422163	0.0334686113025062
y_0 (km)	-0.001665618452110	-0.001673506354602
$\dot{x}_0$ (km/s)	0.0253396821873571	0.0254287103035307
$\dot{y}_0$ (km/s)	0.0013989003488525	0.0014034037316567

Table 13. RMS for Large Sample rate

	Process Noise	Process plus Measurement Noise
RMS Angle	3.4130e-03	2.0706e-02
RMS Range	7.3775e-01	2.2073e+00

Figure 15 shows the relative trajectory of the motion of the deputy satellite with respect to the chief satellite. The conclusion made above matches the plot obtained for relative motion. Figure 15 shows the relative trajectory when the system has both process plus measurement noise. The trajectory generated using the true state vector with the full nonlinear equation is labelled as “True IC/Nonlinear”. The trajectory generated using the computed state vector with the second-order dynamics is labeled as “Computed IC/2nd Order”, and the line-of-sight direction vectors are labelled as “LOS direction”.

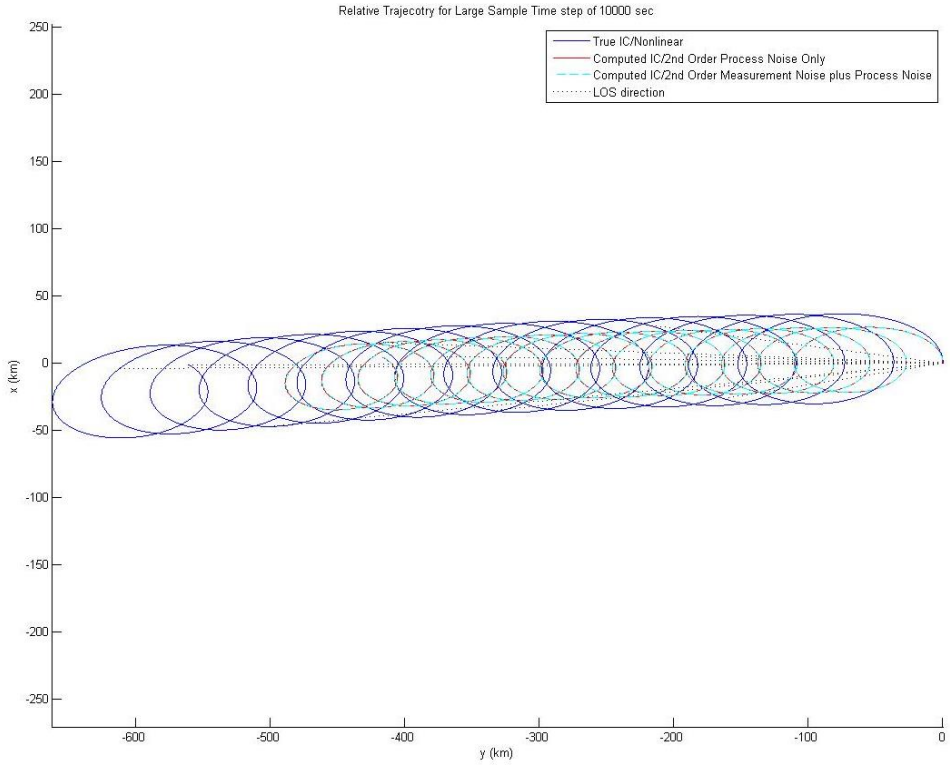

Figure 15. Relative Orbit with Sample Time Period of 10000 s, Process plus Measurement Noise

CHAPTER 5

MACAULAY RESULTANT METHOD

The problem of initial relative-orbit determination requires estimation of three components of the relative position vector and three components of the relative velocity vector between the chief and deputy satellite. So there are a total of six unknowns that satisfy six coupled second-degree polynomial equations. In earlier discussed methods, the polynomial nature of the measurement equations was not exploited. The nonlinear combinations of the initial states were considered to be independent which increased the number of unknowns from six to twenty-five in the Cartesian-component formulation and up to twenty-one in the separation-magnitude formulation. In this method, the multivariate polynomial system of equations are solved using Macaulay resultant. Resultant theory appears to be a less familiar subject in engineering disciplines, when compared to linear algebra[13]. In this theory, the system of multivariate polynomial equations is projected to a single univariate polynomial equation, the resultant polynomial equation; and using a matrix polynomial structure, this equation can be solved by computing a generalized eigen decomposition. Because the resultant polynomial is zero if and only if the polynomial system has a common root, this procedure is often interpreted as a means to finding the intersection of algebraic curves.

Resultant Polynomial Formulation

Consider a set of m coupled or multivariate polynomial equations in n variables given in Eq. (38). Polynomial $p_j(x_i)$ for j = 1,2 … m and i = 1,2 … n has degree d_j, i.e., the monomial appearing in $p_j(x_i)$ with the largest exponent sum equals d_j. Coefficient c_k^j denotes a constant multiplier for monomial k appearing in the j^{th} equation.

$$\begin{aligned} p_1(x_1, x_2 \ldots x_n) &= 0 \\ p_2(x_1, x_2 \ldots x_n) &= 0 \\ &\ldots \\ p_m(x_1, x_2, \ldots x_n) &= 0 \end{aligned} \tag{38}$$

When m > n, one should expect no solutions are possible except in special cases. On the other hand when m < n, an infinite number of non-unique solutions exist. The case where m = n occurs most often when the equation set represents an applied system, such as in relative initial-orbit determination problem. Reference 11 gives a summary of the various resultant polynomial forms that can be used in the cases m > n, m < n, and m = n. When m = n, one should expect a finite number of unique solutions. When the number of equations and variables is equal (m = n), and when the equation set is homogenous, the Macaulay resultant polynomial is a popular technique. Polynomial equations are considered homogenous in each equation, when all the terms have the same degree. If this is not the case, it can be homogenized by a simple process of introducing an extra variable. To homogenize Eq. (38), replace every variable x_i by x_i/x_h and clear all denominators in all equations, where x_h denotes the new homogenizing unknown variable[11]. After this process, every monomial in the j^{th} equation will have degree equal to d_j.

For a homogenous m = n equation set, the Macaulay resultant polynomial R is expressed as[12,13,14]

$$R = \frac{\det \mathbf{N}}{\det \mathbf{D}} \tag{39}$$

Where R is of scalar dimension, **N** has dimension $n_N \times n_N$, and **D** has dimension $n_D \times n_D$. Although dimension n_D is not easily expressed by a simple formula, dimension n_N is given generally by the relation

$$n_N = (n-1+d)!/(n-1)!d! \tag{40}$$

Where parameter d, sometimes called the system degree, is defined as

$$d = 1 + \sum_{j=1}^{m} (d_j - 1) \tag{41}$$

Square matrices **N** and **D** are constructed from the polynomial coefficients, and either a set of unspecified coefficients c_{xi} originating from an appended equation, which can be required to recover an equal number of equations and variables, or one of the unknown variables x_{i*} (i.e., x_i with $i = i^*$) chosen to be solved for first. Rows of the **N** matrix represents elementary members and, through the determinant combinations, resultant R is a special kind of member of modular system. The basic tenet of resultant theory is that R = 0, or equivalently **N** is rank deficient, if and only if the equation set has a finite solution, assuming matrix **D** is full rank. If matrix **D** is rank deficient, then matrix **N** (and **D**) must be modified by a reduction process. If R = 0, null space vector $\boldsymbol{\chi}_i$ are computed from

$$\mathbf{N}\,\boldsymbol{\chi}_i = 0 \text{ for } i = 1, 2 \ldots q \tag{42}$$

Where q denotes the rank deficiency of **N**. Elements of the vector $\boldsymbol{\chi}_i$ are proportional to monomial functions of the variables. By taking certain combinations of the $\boldsymbol{\chi}_i$ elements, the unknown variables can be computed.

The matrix **N** is constructed by first labelling the columns and rows through a systematic monomial combinatory process. Denote the monomial $x_1^{a1} \ldots x_n^{an}$ as x^a where a

= (a_1, … an) with integer a_i's. Define X^N as the set of all monomials of degree d across the n variables x_i as[12]

$$X^N = \{x^a \mid a_1 + \ldots + a_n = d\} \tag{43}$$

For example, with n = 3 representing x_1,x_2,x_3 and d = 3, the set X^N is

$$X^N = \{x_1^3, x_1^2x_2, x_1^2x_3, x_1x_2^2, x_1x_3^2, x_1x_2x_3, x_2^3, x_2^2x_3, x_2x_3^2, x_3^3\} \tag{44}$$

Note $n_N = 10$ and the set X^N contains ten monomial elements, which are used to label the ten columns of matrix N. Next define the i^{th} subset of X^N as

$$X_i^N = \{x^a \mid a_i \geq d_i \text{ and } a_j < d_j \text{ for all } j < i\} \text{ for } i = 1, 2 \ldots n \tag{45}$$

In this example with $d_1 = 1$, $d_2 = 2$, and $d_3 = 2$, the subset X_1^N, X_2^N, X_3^N of X^N are

$$\begin{gathered} X_1^N = \{x_1^3, x_1^2x_2, x_1^2x_3, x_1x_2^2, x_1x_3^2, x_1x_2x_3\} \\ X_2^N = \{x_2^3, x_2^2x_3\} \\ X_3^N = \{x_2x_3^2, x_3^3\} \end{gathered} \tag{46}$$

Sets of homogenous degree d polynomials P_i^N corresponding to the subsets X_i^N are now constructed. The general syntax for the i^{th} polynomial subset is P_i^N is

$$P_i^N = \frac{X_i^N}{x_i^{d_i}} p_i \tag{47}$$

Continuing the specific example, the subsets P_1^N, P_2^N, P_3^N of P^N are

$$\begin{gathered} P_1^N = \{x_1^2p_1, x_1x_2p_1, x_1x_3p_1, x_2^2p_1, x_3^2p_1, x_2x_3p_1\} \\ P_2^N = \{x_2p_2, x_3p_2\} \\ P_3^N = \{x_2p_3, x_3p_3\} \end{gathered} \tag{48}$$

And thus the polynomial set is

$$P^N = \{x_1^2p_1, x_1x_2p_1, x_1x_3p_1, x_2^2p_1, x_3^2p_1, x_2x_3p_1, x_2p_2, x_3p_2, x_2p_3, x_3p_3\} \tag{49}$$

The set P^N contains ten polynomial elements, which are used to label the ten rows of matrix **N**. The coefficients in these polynomials are then inserted into the entries of the **N** matrix

based on the row and column labels. Suppose the original three equations in three variables are[12]

$$\begin{aligned} p_1 &= c^1_{x_1}x_1 + c^1_{x_2}x_2 + c^1_{x_3}x_3 = 0 \\ p_2 &= c^2_{x_1x_1}x_1^2 + c^2_{x_2x_2}x_2^2 + c^2_{x_3x_3}x_3^2 + c^2_{x_1x_2}x_1x_2 + c^2_{x_2x_3}x_2x_3 + c^2_{x_3x_1}x_3x_1 = 0 \\ p_3 &= c^3_{x_1x_2}x_1^2 + c^3_{x_2x_2}x_2^2 + c^3_{x_3x_3}x_3^2 + c^3_{x_1x_2}x_1x_2 + c^3_{x_2x_3}x_2x_3 + c^3_{x_3x_1}x_3x_1 = 0 \end{aligned} \quad (50)$$

Matrix **N** is constructed as[7]

$$\boldsymbol{N} = \begin{array}{c} \begin{matrix} x_1^3 & x_1^2x_2 & x_1^2x_3 & x_1x_2^2 & x_1x_3^2 & x_1x_2x_3 & x_2^3 & x_2^2x_3 & x_2x_3^2 & x_3^3 \end{matrix} \\ \begin{bmatrix} c^1_{x_1} & c^1_{x_2} & c^1_{x_3} & 0 & 0 & 0 & 0 & 0 & 0 & 0 \\ 0 & c^1_{x_1} & 0 & c^1_{x_2} & 0 & c^1_{x_3} & 0 & 0 & 0 & 0 \\ 0 & 0 & c^1_{x_1} & 0 & c^1_{x_3} & c^1_{x_2} & 0 & 0 & 0 & 0 \\ 0 & 0 & 0 & c^1_{x_1} & 0 & 0 & c^1_{x_2} & c^1_{x_3} & 0 & 0 \\ 0 & 0 & 0 & 0 & c^1_{x_1} & 0 & 0 & 0 & c^1_{x_2} & c^1_{x_3} \\ 0 & 0 & 0 & 0 & 0 & c^1_{x_1} & 0 & c^1_{x_2} & c^1_{x_3} & 0 \\ 0 & c^2_{x_1x_1} & 0 & c^2_{x_1x_2} & 0 & c^2_{x_3x_1} & c^2_{x_2x_2} & c^2_{x_2x_3} & c^2_{x_3x_3} & 0 \\ 0 & 0 & c^2_{x_1x_1} & 0 & c^2_{x_3x_1} & c^2_{x_1x_2} & 0 & c^2_{x_2x_2} & c^2_{x_2x_3} & c^2_{x_3x_3} \\ 0 & c^3_{x_1x_1} & 0 & c^3_{x_1x_2} & 0 & c^3_{x_3x_1} & c^3_{x_2x_2} & c^3_{x_2x_3} & c^3_{x_3x_3} & 0 \\ 0 & 0 & c^3_{x_1x_1} & 0 & c^3_{x_3x_1} & c^3_{x_1x_2} & 0 & c^3_{x_2x_2} & c^3_{x_2x_3} & c^3_{x_3x_3} \end{bmatrix} \end{array} \begin{matrix} x_1^2p_1 \\ x_1x_2p_1 \\ x_1x_3p_1 \\ x_2^2p_1 \\ x_3^2p_1 \\ x_2x_3p_1 \\ x_2p_2 \\ x_3p_2 \\ x_2p_3 \\ x_3p_3 \end{matrix} \quad (51)$$

Here, matrix **N** is constructed in terms of the polynomial coefficients. But as mentioned earlier, it can also be constructed with the polynomial coefficients along with either a set of unspecified coefficients c_{xi} originating from an appended equation; hence, the resultant is written as R (c_k^j,c_{i*}) or the variables x_{i*} chosen to be solved for first; hence, the resultant is written as R (c_k^j,x_{i*}). For the latter method, the polynomial equations are first restructured such that x_{i*} is imbedded as part of the coefficients. This imbedding process subtracts one variable from the system making the total count of unknown's n-1. The

homogenization process is then performed and adds one variable to the system making the total count of unknowns equal to the original value of n. Thus, no additional equation is needed here (m = n). In this thesis, matrix **N** is constructed with the polynomial coefficients and a variable x_{i*} which is chosen to be solved for first.

Once matrix **N** is available, matrix **D** is formed by well-defined procedure described here.[11] As mentioned earlier, reference 11 provides a summary for various resultant cases. Matrix **D** is the minor of matrix **N** and the procedure determines which columns and rows of **N** are to be retained to form **D**. In the next section, some of these monomials will be reduced depending upon whether the exponents are "big" or "small".

Each variable will be associated with a particular equation. For example the first variable, x_1, will be associated with the first equation, p_1. The second variable, x_2, will be associated with the second equation, p_2, etc. The degrees of the associated equation define "bigness" for the exponents of that variable. Specifically, since d_1 (the degree of p_1) is 1, if the exponent of x_1 is greater than or equal to 1, it is considered big. Since $d_2 = 2$, whenever the exponent of x_2 is greater than or equal to 2, it is considered big. The degree of p_3 is 2, therefore, whenever the exponent of x_3 is greater than or equal to 3, it considered big. For example, consider the monomial $x_1^2x_3$. The exponent of x_1 is 2. This is greater than d_1, and is considered big. The exponent of x_3 is 1. This is less than d_3, and is therefore small.

Next step in forming matrix **D** is to determine the reduced monomials. If for a particular monomial of degree d the exponent of only one variable is big, the monomial is said to be reduced. For example, in the monomial $x_1^2x_2$, the exponent of x_1 is greater than d_1, hence considered big, and the exponent of x_2 is less than d_2, hence considered small. Here, the exponent of one variable is small and other exponent is big so the monomial $x_1^2x_2$

is reduced. Another example is of monomial $x_1x_2^2$. Here, the exponent of x_1 is equal to d_1, hence considered big, and the exponent of x_2 is equal to d_2, hence also considered to be big. Since the exponent of both variable is big thus the monomial $x_1x_2^2$ is not reduced.

The denominator of the Macaulay Resultant is the determinant of the matrix **D**. It consists of the elements which have row and column monomial labels which are not reduced. For this specific example, Matrix **D** is thus[7]

$$D = \begin{matrix} x_1x_2^2 & x_1x_3^2 \\ \begin{bmatrix} c_{x_1}^1 & 0 \\ 0 & c_{x_1}^1 \end{bmatrix} & \begin{matrix} x_2^2p_1 \\ x_3^2p_1 \end{matrix} \end{matrix} \tag{52}$$

Macaulay discovered that when matrix **D** has full rank, any factors appearing in the denominator of Eq. **(**39**)** also precisely appear in the numerator, and thus can be cancelled out. In the case where matrix **D** is rank deficient, the Eq. (39) expression is indeterminate and both **N** and **D** must be modified by a reduction process, which is similar to l'Hopital's rule for an indeterminate limit of a rational function. Here, the rank deficient **D** situation is not examined.

Matrices **N** and **D** are constructed as described in Eqs. (43), (45), (47), and method of "big" vs "small". Resultant $R(c_k^j, x_{i*})$ becomes a polynomial in the single unknown x_{i*}[13,15] and the values of x_{i*} that make $R(c_k^j, x_{i*}) = 0$ are sought. The distinguishing feature of this formulation is that computation of the unknown root x_{i*} can be converted to an equivalent companion matrix eigenvalue computation based on matrix numerical routines.[13,15] The expanded matrix polynomial form of $N(c_k^j, x_{i*})$ is

$$N(c_k^j, x_{i*}) = N_p(c_k^j)x_{i*}^p + N_{p-1}(c_k^j)x_{i*}^{p-1} + \cdots + N_1(c_k^j)x_{i*} + N_0(c_k^j) \tag{53}$$

Where each matrix $N_i(c_k^j)$ has dimension $n_N \times n_N$ and p denotes the maximum degree of all x_{i*} terms appearing in the original equation set. Because the leading matrix in Eq. (53) is not equal to the identity matrix, the Eq. (53) polynomial is more naturally companioned

with the two-matrix generalized eigen decomposition problem indicated below with eigenvalue λ and eigenvector ϕ.

$$\lambda \mathbf{B}\boldsymbol{\phi} = \mathbf{A}\boldsymbol{\phi} \tag{54}$$

Companion matrices **A** and **B** appearing in EQ. (54) are given below where $I_{nN\times nN}$ denotes the $n_N \times n_N$ identity matrix and $0_{nN\times nN}$ the $n_N \times n_N$ zero matrix.

$$\mathbf{A} = \begin{bmatrix} 0_{n_N\times n_N} & I_{n_N\times n_N} & 0_{n_N\times n_N} & \cdots & 0_{n_N\times n_N} \\ 0_{n_N\times n_N} & 0_{n_N\times n_N} & I_{n_N\times n_N} & \cdots & 0_{n_N\times n_N} \\ \cdots & \cdots & \cdots & \cdots & \cdots \\ 0_{n_N\times n_N} & 0_{n_N\times n_N} & 0_{n_N\times n_N} & \cdots & I_{n_N\times n_N} \\ -N_0(c_k{}^j) & -N_1(c_k{}^j) & -N_2(c_k{}^j) & \cdots & -N_{p-1}(c_k{}^j) \end{bmatrix}$$

$$\mathbf{B} = \begin{bmatrix} I_{n_N\times n_N} & 0_{n_N\times n_N} & \cdots & 0_{n_N\times n_N} & 0_{n_N\times n_N} \\ 0_{n_N\times n_N} & I_{n_N\times n_N} & \cdots & 0_{n_N\times n_N} & 0_{n_N\times n_N} \\ \cdots & \cdots & \cdots & \cdots & \cdots \\ 0_{n_N\times n_N} & 0_{n_N\times n_N} & \cdots & I_{n_N\times n_N} & 0_{n_N\times n_N} \\ 0_{n_N\times n_N} & 0_{n_N\times n_N} & \cdots & 0_{n_N\times n_N} & -N_p(c_k{}^j) \end{bmatrix} \tag{55}$$

Thus variable x_{i*} is computed from the Eigen decomposition problem in Eq. (54). With this value, matrix **N** is evaluated and the corresponding null space vectors $\boldsymbol{\chi}_i$ are computed from Eq. (42), from which the remaining variables x_i are finally computed.

In order to illustrate the Macaulay method, the following system of two polynomial equations will be used, where variable x_1 is chosen as the initial variable to be solved for. After imbedding x_1 as part of the coefficients, the polynomial equations will be given as:

$$\begin{aligned} p_1(x_2) &= x_2 + (-3x_1 + 5) = 0 \\ p_2(x_2) &= x_2^2 + (x_1^2 - 5) = 0 \end{aligned} \tag{56}$$

Here we have two inhomogeneous equations in one variable. The equations must first be homogenized. This is done by adding a third variable, x_h. Specifically x_2 is replaced by x_2/x_h, and the factors of x_h are cleared from the denominators. In the above example this leads to following two equations:

$$\mathrm{p}_1(x_2, x_h) = x_2 + (-3x_1 + 5)x_h = 0$$
$$\mathrm{p}_2(x_2, x_h) = x_2^2 + (x_1^2 - 5)x_h^2 = 0 \quad (57)$$

This is the homogenized version of the original system.

All the monomials in a given equation are constrained to have the same degree because of the homogenization. The "overall degree" of the system is determined from the degrees of the individual homogenous equations by using Eq. (41):

$$\mathrm{d} = 1 + \sum_{i=1}^{m} (\mathrm{d}_i - 1)$$

Where

m = the number of equations

d_i = the degree of the i^{th} equation

For the homogenous polynomials above, the degrees are:

EQUATION	DEGREE
p_1	$d_1 = 1$
p_2	$d_2 = 2$

Therefore,

$$d = 1 + (1 - 1) + (2 - 1) = 2$$

The number of variables in the inhomogeneous equations is two. Since in restructured polynomials the variable x_1 is imbedded as part of the coefficients, the total count of unknown is one. Since one additional variable has been added to homogenize the equations, the number of variables in the homogeneous equations is restored to two again, providing an equal number of equations and variables. Hence, the numerator matrix sixe would be given by using Eq. (40) as:

Numerator Matrix Size (n_N) = (n-1+d)!/(n-1)!d!

For the two polynomial equations, the "overall degree" was d = 2 and n equals 2. Thus for this example, n_N= 3. The matrix **N** and **D** is constructed using the method described for generating Eq. (51) and Eq. (52), respectively.

$$\mathbf{N} = \begin{matrix} x_2^2 & x_2x_h & x_h^2 \end{matrix} \begin{bmatrix} 1 & (-3x_1+5) & 0 \\ 0 & 1 & (-3x_1+5) \\ 1 & 0 & (x_1^2-5) \end{bmatrix} \begin{matrix} x_2p_1 \\ x_hp_1 \\ p_2 \end{matrix} \tag{58}$$

$$\mathbf{D} = \begin{matrix} x_2 & x_h \end{matrix} \begin{bmatrix} 1 \end{bmatrix} \begin{matrix} x_hp_1 \end{matrix} \tag{59}$$

The matrix polynomial form of **N** is

$$\mathbf{N} = \begin{bmatrix} 0 & 0 & 0 \\ 0 & 0 & 0 \\ 0 & 0 & 1 \end{bmatrix} x_1^2 + \begin{bmatrix} 0 & -3 & 0 \\ 0 & 0 & -3 \\ 0 & 0 & 0 \end{bmatrix} x_1 + \begin{bmatrix} 1 & 5 & 0 \\ 0 & 1 & 5 \\ 1 & 0 & -5 \end{bmatrix} \tag{60}$$

Leading to the generalized Eigen problem matrices A and B given below with p = 2.

$$\mathbf{A} = \begin{bmatrix} 0 & 0 & 0 & 1 & 0 & 0 \\ 0 & 0 & 0 & 0 & 1 & 0 \\ 0 & 0 & 0 & 0 & 0 & 1 \\ -1 & -5 & 0 & 0 & 3 & 0 \\ 0 & -1 & -5 & 0 & 0 & 3 \\ -1 & 0 & 5 & 0 & 0 & 0 \end{bmatrix} \mathbf{B} = \begin{bmatrix} 1 & 0 & 0 & 0 & 0 & 0 \\ 0 & 1 & 0 & 0 & 0 & 0 \\ 0 & 0 & 1 & 0 & 0 & 0 \\ 0 & 0 & 0 & 0 & 0 & 0 \\ 0 & 0 & 0 & 0 & 0 & 0 \\ 0 & 0 & 0 & 0 & 0 & 1 \end{bmatrix} \tag{61}$$

The finite real eigenvalues are $x_1 = 1$ and $x_1 = 2$. Evaluating **N** at the first eigenvalue leads to the single null space vector $\boldsymbol{\chi}_1$, shown in Eq. (62). Elements of vector $\boldsymbol{\chi}_1$ are in proportion to the corresponding column labels. Since the null space vector is non-unique, choose $x_h^2 = 1$, or $x_h = 1$, and dividing the second element by x_h yields the solution $(x_1, x_2) = (1,-2)$, also shown in Eq. (62).

$$x_1 = 1, \quad \boldsymbol{\chi}_1 = \begin{bmatrix} 4 \\ -2 \\ 1 \end{bmatrix} \begin{matrix} x_2^2 \\ x_2x_h \\ x_h^2 \end{matrix}, \; x_h^2 = 1 \rightarrow x_h = 1, x_2 = \frac{x_2x_h}{x_h} = -2 \tag{62}$$

Evaluating N at the second eigenvalue leads to the single null space vector $\boldsymbol{\chi}_1$, shown in Eq. (63). Again choose $x_h^2 = 1$, or $x_h = 1$, and dividing the second element by x_h yields the solution $(x_1, x_2) = (2, 1)$, also shown in Eq. (63).

$$x_1 = 2, \quad \boldsymbol{\chi}_1 = \begin{bmatrix} 1 \\ 1 \\ 1 \end{bmatrix} \begin{matrix} x_2^2 \\ x_2 x_h \\ x_h^2 \end{matrix}, \quad x_h^2 = 1 \rightarrow x_h = 1 \, , x_2 = \frac{x_2 x_h}{x_h} = 1 \tag{63}$$

Macaulay Resultant for IROD

The authors in reference 7 has presented an application of the Macaulay resultant method by solving the initial relative-orbit determination problem using the Cartesian-component formulation. In the three dimensional case, there are total six unknown components of the relative position vector and the velocity vector. On each measurement time, azimuth and elevation angle measurements are observed. Since there are six unknowns, a total of six angle measurements are required at three different measurement time, i.e., Eq. (16). After imbedding and homogenization, m =6, n = 6, $d_1 = 2$, $d_2 = 2$, $d_3 = 2$, $d_4 = 2$, $d_5 = 2$, $d_6 = 2$, d= 7 and $n_N = 792$. The authors have solved the IROD using the Macaulay method for the two-dimensional case, where m = 4, n = 4, $d_1 = 2$, $d_2 = 2$, $d_3 = 2$, d = 5, and $n_N = 56$.[7] The Macaulay method performance was checked for different scenarios such as varying plant noise, variation in measurement noise etc. It has been shown that the method has an advantage of using less number of measurements in comparison to other published methods. However, one disadvantage that has been pointed out is high algebraic complexity. Another disadvantage is of high dimensionality when the equation and/or variable count grows.

CHAPTER 6

MINIMAL-MEASUREMENT SOLUTION USING SEPARATION-MAGNITUDE FORMULATION

The Macaulay Resultant method requires a total of six angle measurements when the IROD problem is solved using the Cartesian-component formulation with the three-dimensional case, which leads to the matrix **N** of size 792×792. To reduce algebraic complexity, and high dimensionality, the Macaulay resultant method is used with the separation-magnitude formulation. The separation-magnitude formulation was based on the fact that at the time of the first observation, the initial direction of the deputy satellite with respect to the chief satellite is already known, and it is only the relative magnitude that needs to be computed for complete knowledge of relative position vector. Thus, reducing the number of unknowns, i.e. the relative position magnitude and the relative velocity vector component, to four in the three-dimensional case. The Macaulay method is applied on the IROD problem using the concept of separation-magnitude formulation and now a total of four measurement equations are required, which leads to the matrix **N** of size 56×56. This shows that the separation-magnitude formulation succeed in overcoming the disadvantages related to the Cartesian-component formulation. The number of measurement equations is reduced to four, and the algebraic complexity is also reduced because of the decrease in the size of matrix **N.**

The second-order dynamics equation of motion, Eq. (14), first needs to be reformulated to apply the Macaulay resultant method. Although the method can be applied the three-dimensional case, for the simplicity, a two-dimensional case is presented, hence there are three unknowns ($\dot{x}_0, \dot{y}_0, r_0$) which will require three additional measurements of unit-direction-vector at different time to solve for the initial relative magnitude of the position vector and the relative velocity vector. At any point of time, the relation between the relative position components and the unit-direction-vector observation can be written as:

$$x_i u_{i(2)} - y_i u_{i(1)} = 0 \tag{44}$$

$$i = 1, 2, 3$$

Where, i represents the number of measurement, and $u_{i(2)}$ and $u_{i(1)}$ are the components of the unit-direction-vector observation at measurement time i. The substitution of the second-order dynamics equation of motion in Eq. (64) can be expressed as:

$$A_i r_0 + B_i \dot{x}_0 + C_i \dot{y}_0 + D_i r_0^2 + E_i \dot{x}_0^2 + H_i \dot{y}_0^2 + I_i r_0 \dot{x}_0 + J_i r_0 \dot{y}_0 + K_i \dot{x}_0 \dot{y}_0 = 0 \tag{65}$$

$$i = 1, 2, 3$$

$$A_i = (F_1^i u_{01} u_{i(2)} - G_1^i u_{01} u_{i(1)} + G_2^i u_{02} u_{i(1)})$$

$$B_i = (F_2^i u_{i(2)} - G_3^i u_{i(1)})$$

$$C_i = (F_3^i u_{i(2)} - G_4^i u_{i(1)})$$

$$D_i = (F_4^i u_{01}^2 u_{i(2)} + F_5^i u_{02}^2 u_{i(2)} + F_8^i u_{01} u_{02} u_{i(2)} - G_5^i u_{01}^2 u_{i(1)} - G_6^i u_{02}^2 u_{i(1)} - G_9^i u_{01} u_{02} u_{i(1)})$$

$$E_i = (F_6^i u_{i(2)} - G_7^i u_{i(1)})$$

$$H_i = (F_7^i u_{i(2)} - G_8^i u_{i(1)})$$

$$I_i = (F_9^i u_{01} u_{i(2)} - G_{10}^i u_{01} u_{i(1)} - G_{12}^i u_{02} u_{i(1)})$$

$$J_i = (F^i_{10}u_{01}u_{i(2)} + F^i_{11}u_{02}u_{i(2)} - G^i_{11}u_{01}u_{i(1)})$$

$$K_i = (F^i_{12}u_{i(2)} - G^i_{13}u_{i(1)})$$

$$F^i_1 = (4 - 3\cos(n_0t_i)) \qquad G^i_1 = 6(\sin(n_0t_i) - n_0t_i)$$

$$F^i_2 = \frac{1}{n_0}(\sin(n_0t_i)) \qquad G^i_2 = 1$$

$$F^i_3 = \frac{2}{n_0}(1 - \cos(n_0t_i)) \qquad G^i_3 = \frac{2}{n_0}(-1 + \cos(n_0t_i))$$

$$F^i_4 = \frac{3}{2R_0}(7 - 10\cos(n_0t_i) + 3\cos(2n_0t_i) + 12n_0t_i\sin(n_0t_i) - 12n_0^2t_i^2) \qquad G^i_4 = \frac{1}{n_0}(4\sin(n_0t_i) - 3n_0t_i)$$

$$F^i_5 = \frac{3}{2R_0}(1 - \cos(n_0t_i)) \qquad G^i_5 = \frac{3}{4R_0}(40\sin(n_0t_i) + 3\sin(2n_0t_i) - 22n_0t_i - 24n_0t_i\cos(n_0t_i))$$

$$F^i_6 = \frac{1}{2n_0^2R_0}(-3 + 4\cos(n_0t_i) - \cos(2n_0t_i)) \qquad G^i_6 = \frac{3}{R_0}(\sin(n_0t_i) - n_0t_i)$$

$$F^i_7 = \frac{1}{2n_0^2R_0}(6 - 10\cos(n_0t_i) + 4\cos(2n_0t_i) + 12nt_i\sin(n_0t_i) - 9n_0^2t_i^2) \qquad G^i_7 = \frac{1}{4n_0^2R_0}(8\sin(n_0t_i) - \sin(2n_0t_i) - 6n_0t_i)$$

$$F^i_8 = \frac{6}{R_0}(-\sin(n_0t_i) + n_0t_i) \qquad G^i_8 = \frac{1}{n_0^2R_0}(10\sin(n_0t_i) + \sin(2n_0t_i) - 6n_0t_i - 6n_0t_i\cos(n_0t_i))$$

$$F^i_9 = \frac{3}{n_0R_0}(4\sin(n_0t_i) - \sin(2n_0t_i) - 4n_0t_i + 2n_0t_i\cos(n_0t_i)) \qquad G^i_9 = \frac{3}{R_0}(1 - \cos(n_0t_i))$$

$$F_{10}^{i} = \frac{3}{n_0 R_0}(4 - 6\cos(n_0 t_i) + 2\cos(2n_0 t_i) + 7n_0 t_i \sin(n_0 t_i) - 6n_0^2 t_i^2)$$

$$G_{10}^{i} = \frac{3}{2n_0 R_0}(-5 + 4\cos(n_0 t_i) + \cos(2n_0 t_i) + 4n_0 t_i \sin(n_0 t_i))$$

$$F_{11}^{i} = \frac{3}{n_0 R_0}(-\sin(n_0 t_i) + (n_0 t_i))$$

$$G_{11}^{i} = \frac{3}{n_0 R_0}(12\sin(n_0 t_i) + \sin(2n_0 t_i) - 7n_0 t_i - 7n_0 t_i \cos(n_0 t_i))$$

$$F_{12}^{i} = \frac{1}{n_0^2 R_0}(7\sin(n_0 t_i) - 2\sin(2n_0 t_i) - 6n_0 t_i + 3n_0 t_i \cos(n_0 t_i))$$

$$G_{12}^{i} = \frac{1}{3n_0 R_0}(-\sin(n_0 t_i) + n_0 t_i)$$

$$G_{13}^{i} = \frac{1}{n_0^2 R_0}(-3 + 2\cos(n_0 t_i) + \cos(2n_0 t_i) + 3n_0 t_i \sin(n_0 t_i))$$

The next step in the Macaulay Resultant method is to choose a variable which will be solved first. Here, the magnitude of the relative position vector (r_0) is chosen as the first variable to be solved for. Hence, imbedding the r_0 into the coefficient of other monomials as a parameter will transform the equation as:

$$E_i \dot{x}_0^2 + H_i \dot{y}_0^2 + K_i \dot{x}_0 \dot{y}_0 + (B_i + I_i r_0)\dot{x}_0 + (C_i + J_i r_0)\dot{y}_0 + (A_i r_0 + D_i r_0^2) = 0 \qquad (66)$$

In Eq. (66), now the unknowns are $\dot{x}_0$ and $\dot{y}_0$, which reduces the number of unknowns to two. The homogenizing of Eq. (66) will recover the original number of unknowns. To homogenize Eq. (66), replace $\dot{x}_0$ and $\dot{y}_0$ with $\dot{x}_0/x_h$ and $\dot{y}_0/x_h$, and after clearing all denominators, the homogenized equation set can be written as:

$$E_i \dot{x}_0^2 + H_i \dot{y}_0^2 + K_i \dot{x}_0 \dot{y}_0 + (B_i + I_i r_0)\dot{x}_0 x_h + (C_i + J_i r_0)\dot{y}_0 x_h + (A_i r_0 + D_i r_0^2)x_h^2 = 0 \qquad (67)$$

$$i = 1, 2, 3$$

Eq. (67) represents three equations with the total of three unknowns ($\dot{x}_0$, $\dot{y}_0$, x_h). Hence, the homogenization recovers the original number of unknowns. Here, m = 3, n = 3, d_1 = 2,

$d_2 = 2$, $d_3 = 2$, and $n_N = 15$. It can be noticed that with the Cartesian-component formulation, in the two-dimensional cae, the size of the **N** matrix was 56×56, here it is only 15×15 with the separation-magnitude formulation. Thus, decreasing the number of unknowns greatly reduce the dimension of the problem. The matrices **N** and **D** are constructed using the method described for generating Eq. (51) and Eq. (52), respectively.

$$N = N_2 r_0^2 + N_1 r_0 + N_0 \tag{68}$$

Rows of Matrix **N** have these monomials:

$$\{\dot{x}_0^4 \;\; \dot{x}_0^2\dot{y}_0 \;\; \dot{x}_0^3 x_h \;\; \dot{x}_0^2\dot{y}_0^2 \;\; \dot{x}_0^2\dot{y}_0 x_h \;\; \dot{x}_0^2 x_h^2 \;\; \dot{x}_0\dot{y}_0^3 \;\; \dot{x}_0\dot{y}_0^2 x_h \;\; \dot{x}_0\dot{y}_0 x_h^2 \;\; \dot{x}_0 x_h^3 \;\; \dot{y}_0^4 \;\; \dot{y}_0^3 x_h \;\; \dot{y}_0^2 x_h^2 \;\; \dot{y}_0 x_h^3 \;\; x_h^4\}$$

Columns of Matrix **N** have these polynomials:

$$\{p_1\dot{x}_0^2, p_1\dot{y}_0, p_1\dot{x}_0 x_h, p_1\dot{y}_0^2, p_1\dot{y}_0 x_h, p_1 x_h^2, p_2\dot{x}_0\dot{y}_0, p_2\dot{x}_0 x_h, p_2\dot{y}_0^2, p_2\dot{y}_0 x_h, p_2 x_h^2, p_3\dot{x}_0\dot{y}_0, p_3\dot{x}_0 x_h, p_3 x_h^2\}^T$$

$$N_2 = \begin{bmatrix}
0 & 0 & 0 & 0 & 0 & D_1 & 0 & 0 & 0 & 0 & 0 & 0 & 0 & 0 & 0 \\
0 & 0 & 0 & 0 & 0 & 0 & 0 & 0 & D_1 & 0 & 0 & 0 & 0 & 0 & 0 \\
0 & 0 & 0 & 0 & 0 & 0 & 0 & 0 & 0 & D_1 & 0 & 0 & 0 & 0 & 0 \\
0 & 0 & 0 & 0 & 0 & 0 & 0 & 0 & 0 & 0 & 0 & 0 & D_1 & 0 & 0 \\
0 & 0 & 0 & 0 & 0 & 0 & 0 & 0 & 0 & 0 & 0 & 0 & 0 & D_1 & 0 \\
0 & 0 & 0 & 0 & 0 & 0 & 0 & 0 & 0 & 0 & 0 & 0 & 0 & 0 & D_1 \\
0 & 0 & 0 & 0 & 0 & 0 & 0 & 0 & D_2 & 0 & 0 & 0 & 0 & 0 & 0 \\
0 & 0 & 0 & 0 & 0 & 0 & 0 & 0 & 0 & D_2 & 0 & 0 & 0 & 0 & 0 \\
0 & 0 & 0 & 0 & 0 & 0 & 0 & 0 & 0 & 0 & 0 & 0 & D_2 & 0 & 0 \\
0 & 0 & 0 & 0 & 0 & 0 & 0 & 0 & 0 & 0 & 0 & 0 & 0 & D_2 & 0 \\
0 & 0 & 0 & 0 & 0 & 0 & 0 & 0 & 0 & 0 & 0 & 0 & 0 & 0 & D_2 \\
0 & 0 & 0 & 0 & 0 & 0 & 0 & 0 & D_3 & 0 & 0 & 0 & 0 & 0 & 0 \\
0 & 0 & 0 & 0 & 0 & 0 & 0 & 0 & 0 & D_3 & 0 & 0 & 0 & 0 & 0 \\
0 & 0 & 0 & 0 & 0 & 0 & 0 & 0 & 0 & 0 & 0 & 0 & 0 & D_3 & 0 \\
0 & 0 & 0 & 0 & 0 & 0 & 0 & 0 & 0 & 0 & 0 & 0 & 0 & 0 & D_3
\end{bmatrix}$$

$$N_1 = \begin{bmatrix} 0 & 0 & I_1 & 0 & J_1 & A_1 & 0 & 0 & 0 & 0 & 0 & 0 & 0 & 0 & 0 \\ 0 & 0 & 0 & 0 & I_1 & 0 & 0 & J_1 & A_1 & 0 & 0 & 0 & 0 & 0 & 0 \\ 0 & 0 & 0 & 0 & 0 & I_1 & 0 & 0 & J_1 & A_1 & 0 & 0 & 0 & 0 & 0 \\ 0 & 0 & 0 & 0 & 0 & 0 & 0 & I_1 & 0 & 0 & 0 & J_1 & A_1 & 0 & 0 \\ 0 & 0 & 0 & 0 & 0 & 0 & 0 & 0 & I_1 & 0 & 0 & 0 & J_1 & A_1 & 0 \\ 0 & 0 & 0 & 0 & 0 & 0 & 0 & 0 & 0 & I_1 & 0 & 0 & 0 & J_1 & A_1 \\ 0 & 0 & 0 & 0 & I_2 & 0 & 0 & J_2 & A_2 & 0 & 0 & 0 & 0 & 0 & 0 \\ 0 & 0 & 0 & 0 & 0 & I_2 & 0 & 0 & J_2 & A_2 & 0 & 0 & 0 & 0 & 0 \\ 0 & 0 & 0 & 0 & 0 & 0 & 0 & I_2 & 0 & 0 & 0 & J_2 & A_2 & 0 & 0 \\ 0 & 0 & 0 & 0 & 0 & 0 & 0 & 0 & I_2 & 0 & 0 & 0 & J_2 & A_2 & 0 \\ 0 & 0 & 0 & 0 & 0 & 0 & 0 & 0 & 0 & I_2 & 0 & 0 & 0 & J_2 & A_2 \\ 0 & 0 & 0 & 0 & I_3 & 0 & 0 & J_3 & A_3 & 0 & 0 & 0 & 0 & 0 & 0 \\ 0 & 0 & 0 & 0 & 0 & I_3 & 0 & 0 & J_3 & A_3 & 0 & 0 & 0 & 0 & 0 \\ 0 & 0 & 0 & 0 & 0 & 0 & 0 & 0 & I_3 & 0 & 0 & 0 & J_3 & A_3 & 0 \\ 0 & 0 & 0 & 0 & 0 & 0 & 0 & 0 & 0 & I_3 & 0 & 0 & 0 & J_3 & A_3 \end{bmatrix}$$

$$N_0 = \begin{bmatrix} E_1 & K_1 & B_1 & H_1 & C_1 & 0 & 0 & 0 & 0 & 0 & 0 & 0 & 0 & 0 & 0 \\ 0 & E_1 & 0 & K_1 & B_1 & 0 & H_1 & C_1 & 0 & 0 & 0 & 0 & 0 & 0 & 0 \\ 0 & 0 & E_1 & 0 & K_1 & B_1 & 0 & H_1 & C_1 & 0 & 0 & 0 & 0 & 0 & 0 \\ 0 & 0 & 0 & E_1 & 0 & 0 & K_1 & B_1 & 0 & 0 & H_1 & C_1 & 0 & 0 & 0 \\ 0 & 0 & 0 & 0 & E_1 & 0 & 0 & K_1 & B_1 & 0 & 0 & H_1 & C_1 & 0 & 0 \\ 0 & 0 & 0 & 0 & 0 & E_1 & 0 & 0 & K_1 & B_1 & 0 & 0 & H_1 & C_1 & 0 \\ 0 & E_2 & 0 & K_2 & B_2 & 0 & H_2 & C_2 & 0 & 0 & 0 & 0 & 0 & 0 & 0 \\ 0 & 0 & E_2 & 0 & K_2 & B_2 & 0 & H_2 & C_2 & 0 & 0 & 0 & 0 & 0 & 0 \\ 0 & 0 & 0 & E_2 & 0 & 0 & K_2 & B_2 & 0 & 0 & H_2 & C_2 & 0 & 0 & 0 \\ 0 & 0 & 0 & 0 & E_2 & 0 & 0 & K_2 & B_2 & 0 & 0 & H_2 & C_2 & 0 & 0 \\ 0 & 0 & 0 & 0 & 0 & E_2 & 0 & 0 & K_2 & B_2 & 0 & 0 & H_2 & C_2 & 0 \\ 0 & E_3 & 0 & K_3 & B_3 & 0 & H_3 & C_3 & 0 & 0 & 0 & 0 & 0 & 0 & 0 \\ 0 & 0 & E_3 & 0 & K_3 & B_3 & 0 & H_3 & C_3 & 0 & 0 & 0 & 0 & 0 & 0 \\ 0 & 0 & 0 & 0 & E_3 & 0 & 0 & K_3 & B_3 & 0 & 0 & H_3 & C_3 & 0 & 0 \\ 0 & 0 & 0 & 0 & 0 & E_3 & 0 & 0 & K_3 & B_3 & 0 & 0 & H_3 & C_3 & 0 \end{bmatrix}$$

Matrix **D** can be shown as:

$$D = \begin{bmatrix} E_1 & 0 & A_1 r_0 + D_1 r_0^2 \\ 0 & E_1 & F_1 \\ 0 & B_3 + H_3 r_0 & 0 \end{bmatrix}$$

Leading to the generalized eigen problem matrices A and B given below:

$$A = \begin{bmatrix} 0_{15\times15} & I_{15\times15} & 0_{15\times15} \\ 0_{15\times15} & 0_{15\times15} & I_{15\times15} \\ -N_0 & -N_1 & -N_2 \end{bmatrix} \quad B = \begin{bmatrix} I_{15\times15} & 0_{15\times15} & 0_{15\times15} \\ 0_{15\times15} & I_{15\times15} & 0_{15\times15} \\ 0_{15\times15} & 0_{15\times15} & N_3 \end{bmatrix}$$

Thus the variable r_0 is computed from the eigen decomposition problem in Eq. (54). With this value, matrix N is evaluated and the corresponding null space vectors are computed from Eq. (42), from which the remaining variables $\dot{x}_0$, and $\dot{y}_0$ are finally computed.

Performance Test

To test and evaluate the performance of the new relative IROD solution, a two-dimensional xy planar numerical example is presented. As mentioned in chapter 4, the RMS of angle residual and of range ratio will be calculated to check the performance metric. A root-mean-square value of the angle residual that is close to zero indicates that the predicted angles are close to the originally collected measurement angles. The largest and worst possible RMS error value is equal to π radians away from its corresponding true line-of-sight measurement. For range ratio RMS, a value near one indicates the predicted ranges are close to the true ranges.

Several factors including noise type and level, and sample rate are varied to explore certain aspects of the IROD performance. Two types of noise are used to test this IROD technique: process noise and process plus the measurement noise. As mentioned earlier, the term process noise refers to generating the measurements with a higher fidelity model (nonlinear simulation) than the model on which the estimation solution is based (i.e., the second-order model). Measurement noise level is considered across the range 10^{-8} to 10^{-3} radians. Measurement sample rate is varied across a wide range of cases from 100 seconds to 10000 seconds to show dependency on temporal distribution of the measurements.

Estimating initial conditions with process noise and measurement noise

The IROD solution calculated using the Macaulay Resultant method is tested and validated here. A two-dimensional coplanar orbit is considered again. For the nonlinear

simulation, the true measurements are generated by choosing a set of initial conditions and propagating them forward using two-body dynamics and a fourth order Runge-Kutta numerical integrator with time step equal to one second. Both process noise and process plus measurement noise cases are considered. Process noise is introduced by using the second-order solution in the IROD technique. In the case with measurement corruption, Gaussian noise with a standard deviation of $\sigma = 10^{-6}$ rad is added to each measurement. For simplicity, measurements are taken at equal time steps. It is not necessary that measurements always be taken at equal time increments, but the time at which a measurement is taken must be recorded. Measurements for this case are sampled at equal time step increments of 1000 s. The initial conditions for this case are given below, in terms of circular chief orbit elements and the deputy's relative states with $\mu = 398600.436\ km^3/s^2$.

Chief:	Deputy:	Sample:
R_0 = 7100 km	$x_0 = 0.2$ km	t_1 = 1000 s
Ω_0 = 45 deg,	$y_0 = 0$ km	t_2 = 2000 s
θ_0 = 0 deg	$\dot{x}_0 = 0.002$ km/s	t_3 = 3000 s
i_0 = 70 deg	$\dot{y}_0 = 0.02$ km/s	

(69)

Five real finite roots from the Macaulay resultant polynomial are computed for Eq. (69). These roots are equivalent to the orbit determination solution for r_0. After taking each of these solutions and generating the associated null space vector, the remaining two initial states $\dot{x}_0, \dot{y}_0$ for the orbit determination solutions are computed. Table 14 shows the five root values and the initial state conditions. Based on comparison of individual initial states with the known exact values, the fifth solution in Table 14 indicates the IROD method using the Macaulay resultant framework is able to successfully recover the true initial conditions with process noise plus measurement noise. One point worth mentioning is when all five solution

are substituted into the original measurement equations, the equation residuals are all almost zero indicating all five sets of initial states are valid solutions. Utilization of the second-order dynamics model in the orbit determination problem permits multiple solutions. The fifth solution is clearly the one being sought, as the first four solutions have larger position and velocity values, possibly to the extent that the underlying second-order solution becomes inaccurate. Since the true initial conditions are unknown in a realistic application, the best solution can be identified by comparing the RMS of the angle residuals. RMS angle values are also listed in Table 14. Note that the fifth solution has minimum RMS. It can be noticed that the unobservable nature when using a linear dynamics model in relative orbit determination has been exchanged for a multiple solutions when using a nonlinear dynamics model.

Table 14. Estimated Initial Conditions with Process Noise & Measurement Noise

Resultant Root	x_0 (km)	y_0(Km)	$\dot{x}_0$ (Km/s)	$\dot{y}_0$ (km/s)	RMS angle
-2.2660e+04	-2.2660e+04	-1.1079e-02	5.8066e+01	1.8316e+01	2.6060e-06
2.1139e+04	2.1139e+04	1.0334e-02	-1.2443e+01	-4.1399e+01	1.1364e-08
1.4158e+04	1.4158e+04	6.9220e-03	-1.0810e+01	-2.4651e+01	8.1612e-09
3.8885e+03	3.8885e+03	1.9010e-03	-6.9412e+01	3.1486e+01	1.9235e-06
1.9790e-01	1.9790e-01	9.6750e-08	1.9748e-03	1.9754e-02	4.4187e-13

Figure 16 shows the trajectory of relative motion between the chief and deputy satellite for the 2.5 orbits of the chief satellite. The trajectory generated using the true state vector with the full nonlinear equations is labelled as “True IC/Nonlinear”. The trajectory generated using the computed state vector with the second order dynamics is labeled as “Computed IC/2nd Order”. And, the line-of-sight direction vector is labelled as “LOS direction”. It is clear from the figure and the table that the Macaulay resultant method is performing well under these conditions.

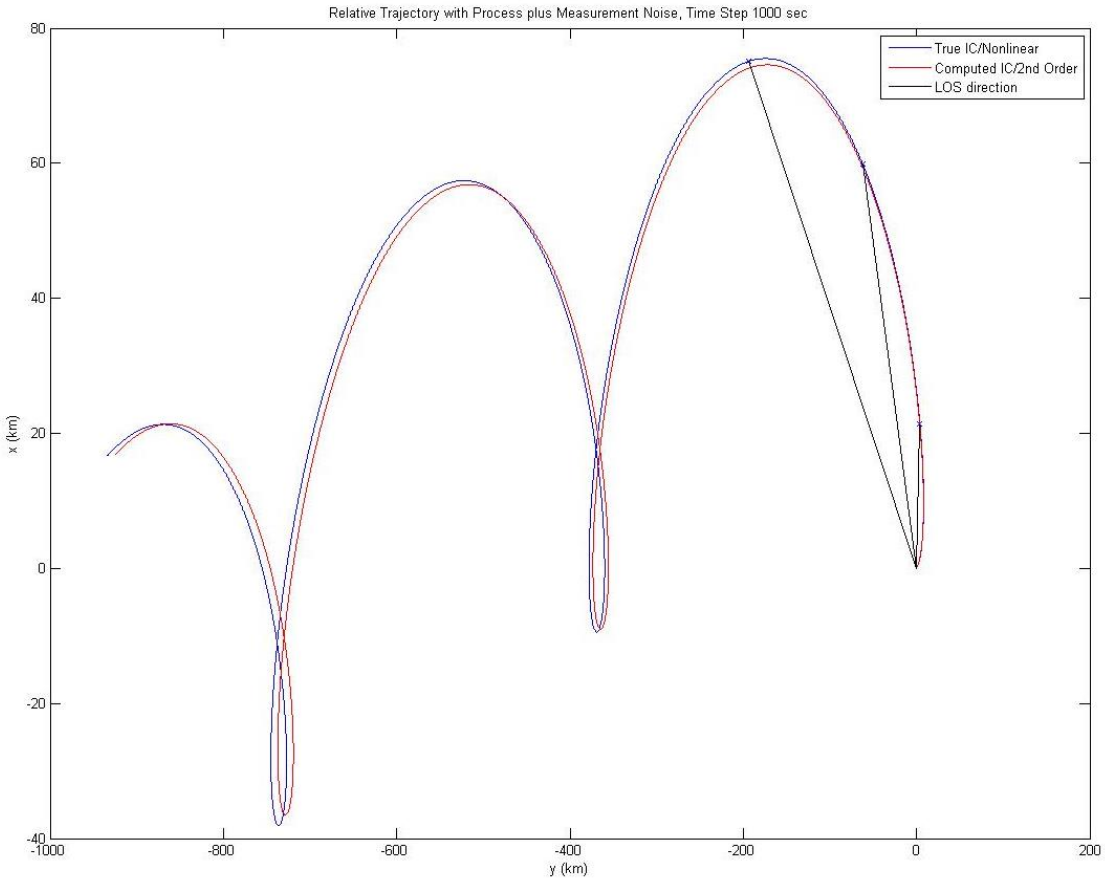

Figure 16. Relative orbit with Process plus Measurement Noise, time step of 1000 s

Effect of varying the measurement noise on estimation of initial conditions

In order to determine how the Macaulay resultant method will work with varying noise level, the same initial conditions are run with six different levels of measurement noise added to the process noise. The initial conditions are held constant at each run and the standard deviation of Gaussian noise is changed. Table 15 shows the values of the initial state conditions for the different values of standard deviation of Gaussian noise. Finite real roots from the Macaulay resultant polynomial are computed for each run having different value of standard deviation of Gaussian noise. These roots are equivalent to orbit

determination solution for r_0. After taking each of these solutions and generating the associated null space vector, the remaining two initial states $\dot{x}_0, \dot{y}_0$ for the orbit determination solutions are computed. RMS angle is also listed in Table 15. From Table 15, it can be seen, the largest level of the measurement noise ($\sigma = 10^{-3}$ rad) produces the highest error as expected, hence it hinders the ability of the IROD method. So it is desirable that the camera should take high precision measurement to reduce the corruption of the solution.

Figures 17 and 18 show the relative trajectory of the deputy satellite with respect to the chief satellite for 2.5 orbits of the chief satellite when the system has process plus measurement noise. The trajectory generated using the true state vectors with the full nonlinear equations is labelled as "True IC/Nonlinear". The trajectory generated using the computed state vectors with the second-order dynamic is labeled as "Computed IC/2nd Order". And, the line-of-sight direction vector is labelled as "LOS direction". In Figure 17 the relative trajectory is propagated with measurement noise of 10^{-8} rad standard deviation. And, as expected, the relative trajectory propagated with the second-order dynamics and the estimated initial conditions is able to follow the true relative trajectory. In Figure 18 the estimated relative trajectory generated with the process plus the measurement noise of 10^{-3} rad is compared with the true relative trajectory. It is clear from the figure and the table that the separation-magnitude formulation is performing well with the Macaulay resultant method when the measurements are less corrupted.

Table 15. Estimated Initial Conditions with Process Noise & Varying Level of Measurement Noise

σ	Real Lambda	x_0	y_0	$\dot{x}_0$	$\dot{y}_0$	RMS Angle
10^{-8}	-2.2660e+04	-2.2660e+04	2.8132e-05	5.8066e+01	1.8316e+01	3.2965e-06
	2.1139e+04	2.1139e+04	-2.6242e-05	-1.2444e+01	-4.1400e+01	2.2186e-08
	1.4158e+04	1.4158e+04	-1.7577e-05	-1.0810e+01	-2.4651e+01	5.3761e-09
	3.8883e+03	3.8883e+03	-4.8272e-06	-6.9412e+01	3.1486e+01	3.8419e-07
	1.9781e-01	**1.9781e-01**	**-2.4557e-10**	**1.9748e-03**	**1.9752e-02**	**5.5219e-13**
10^{-7}	-2.2660e+04	-2.2660e+04	-1.5216e-03	5.8066e+01	1.8316e+01	1.5730e-06
	2.1139e+04	2.1139e+04	1.4195e-03	-1.2443e+01	-4.1400e+01	3.0796e-08
	1.4158e+04	1.4158e+04	9.5074e-04	-1.0810e+01	-2.4651e+01	5.8302e-09
	3.8883e+03	3.8884e+03	2.6110e-04	-6.9412e+01	3.1486e+01	3.5048e-07
	1.9776e-01	**1.9782e-01**	**1.3284e-08**	**1.9747e-03**	**1.9751e-02**	**8.0269e-13**
10^{-6}	-2.2660e+04	-2.2660e+04	-1.1079e-02	5.8066e+01	1.8316e+01	1.4705e-06
	2.1139e+04	2.1139e+04	1.0334e-02	-1.2443e+01	-4.1399e+01	7.1638e-08
	1.4158e+04	1.4158e+04	6.9220e-03	-1.0810e+01	-2.4651e+01	2.0727e-08
	3.8885e+03	3.8885e+03	1.9010e-03	-6.9412e+01	3.1486e+01	1.9722e-07
	1.9790e-01	**1.9790e-01**	**9.6750e-08**	**1.9748e-03**	**1.9754e-02**	**9.0099e-13**
10^{-5}	-2.2660e+04	-2.2660e+04	-6.6593e-02	5.8066e+01	1.8316e+01	1.4613e-06
	2.1138e+04	2.1138e+04	6.2119e-02	-1.2443e+01	-4.1398e+01	5.1016e-08
	1.4160e+04	1.4160e+04	4.1612e-02	-1.0811e+01	-2.4654e+01	1.1356e-08
	3.8888e+03	3.8888e+03	1.1428e-02	-6.9412e+01	3.1486e+01	4.6446e-07
	2.0010e-01	**2.0010e-01**	**5.8804e-07**	**1.9771e-03**	**1.9799e-02**	**9.8617e-13**
10^{-4}	-2.2650e+04	-2.2650e+04	2.4210e+00	5.8033e+01	1.8312e+01	1.7451e-06
	2.1150e+04	2.1150e+04	-2.2607e+0	-1.2457e+01	-4.1428e+01	2.2121e-08
	1.4136e+04	1.4136e+04	-1.5110e+0	-1.0809e+01	-2.4599e+01	5.9361e-09
	3.8481e+03	3.8481e+03	-4.1131e-01	-6.9338e+01	3.1530e+01	3.4071e-07
	1.5078e-01	**1.5078e-01**	**-1.6116e-05**	**1.9418e-03**	**1.8872e-02**	**4.8242e-12**
10^{-3}	-2.2697e+04	-2.2697e+04	-7.3809e+0	5.8172e+01	1.8333e+01	3.0133e-06
	2.1031e+04	2.1030e+04	6.8389e+00	-1.2401e+01	-4.1097e+01	9.8621e-08
	1.4371e+04	1.4371e+04	4.6733e+00	-1.0867e+01	-2.5121e+01	6.0901e-09
	3.9662e+03	3.9662e+03	1.2898e+00	-6.9513e+01	3.1403e+01	1.4981e-06
	6.2064e-01	**6.2064e-01**	**2.0183e-04**	**2.1805e-03**	**2.6567e-02**	**5.6921e-12**

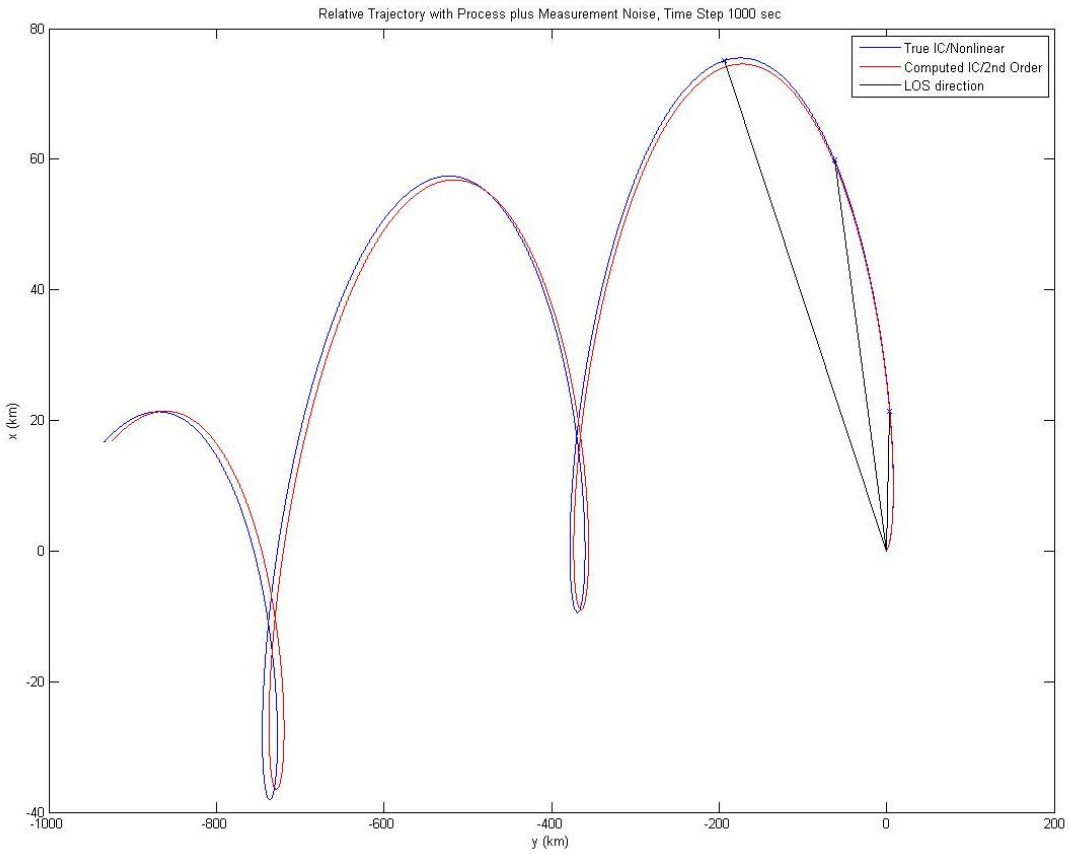

Figure 17. Relative orbit with Process plus Measurement Noise of 10^{-8} rad of standard deviation

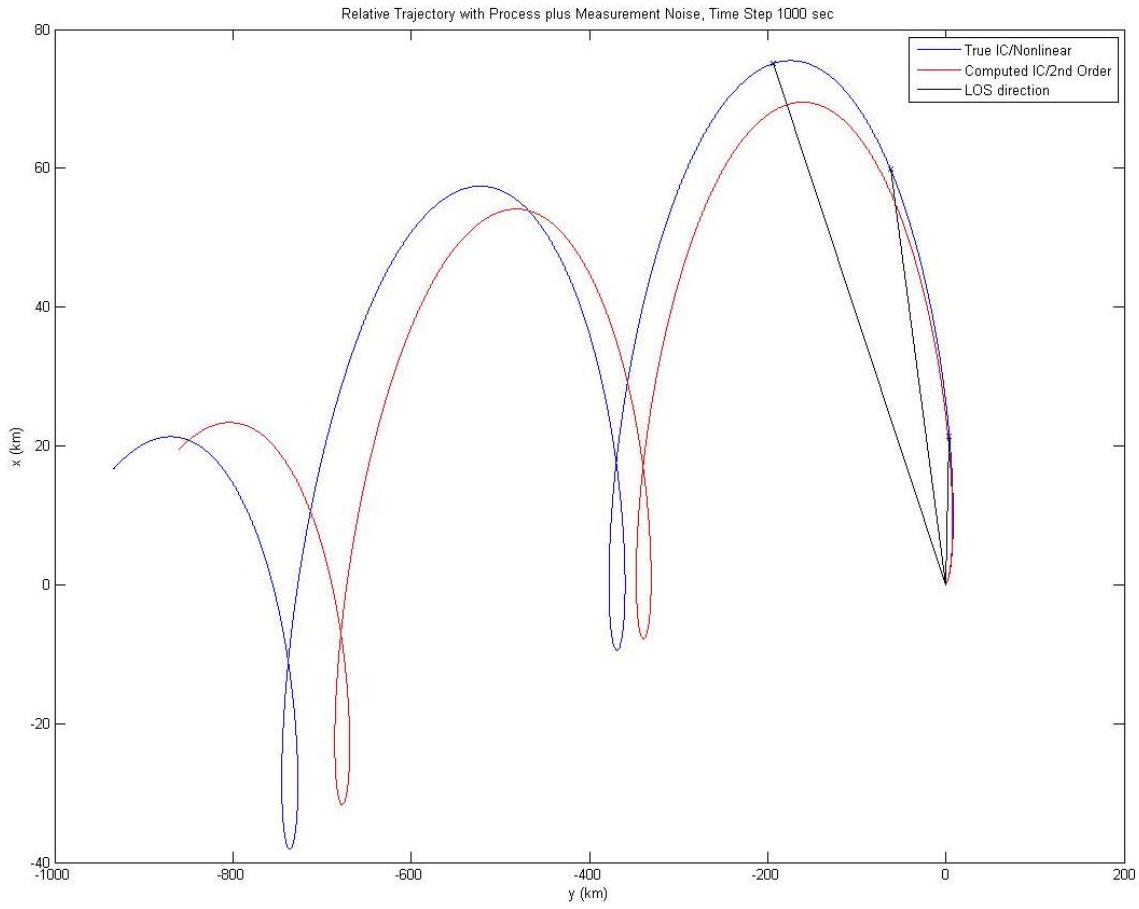

Figure 18. Relative orbit with Process plus Measurement Noise of 10^{-3} rad of standard deviation

Effect of varying sample time period on estimation of initial conditions

To present the potential of this method with varying sample time, the same initial conditions are run with five different sample time periods. Each run is made with the process noise plus Gaussian measurement noise with a standard deviation of $\sigma = 10^{-6}$ rad. The initial state vector is estimated using the time interval of 2000 s, 4000 s, 5000 s and 7000 s. As mentioned earlier, the basic tenet of the Macaulay resultant method is the matrix **N** has to be rank deficient. With the time period of 3000 s, and 6000 s, the matrix **N** was full rank, hence those are not discussed in this thesis.

Tables 16 and 17 show the estimated initial conditions and the RMS associated with angle residual and range ratio estimation for different sample time period, respectively. It can be seen from both tables that the Macaulay resultant method is able to estimate the initial conditions. One thing to notice is, although the estimation of relative position vector is poor as the sample time period is increased, the estimation of the velocity vector is still accurate. The performance of the IROD method can be sensitive to a uniform sample rate and thus should be given careful consideration.

Figures 19 - 23 show the trajectory of the relative motion between the deputy satellite and the chief satellite for the sample time period of 1000 s, 2000 s, 4000 s, 5000 s, and 7000 s. The trajectory generated using the true state vector with the full nonlinear equations is labelled as "True IC/Nonlinear". The trajectory generated using the computed state vector with the second-order dynamics is labeled as "Computed IC/2nd Order". And, the line-of-sight direction vector is labelled as "LOS direction". As expected after observing the above tables, the relative trajectory propagated with the estimated initial state vector using the second-order dynamics is following the true relative trajectory. In the redundant-

measurement solution, it was seen that as the sample period was increased, the computed relative trajectory was of poor accuracy. Here, it can be seen from the tables and figures that the minimum-measurement solution maintains accuracy for large sample periods.

Table 16. Estimated Initial Conditions with Varying Time Interval

Sample Period	Real Lambda	x_0	y_0	$\dot{x}_0$	$\dot{y}_0$
	Exact	**0.2**	**0**	**.002**	**.02**
1000	-2.2660e+04	-2.2660e+04	1.9599e-02	5.8066e+01	1.8316e+01
	2.1139e+04	2.1139e+04	-1.8282e-02	-1.2444e+01	-4.1400e+01
	1.4158e+04	1.4158e+04	-1.2245e-02	-1.0810e+01	-2.4651e+01
	3.8884e+03	3.8884e+03	-3.3630e-03	-6.9412e+01	3.1486e+01
	1.9776e-01	1.9776e-01	-1.7104e-07	1.9746e-03	1.9751e-02
2000	2.2151e+04	2.2151e+04	2.4217e-02	-1.2029e+01	-4.3364e+01
	3.3917e+02	3.3917e+02	3.7081e-04	-5.6637e-01	-8.2849e-01
	2.5030e-01	2.5030e-01	2.7365e-07	1.9701e-03	2.0358e-02
4000	1.1694e-01	1.1694e-01	-9.0001e-08	2.1153e-03	1.9985e-02
5000	1.0802e-01	1.0802e-01	-1.1764e-07	2.1675e-03	2.0332e-02
7000	1.0702e-01	1.0803e-01	-1.1754e-07	2.1475e-03	2.0132e-02

Table 17. RMS with Varying Sample Time Period

Sample Period	Real Lambda	RMS Angle	RMS Range Ratio	RMS velocity
1000	-2.2660e+04	2.9150e-06	7.7999e+02	3.8125e+03
	2.1139e+04	3.0173e-08	2.2246e+03	2.0948e+03
	1.4158e+04	1.0958e-08	9.7329e+02	9.6491e+02
	3.8884e+03	3.3408e-07	6.9707e+03	1.3758e+04
	1.9776e-01	7.1000e-13	9.8759e-01	9.8766e-01
2000	9.5156e+01	1.0470e-08	2.3946e+03	1.9324e+03
	1.0124e+02	2.0209e-10	1.5136e+01	2.5882e+01
	9.4950e-03	1.7675e-11	1.0217e+00	1.0222e+00
4000	1.1694e-01	2.5626e-12	9.9280e-01	9.9153e-01
5000	1.0802e-01	1.1517e-11	1.0090e+00	1.0087e+00
7000	1.0702e-01	7.7567e-10	9.9248e-01	9.9379e-01

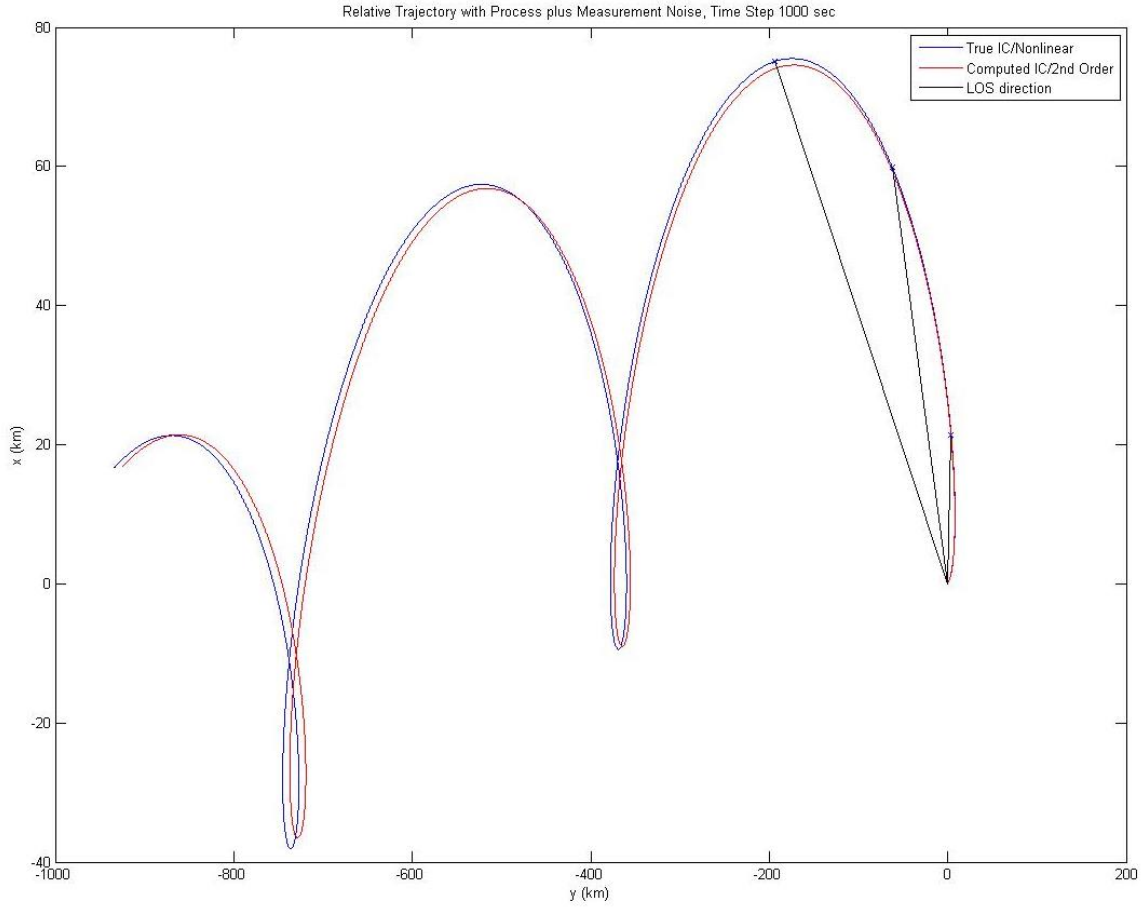

Figure 19. Relative Orbit with Process plus 10^{-6} rad of Measurement Noise, Time Step of 1000 s

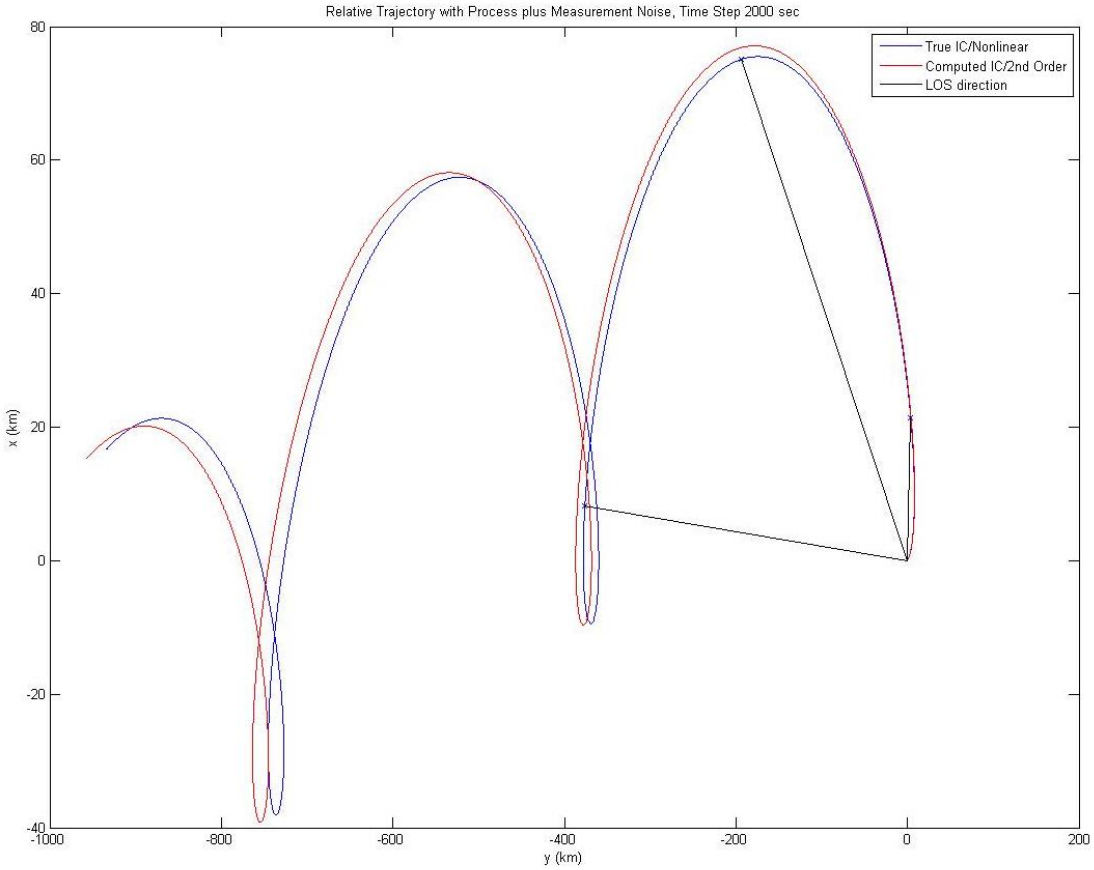

Figure 20. Relative Orbit with Process plus 10^{-6} rad of Measurement Noise, Time Step of 2000 s

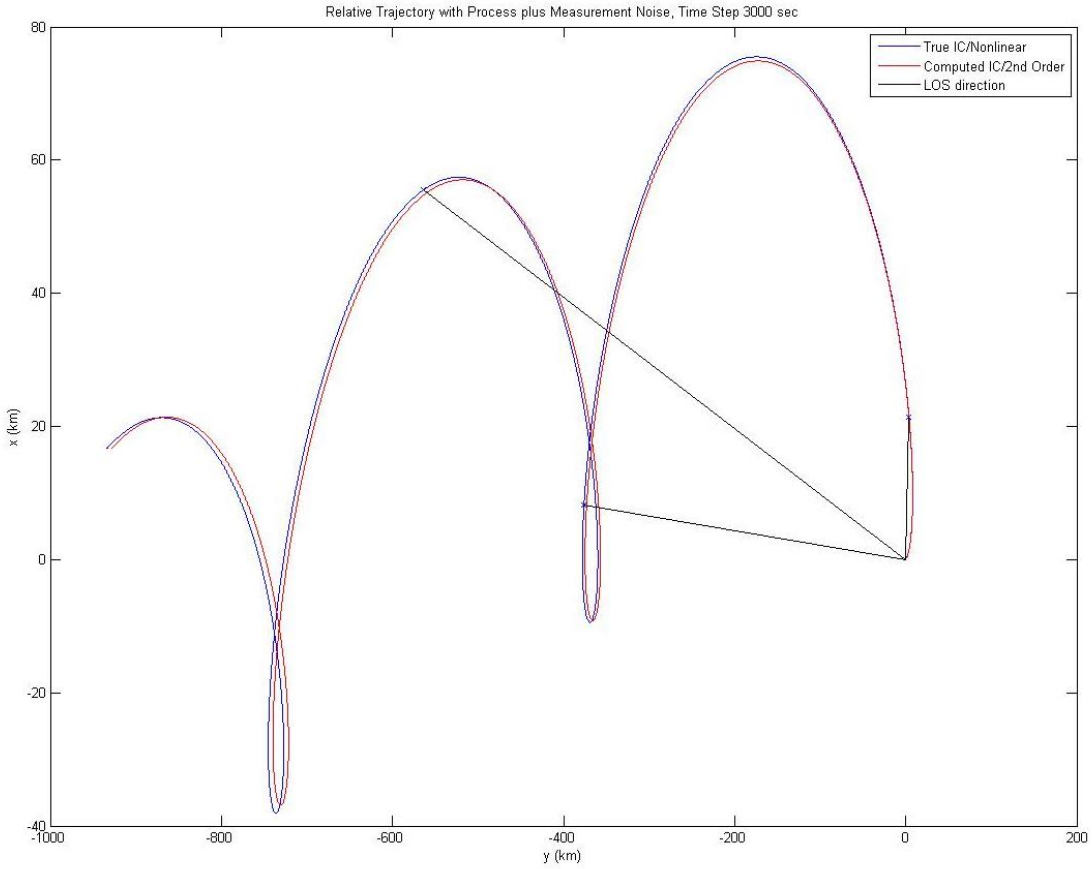

Figure 21. Relative Orbit with Process plus 10^{-6} rad of Measurement Noise, Time Step of 4000 s

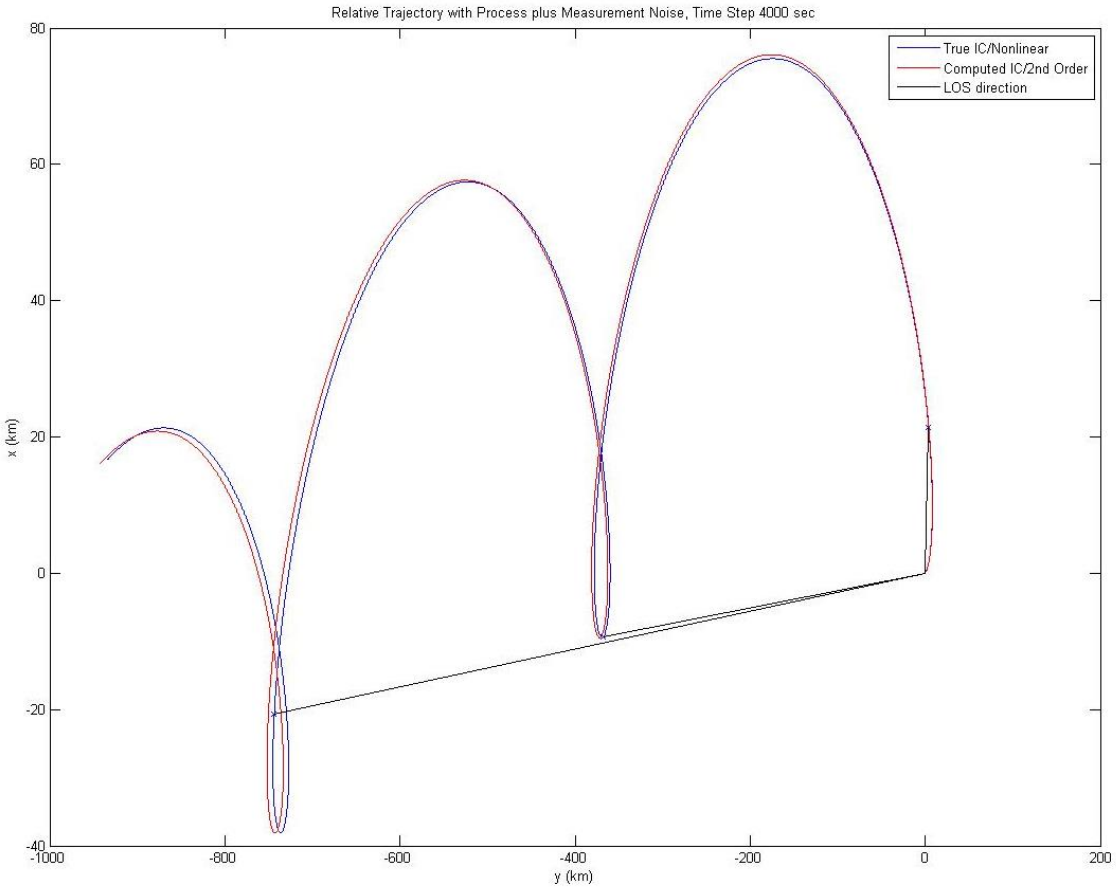

Figure 22. Relative Orbit with Process plus 10^{-6} rad of Measurement Noise, Time Step of 5000 s

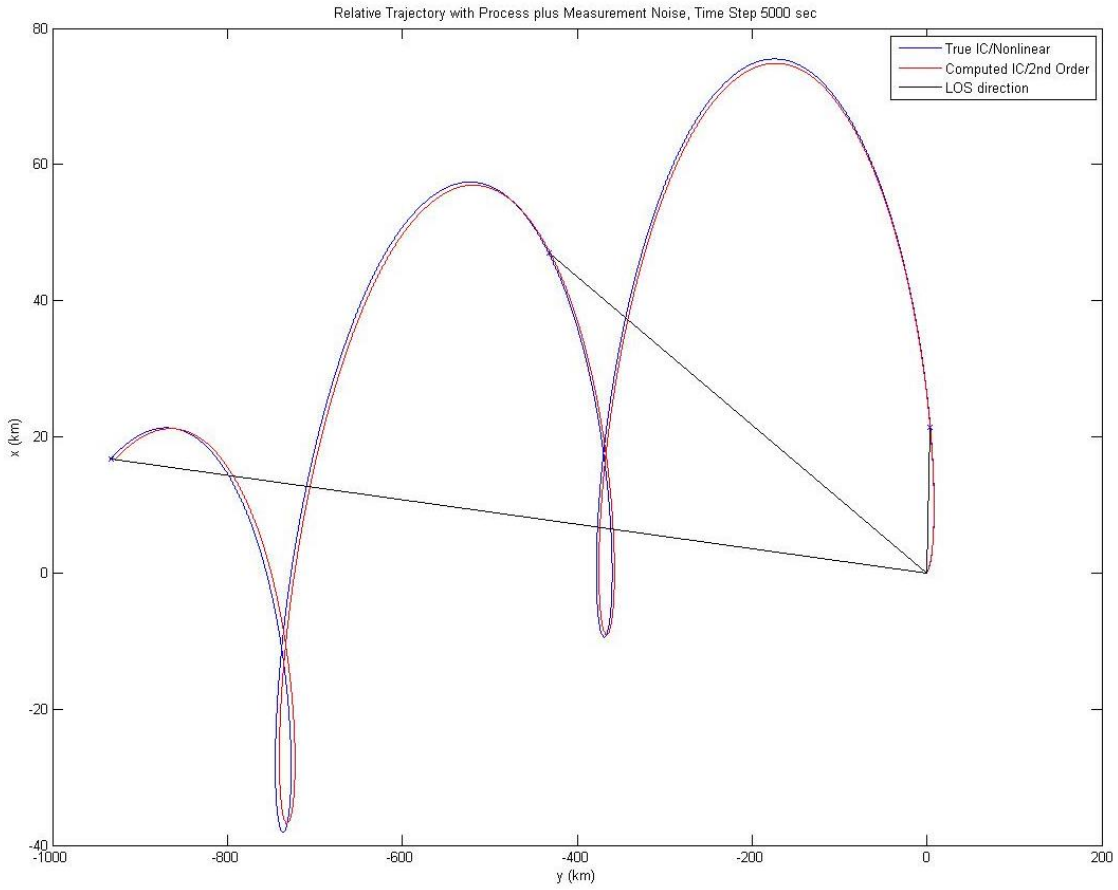

Figure 23. Relative Orbit with Process plus 10^{-6} rad of Measurement Noise, Time Step of 7000 s

Fast Sample Rate

In order to show the effect of a fast sample rate, the same model parameters are run with the sample period reduced from 1000 s to 150 s. Both process noise and the measurement noise of standard deviation 10^{-6} rad is added to the system.

In Figures 7 and 15, the relative orbit and line-of-sight representations were plotted for the sample rate of 1000 s and 150 s, respectively, with the redundant-measurement solution and the separation-magnitude formulation. Figure 15 showed that such a small sample does not give much information on the shape and drift behavior of the relative orbit trajectory. Here, with sample period of 150 s, the results are accurate, as it can be seen from Tables 18 and 19.

Table 18. Estimated Initial Conditions with Time Step of 150 s

Sample Period	Real Lambda	x_0	y_0	$\dot{x}_0$	$\dot{y}_0$
	Exact	**0.2**	**0**	**.002**	**.02**
150	1.4542e+04	1.4542e+04	-1.4868e-03	-1.1534e+01	-2.6314e+01
	-1.3676e+03	-1.3676e+03	1.3983e-04	2.1458e+00	-2.0899e+00
	2.0006e-01	2.0006e-01	-2.0455e-08	2.0006e-03	2.0006e-02

Table 19. RMS with Time Step of 150 s

Sample Period	Real Lambda	RMS Angle	RMS Range Ratio	RMS velocity
150	1.4542e+04	5.9927e-10	1.1247e+03	1.1187e+03
	-1.3676e+03	1.3556e-12	1.9226e+02	2.1476e+02
	2.0006e-01	4.2979e-13	9.5794e-01	9.5796e-01

The Macaulay resultant method is able to provide better results than the redundant-measurement solution when used with separation-magnitude formulation. Figure 24 shows the relative orbit of deputy satellite with respect to chief satellite when the sample period is 150 s.

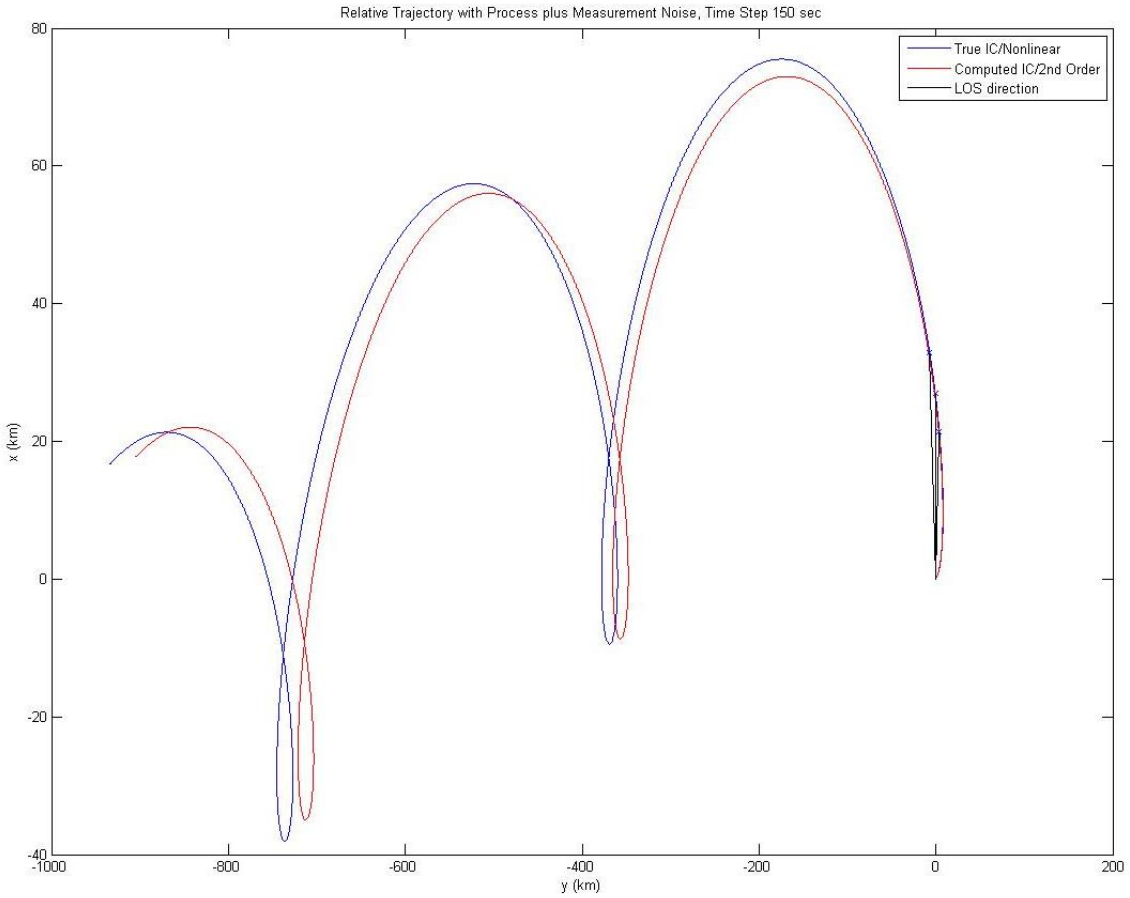

Figure 24. Relative Orbit with Process plus 10^{-6} rad of Measurement Noise, Fast sample period of 150 s

Slow Sample Rate

As mentioned earlier in chapter 4, large separations between the chief and deputy satellites, large time periods between the measurements, and very large drift rates can also prevent the success of the IROD method. Since the IROD method is fundamentally based on the second-order solution, it ceases to be valid where the second-order solution is no longer suitable.

Table 12 shows the estimation results for the slow sample time of 10000 s, using the redundant-measurement solution, and the estimated initial conditions were very poor. Here, the limit of slow sample rate is further increased by taking samples at 14000 s. Table 20 shows the estimation result of the minimal-measurement solution for a sample period of 14000 s. Table 21 shows the RMS error associated with angle residual and range ratio, and further provides evidence that even large sample periods do not hinder the accuracy of the solution. It can be said that the Macaulay method extends the upper limit on the slow sample periods.

Table 20. Estimated Initial Conditions with Time Step of 140000 s

Sample Period	Real Lambda	x_0	y_0	$\dot{x}_0$	$\dot{y}_0$
	Exact	**0.2**	**0**	**.002**	**.02**
14000	1.4542e+04	1.4542e+04	-1.4868e-03	-1.1534e+01	-2.6314e+01
	-1.3676e+03	-1.3676e+03	1.3983e-04	2.1458e+00	-2.0899e+00
	2.0006e-01	2.0006e-01	-2.0455e-08	2.0006e-03	2.0006e-02

Table 21. RMS with Slow Time Step of 14000 s

Sample Period	Real Lambda	RMS Angle	RMS Range Ratio	RMS velocity
14000	1.4542e+04	1.6336e-03	2.3033e+05	8.2169e+05
	-1.3676e+03	3.2510e-02	4.6490e+05	1.8021e+06
	2.0006e-01	2.3425e-09	1.0402e+00	1.0174e+00

Figure 25 shows the relative trajectory of the motion of the deputy satellite with respect to the chief satellite. The conclusion made above matches the plot obtained for relative motion. The trajectory generated using the true state vectors with the full nonlinear equations is labelled as "True IC/Nonlinear". The trajectory generated using the computed state vectors with the second-order dynamics is labeled as "Computed IC/2nd Order". And, the line-of-sight direction vector is labelled as "LOS direction".

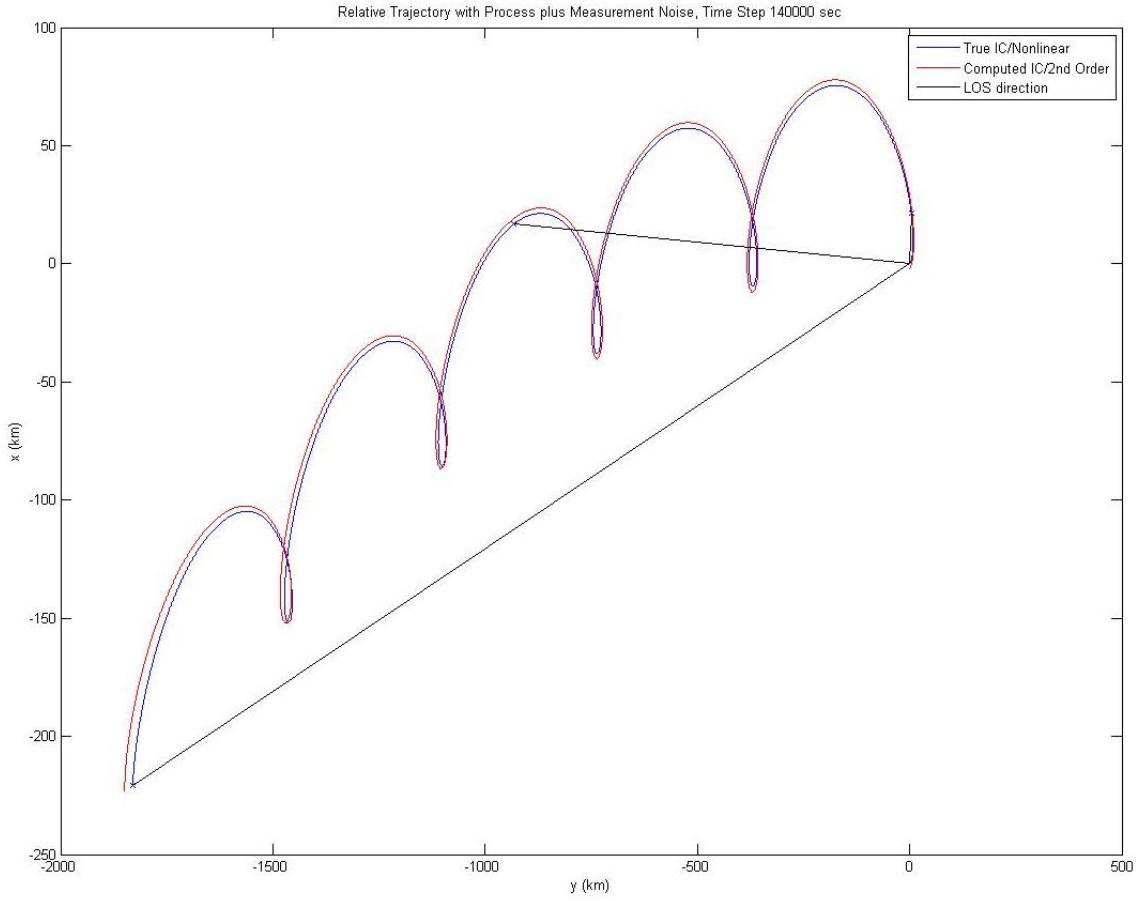

Figure 25. Relative Orbit with Process plus 10^{-6} rad of Measurement Noise, Large sample period of 14000 s

CONCLUSION

A method has been presented for computing the initial state vector using line-of-sight direction vectors. For three dimensional estimations, a total of eight measurements of unit-direction-vectors is required, generating a 21×21 matrix of linear equations. This method requires redundant measurements, but requires less measurements than other published methods. Also, it requires less computational effort than any other published method. With ideal assumptions, the method is able to estimate exact initial conditions, and with more realistic enviornment the technique can recover the initial conditions with a level of precision, depending upon the corruption of measurement noise and the fidelity of the nonlinear solution model. The only requirement will be to use a high precision camera so that the measurements are relatively free of corruptions. It should also be mentioned that the separation-magnitude method uses the unit-direction-vector of initial relative position between the chief and the deputy satellite as a basis for the solution, and may be particularly sensitive to erros in this observation.

The application of the Macaulay resultant method has also been presented in this thesis. The minimal-measurement solution using the separation-magntiude formulation computes the intitial relative position vector and velocity vector of the deputy satellite with respect to the chief satellite. It provides all the imaginary and real solutions possible to the problem of IROD. This method requires minimal number of measurements in comparsion to the published methods, and the redundant-measurement solution method. However, it

adds algebraic complexity to the procdeure which is high in comparison to the redundant-measurement solution method but very less in comparision to the published method. In published method, for the three dimensional case, the matrix obtained has dimension of 792×792 utilizing a total of six angular measurements, but in the presented method the matrix size is of 56×56 processing only two more unit-direction-vector measurement. The Macauly Resultant method is highly dependent on number of measurements and unknowns. Althought the Macaulay Resultant method has some algebraic compleixty in comparison to the discard method, but it improves the limit placed on the IROD method by the redundant-measurement method. The redundant-measurement method provides satisfactory result with the fast sample rate of 150 s and the slow sample rate of 10000 s but the Macaulay Resultant method provides similar satisfactory result with 100 s of fast sample rate and 14000 s of slow sample rate.

REFRENCES

1. Woffinden, D. C. and Geller, D. K., "Observability Criteria for Angles-Only Navigation," IEEE Transactions on Aerospace and Electronic Systems, Vol. 45, No. 3, July, 2009, pp. 1194-1208.
2. G.W. Hill, "Researches in the Lunar Theory," American Journal of Mathematics, Volume 1, 1878, pp. 5-26
3. Chohessy, W. H. and Wiltshire, R. S., "Terminal Guidance System for Satellite Rendezvous", Journal of the Aerospace Sciences, Vol. 27, No. 9, September, 1960, pp. 653-658
4. Patel, H., Lovell, T. A., Allgeier, S., Russell, R., and Sinclair, A. J., "Relative Navigation for Satellites in Close Proximity Using Angle-Only Observations," AAS- 2012-212, Proceedings of the AAS-AIAA Spaceflight Mechanics Meeting, Charleston, South Carolina, January-February, 2012
5. Newman, B., Lovell, T. A., and Pratt, E., "Second Order Nonlinear Initial Orbit Determination for Relative Motion using Volterra Theory," AAS-2014-286,, Proceedings of the AAS- AIAA Spaceflight Mechanics Meeting, Santa Fe, New Mexico, January, 2014
6. Pratt, E., Lovell, T. A., and Newman, B., " A Second Order Method for Initial Relative Orbit Determination Using Angle-Only Observations," AAS-2014-293, Proceedings of the AAS-AIAA Spaceflight Mechanics Meeting, Santa Fe, New Mexico, January, 2014
7. Newman, B., Lovell, T. A., Pratt, E., and Duncan, E., "Quadratic Hexa-Dimensional Solution for Relative Orbit Determination," AIAA 2014-4309, Proceedings of the AIAA-AAS Astrodynamics Specialist Conference, San Diego, California, August, 2014

8. Stringer, M. T., Newman, B., Lovell, T. A., and Omran, A., 'Second Order Nonlinear Initial Value Solution for Relative Motion Using Volterra Theory," AAS-2013-469, Proceedings of the AAS-AIAA Spaceflight Mechanics Meeting, Lihue, Hawai, February, 2013.
9. Newman, B., Lovell, T. A., and Pratt, E., "Second Order Nonlinear Initial Orbit Determination for Relative Motion using Volterra Theory," AAS-2014-286, Proceedings of the AAS-AIAA Spaceflight Mechanics Meeting, Santa Fe, New Mexico, January, 2014.
10. Schaub, H., Junkins, J. L., "Analytical Mechanics of Space Systems," American Institute of Aeronautics and Astronautics, Inc., Reston, Virginia
11. Stiller, P. F., "An Introduction to the Theory of Resultants," ISC-96-02-MATH, Institute for Scientific Computation, Texas A&M University, College Station, Texas 1996.
12. Bajaj, C., Garrity, T., and Warren, J., "On the Applications of Multi-Equational Resultants," CSD-TR-826
13. LeGrand, K.A., DeMars, K. J., and Darling, J. E., "Solutions of Multivariate Polynomial System using Macaulay Resultant Expressions," AAS-104-229, Proceedings of the AAS-AIAA Spaceflight Mechanics Meeting, Santa Fe, New Mexico, January, 2014.
14. Manocha, D., "Computing Selected Solutions of Polynomial Equations," Proceedings of the ACM International Symposium on Symbolic and Algebraic Computation, Oxford, England, July, 1994, pp. 1-8.
15. Manocha, D. and Krishnan, S., "Solving Algebraic Systems Using Matrix Computations," ACM Special Interest Group on Symbolic and Algebraic Manipulation Bulletin, Vol. 30, No. 4, December, 1996, pp. 4-21.
16. Jonsson, G.F. and Vavasis, S. A., "Accurate Solution of Polynomial Equations Using Macaulay Resultant Matrices," Mathematics of Computation, Vol. 74, No. 249, July, 2004, pp. 221-262.